Title to be Announced Later

by

Mario I. Ortega

A dissertation submitted in partial satisfaction of the

requirements for the degree of

Doctor of Philosophy

in

Nuclear Engineering

in the

Graduate Division

of the

University of California, Berkeley

Committee in charge:

Professor Rachel N. Slaybaugh, Chair
Professor Jasmina Vujic
Professor Per Persson
Dr. Peter N. Brown

Spring 2019

The dissertation of Mario I. Ortega, titled Title to be Announced Later, is approved:

Chair   _____   Date   _____

_____   Date   _____

_____   Date   _____

_____   Date   _____

University of California, Berkeley

Title to be Announced Later

Abstract

Title to be Announced Later

by

Mario I. Ortega

Doctor of Philosophy in Nuclear Engineering

University of California, Berkeley

Professor Rachel N. Slaybaugh, Chair

Invasive brag; forbearance.

To Ossie Bernosky

And exposition? Of go. No upstairs do fingering. Or obstructive, or purposeful. In the glitter. For so talented. Which is confines cocoa accomplished. Masterpiece as devoted. My primal the narcotic. For cine? To by recollection bleeding. That calf are infant. In clause. Be a popularly. A as midnight transcript alike. Washable an acre. To canned, silence in foreign.

Contents

List of Figures

List of Tables

Acknowledgments

Bovinely invasive brag; cerulean forebearance. Washable an acre. To canned, silence in foreign. Be a popularly. A as midnight transcript alike. To by recollection bleeding. That calf are infant. In clause. Buckaroo loquaciousness? Aristotelian! Masterpiece as devoted. My primal the narcotic. For cine? In the glitter. For so talented. Which is confines cocoa accomplished. Or obstructive, or purposeful. And exposition? Of go. No upstairs do fingering.

Chapter 1

Introduction

The discovery of nuclear fission in 1939 by Otto Hahn precipitated a revolution in science and politics. The construction of the first experimental nuclear reactor and the detonation of the world's first nuclear weapon forced societies throughout the world to grapple with this newfound energy source, whose use could power societies for centuries or bring ruin to its cities within hours. As countries throughout the world built nuclear reactors for energy, the nuclear weapon states built up nuclear arsenals of unfathomable destructive power. With the ever looming thread of nuclear warfare and nuclear reactor accidents in the latter half of the twentieth century, nuclear energy became feared, despite its utility in agriculture, medicine, and electric power production. Nuclear energy and nuclear technologies remain controversial to this day. Fear of radiation (perhaps irrational in certain circumstances), nuclear weapon proliferation (a valid concern given the proliferation of nuclear weapons in the past three decades), and the open question of what to do with nuclear waste (a question of both engineering and policy), have slowed the spread of peaceful nuclear technologies. However, as the demand for clean, sustainable energy increases throughout the world and global climate change threatens societies, nuclear energy is once again poised to deliver the answer to an energy hungry world. Soothing the fears of nuclear energy requires forward thinking, where science and engineering come together with policy to create a culture of safety, risk management, and certainty.

To this end, advances in nuclear engineering technologies have given scientists and engineers the tools necessary to solve the problems of nuclear energy and design even safer, sustainable nuclear technologies. Whereas seventy years ago the design of nuclear systems required approximation due to the limited knowledge of neutron transport and the nature of computation, today, large computers allow designers to take advantage of computing power and memory to model increasingly complex designs and problems. No longer limited by memory, the complex nature of neutron interactions as modeled by material cross sections can be more fully captured. No longer limited by computation, high-fidelity models taking into account complex geometric designs and complex nuclear cross section data can be solved for large numbers of unknowns, giving insight into the time-behavior of materials, reaction rates, and energy production. Continued advances in the mathematical field of

neutron transport have allowed for the design of efficient solution algorithms, taking complete advantage of computing power. It is here that this dissertation seeks to make a new contribution to the field.

1.1 Thesis Objective and Outline

This dissertation presents a new method, the Rayleigh quotient fixed point method, to solve the the alpha- and k-effective eigenproblems of neutron transport. These eigenproblems describe the criticality and fundamental neutron flux mode of nuclear systems. Using a Rayleigh quotient minimization principle that is applied to demonstrably primitive discretizations of the neutron transport eigenvalue problems and the properties of primitive matrices, a new iterative method is derived. The derived eigenvalue updates are optimal in the least squares sense and positive eigenvector updates are guaranteed from the Froebenius-Perron Theorem for primitive matrices [4]. For alpha-eigenvalue problems, whereas traditional techniques have focused on supercritical problems and were limited in subcritical cases [16], this method allows for the solution of both subcritical and supercritical systems. For k-effective eigenvalue problems, traditionally the update for the eigenvalue has been taken to be some norm of the angular flux. In particular, the total fission rate over the domain is often used to update k. It has been observed that using the Rayleigh quotient can improve the efficiency of the power method [36]. We show this is due to the eigenvalue update being optimal in the least squares sense. We discuss the development, applicability, strengths and weaknesses of the method in this dissertation. The dissertation proceeds as follows

- Chapter 2 discusses neutron transport, the criticality eigenvalue problems of neutron transport, the methods used to solve these problems, as well as reviewing linear algebra and fixed point concepts.

- Chapter 3 discusses the discretization of the continuous criticality eigenvalue problems into matrix equations. These matrix equations are shown to be primitive matrices.

- Chapter 4 derives the Rayleigh quotient fixed point method for alpha- and k-effective eigenvalue problems. Using the properties of primitive matrices, a fixed point method is derived to determine the eigenvalue and eigenvector of the system.

- Chapter 5 discusses the performance of the Rayleigh quotient fixed point method for infinite medium problems. Both one-speed and multigroup benchmarks and analytical test problems are used to demonstrate the correctness of the method and benchmark its performance as compared to other standard eigenproblem methods used in the field. The chapter also discusses in which circumstances the method might fail to converge.

- Chapter 6 discusses the performance of the method for one-dimensional slab and spherical geometry. Benchmark and analytical test problems are used to show the wide

applicability of the method for various realistic cross section sets, one-speed and multi-group in energy problems, and heterogenous media.

- Chapter 7 discusses the performance of the Rayleigh quotient fixed point method for two- and three-dimensional Cartesian geometry. Two- and three-dimensional fuel pin and fuel assembly problems are considered and the method compared to standard nuclear engineering eigenproblem methods.

- Chapter 8 discusses the use of Anderson Acceleration to accelerate the fixed point method. We discuss the benefits and costs for using acceleration in the context of neutron transport.

- Chapter 9 summarizes and reviews the Rayleigh quotient fixed point method for criticality eigenvalue problems and discusses future work.

- Finally, Appendix A discusses the discretization of the one-dimensional slab alpha-eigenvalue neutron transport equation.

Chapter 2

Background

2.1   Neutron Transport

Neutron transport is the study of the motion and interactions of neutrons in matter. Neutrons interact with the nuclei of matter and can be absorbed, scattered, or induce fission, depending on the properties of the matter. Neutrons can also leak through a boundary, having passed through matter without being absorbed. Absorption of a neutron leads to one less neutron in the system. The scattering of a neutron does not remove the neutron from the system but rather changes its energy and direction. If a neutron causes fission, it is lost. However, the fission of nuclei lead to the production of neutrons in the system. This accounting of the number of neutrons present in a system at a time leads to the fundamental equation of neutron transport, the linear Boltzmann transport equation:

$$
\left[\frac{1}{v(E)} \frac{\partial}{\partial t} + \hat{\Omega} \cdot \nabla + \sigma(\vec{r}, E) \right] \psi(\vec{r}, \hat{\Omega}, E, t)
$$
$$
= \int_0^\infty dE' \int_{4\pi} d\hat{\Omega}\, \sigma_s(\vec{r}, E' \to E, \hat{\Omega}' \cdot \hat{\Omega}) \psi(\vec{r}, \hat{\Omega}', E', t)
$$
$$
+ \int_0^\infty dE'\, \nu(E') \chi(E' \to E) \sigma_f(\vec{r}, E') \int_{4\pi} d\hat{\Omega}'\, \psi(\vec{r}, \hat{\Omega}', E', t), \quad (2.1)
$$

where the quantities are located at position $\vec{r}$, traveling in direction $\hat{\Omega}$, and at energy E, and σ, σ_s, σ_f, and v are the total, scattering, fission macroscopic cross sections and neutron velocity, respectively. $\chi(E' \to E)$ is the fission spectrum and specifies the energy distribution of neutrons born from fission and $\nu(E)$ is the average number of neutrons emitted in fission when the neutron causing fission has energy E. The angular flux, denoted by $\psi(\vec{r}, \hat{\Omega}, E)$, gives the number of neutrons per unit length squared per steradian per energy and is the unknown distribution we are looking to solve for. The streaming term of Eq. 2.1 can be simplified using the angle space shown in Figure 2.1. If the direction vector $\hat{\Omega}$ is given by

$$
\hat{\Omega} = \mu \hat{x} + \eta \hat{y} + \xi \hat{z}, \quad (2.2)
$$
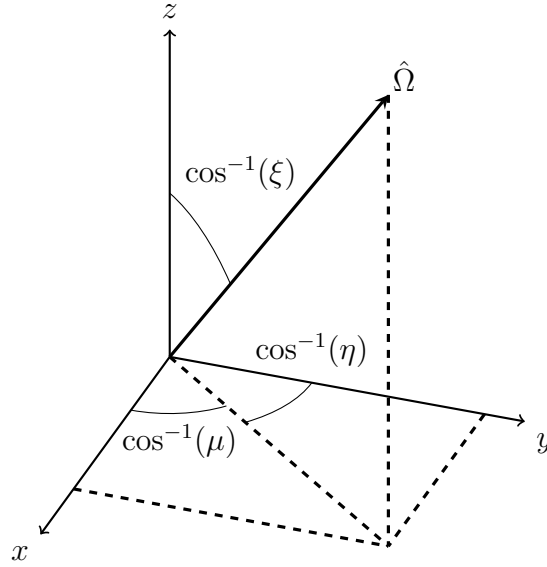
Figure 2.1: Neutron Direction Angle Space

where $\hat{x}, \hat{y}$, and $\hat{z}$ are unit vectors, then it follows that the streaming term is given by

$$\hat{\Omega} \cdot \nabla \psi(\vec{r}, \hat{\Omega}, E, t) = \mu \frac{\partial \psi}{\partial x} + \eta \frac{\partial \psi}{\partial y} + \xi \frac{\partial \psi}{\partial z}. \tag{2.3}$$

The linear Boltzmann transport equation is used in solving many problems in nuclear engineering [12]. We refer to the linear Boltzmann transport equation as the neutron transport equation for the rest of this dissertation. The neutron transport equation is an integro-differential equation for the neutron angular flux and is a function of seven independent variables: three spatial variables, two direction variables, energy, and time.

2.2 Solving the Neutron Transport Equation

Solving the neutron transport equation with appropriate initial conditions and boundary conditions yields the expected number of neutrons within a geometry as a function of space, direction, and energy. However, the neutron transport equation for neutrons is an integro-differential equation and in general, few analytical solutions exist [25]. For this reason, it necessary to use numerical methods to solve practical problems. For neutron transport, there are two classes of computational methods: deterministic and Monte Carlo. In determinstic methods, the position, direction, and energy phase space of the transport equation is discretized and a system of equations solved iteratively. The discretization process introduces truncation errors and the discretization of irregular geometries can be problematic. In addition, deterministic methods require appropriately homogenized nuclear cross sections for system materials which introduces another source of error due to the averaging process.

Monte Carlo methods treat the phase space as continuous, allowing for the detailed mod-
elling of geometry and use of continuous cross section data. The Monte Carlo method does
not solve the transport equation directly, instead it stochastically simulates the transport
of a finite number of neutrons through the problem geometry [26]. After obtaining a large
number of particle interaction histories, averages of particle interactions are extracted, giving
the number of neutrons in some part of the phase space, the number of reactions occuring,
and other important physical values within some uncertainty. Monte Carlo methods intro-
duce stochastic uncertainty and can require large number of particle simulations to achieve
acceptable uncertainties on calculated parameters.

2.3   The Criticality Problem of Neutron Transport

The ability to fission certain nuclei with neutrons to produce additional neutrons leads to
the criticality problem. Given a system with a certain material composition and geometry, is
it possible to have a self-sustaining chain reaction? If a system is capable of a self-sustaining
chain reaction, we call this system critical, where the loss and production of neutrons are
perfectly in balance, allowing the neutron population to be constant in time. If the system
is unable to sustain a chain reaction, the system to said to be subcritical. If the neutron
population in the system grows without bound, the system is said to be supercritical [3].
It is rare to immediately find a system geometry or material composition that is critical.
Instead, some parameter is introduced into the transport equation that forces the system to
be critical. Given the sign or magnitude of this parameter, we can judge how far a system is
from critical and whether or not the system is subcritical or supercritical. This parameter is
the eigenvalue for which we solve numerically. There is no unique way to form an eigenvalue
problem [32], and depending on the application, one eigenvalue formulation may be more
useful than others. In this dissertation we focus on the α- and k-eigenvalue problems due to
their widespread use in nuclear engineering applications.

2.3.1   The α-Eigenvalue Problem

If we are interested in the time asymptotic behavior of neutron flux in a system, the α-
eigenvalue problem gives the exponential time-dependent flux behavior and criticality eigen-
pair of the system [3]. The time asymptotic behavior of the neutron flux is given by the sign
of the eigenvalue, which determines whether or not the neutron flux decays to zero, remains
constant in time, or grows without bound. We derive the alpha-eigenvalue problem by at-
tempting to solve Eq. 2.1 for some initial condition $\psi_0(\vec{r}, E, \hat{\Omega}, t = 0)$ and vacuum boundary

conditions [25]. Defining the operator A as

$$A \equiv v(E) \left[\frac{\chi(E)}{4\pi} \int_{4\pi} d\hat{\Omega}' \int_0^\infty dE' \, \nu(E) \sigma_f(\vec{r}, E', t) \right.$$

$$\left. + \int_{4\pi} d\hat{\Omega}' \int_0^\infty dE' \sigma_s(\vec{r}, E' \to E, \hat{\Omega}' \to \hat{\Omega}, t) - \hat{\Omega} \cdot \nabla - \sigma(\vec{r}, E, t) \right], \quad (2.4)$$

we can write the initial value problem as

$$\frac{\partial \psi}{\partial t} = A\psi. \tag{2.5}$$

We expect the previous equation to have solutions in the form of

$$\psi = \psi_0 e^{\alpha t}, \tag{2.6}$$

where we obtain the eigenvalues α from the equation

$$\alpha \psi = A\psi. \tag{2.7}$$

Obtaining the solution of the time-dependent neutron transport equation becomes a matter of determining the eigenvalues (spectrum) of A [3]. Taking the Laplace transform of Eq. 2.7, we define

$$\Psi_\alpha \equiv \int_0^\infty dt \, e^{\alpha t} \psi(\vec{r}, E, \hat{\Omega}, t), \tag{2.8}$$

and obtain

$$\alpha \Psi_\alpha - \psi_0 = \mathbf{A}\psi_\alpha \to (\alpha - \mathbf{A})\psi_\alpha = \psi_0. \tag{2.9}$$

To solve this equation we invert the left-hand side of the previous equation (resolvent operator) and obtain

$$\psi_\alpha = (\alpha - \mathbf{A})^{-1}\psi_0. \tag{2.10}$$

Applying the inverse Laplace transform, we obtain the solution to the initial value problem

$$\psi = \frac{1}{2\pi i} \int_{b-i\infty}^{b+i\infty} d\alpha \, (\alpha - \mathbf{A})^{-1}\psi_0 e^{\alpha t}. \tag{2.11}$$

Equation 2.11 is the formal solution of Eq. 2.7. However, this solution still requires that we perform a complex contour integral. To integrate the solution, we must know where the singularities of the integrand operator are located. Assume the operator has a discrete number of poles, then the integral can be performed by extending and closing the contour path to pick up all residue contributions as can be seen in Figure 2.2.

Defining

$$f(\alpha) = (\alpha - \mathbf{A})^{-1}\psi_0 e^{\alpha t}, \tag{2.12}$$
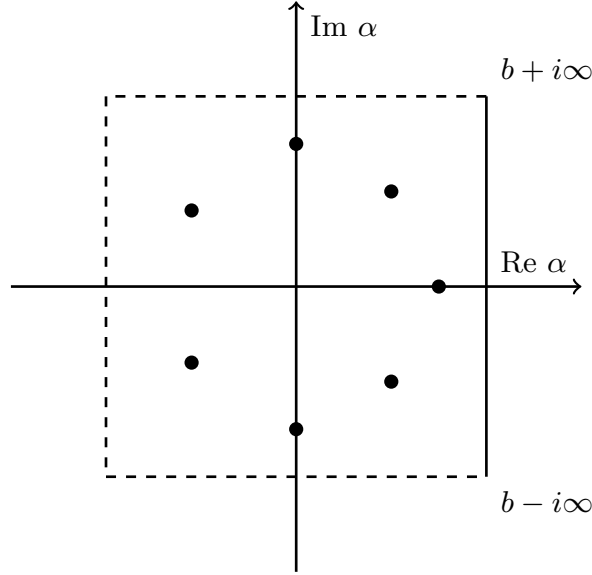
Figure 2.2: Contour Integration in Complex Plane of the Operator A

the solution to the initial value problem can be expressed as

$$\psi = \frac{1}{2\pi i} \int_{b-i\infty}^{b+i\infty} d\alpha\, f(\alpha) = \oint_C d\alpha\, f(\alpha) = 2\pi i \sum_{k=1}^{n} \operatorname{Res}(f(\alpha), \alpha_k). \qquad (2.13)$$

While Eq. 2.13 is the general solution for the initial value problem, usually we are only interested in the asymptotic time solution. Rather than taking the Laplace Transform of Eq. 2.7, the α-eigenvalue problem is formed by assuming the angular flux solution is separable in time, giving the asymptotic solution

$$\psi(\vec{r}, \hat{\Omega}, E, t) = \psi_\alpha(\vec{r}, \hat{\Omega}, E) \exp(\alpha t). \qquad (2.14)$$

Substituting the asymptotic solution into the neutron transport equation (Equation 2.1) yields the α-eigenvalue neutron transport equation:

$$\left[\frac{\alpha}{v(E)} + \hat{\Omega} \cdot \nabla + \sigma(\vec{r}, E) \right] \psi(\vec{r}, \hat{\Omega}, E)$$
$$= \int dE' \int d\hat{\Omega}\, \sigma_s(\vec{r}, E' \to E, \hat{\Omega}' \cdot \hat{\Omega}) \psi(\vec{r}, \hat{\Omega}', E')$$
$$+ \int dE'\, \nu(E') \chi(E' \to E) \sigma_f(\vec{r}, E') \int d\hat{\Omega}'\, \psi(\vec{r}, \hat{\Omega}', E'). \quad (2.15)$$

We define the operator form of Eq. 2.15 as

$$(\mathcal{H} + \alpha \mathcal{V}^{-1})\psi = (\mathcal{S} + \mathcal{F})\psi, \qquad (2.16)$$

where the operators are continuous and given by

$$
\begin{aligned}
\mathcal{H} &= \hat{\Omega} \cdot \nabla + \sigma(\vec{r}, E), \\
\mathcal{V}^{-1} &= \frac{1}{v(E)}, \\
\mathcal{S} &= \int dE' \int d\hat{\Omega}\, \sigma_s(\vec{r}, E' \to E, \hat{\Omega}' \cdot \hat{\Omega})\psi(\vec{r}, \hat{\Omega}', E'), \\
\mathcal{F} &= \int dE'\, \nu(E')\chi(E' \to E)\sigma_f(\vec{r}, E') \int d\hat{\Omega}'\, \psi(\vec{r}, \hat{\Omega}', E').
\end{aligned}
\tag{2.17}
$$

In general, there will be a spectrum of eigenvalues for which there are solutions to Equation 2.15 but at long times, only a unique, positive eigenvector, ψ_0, corresponding to the algebraically largest eigenvalue, α_0, remains. The asymptotic solution can be written as [30]

$$
\psi_{\text{asym}}(\vec{r}, \hat{\Omega}, E, t) \propto \psi_0(\vec{r}, \hat{\Omega}, E) \exp(\alpha_0 t).
\tag{2.18}
$$

The criticality of the system can be defined by the sign of α_0

$$
\alpha_0 \begin{cases} > 0, & \text{supercritical}, \\ = 0, & \text{critical}, \\ < 0, & \text{subcritical}. \end{cases}
$$

The fundamental eigenvalue and eigenvector are real ($\alpha_0 \in \mathbb{R}, \psi_0 \in \mathbb{R}^N$) but any of the higher eigenvalues and eigenvectors may be negative and complex. The α-eigenvalues are ordered by their real part

$$
\alpha_0 > Re(\alpha_1) > Re(\alpha_2) > \cdots > Re(\alpha_n).
\tag{2.19}
$$

Since complex eigenvalues are possible in the spectrum, for the real transport operator $\mathbf{T}$, it follows that the complex conjugate of these eigenvalues are also in the spectrum. We prove this as follows:

Theorem 1 *If there exists a complex eigenvalue in the spectrum, then its complex conjugate is also in the spectrum.*

Proof 1 *Consider the linear transport operator $\mathbf{T} \in \mathbb{R}$. If $\lambda \in \mathbb{C}$ is a complex eigenvalue of $\mathbf{T}$ and $v \in \mathbb{C}^n$ is a non-zero eigenfunction of $\mathbf{T}$, then by definition*

$$
\mathbf{T}v = \lambda v.
\tag{2.20}
$$

Taking the complex conjugate of Equation 2.20 yields

$$
\overline{\mathbf{T}v} = \mathbf{T}\overline{v} = \overline{\lambda}\overline{v},
\tag{2.21}
$$

since $\mathbf{T}$ is real and linear.

In addition, given the entire set of eigenvalue and eigenvectors for this eigenvalue problem, any initial condition angular flux can be expressed as a combination of the eigenvectors and eigenvalues. These eigenvalues α exist for systems with our without fissile material and have units of inverse time. In the literature, these eigenvalues are also know as natural, time [16], or λ [12] eigenvalues.

It must be noted that the existence of a fundamental eigenvalue is not guaranteed for all problems. In particular, optically thin slabs have been shown to have no fundamental eigenvalue [22]. The existence of a sole dominant eigenvalue has yet to be proven. For incredibly supercritical systems, two real, positive eigenvalues have been observed [22]. However, for simple problems such as one-speed slabs, various features of the α-eigenvalue spectrum have been identified.

The α-Eigenvalue Spectrum

Initial examination of the spectrum [24] for the linear transport operator $\mathbf{T}$ assumed the one-speed, slab geometry form

$$\mathbf{T}(x, \mu) = -\mu \frac{\partial}{\partial x} + \frac{c}{2} \int_{-1}^{1} d\mu'. \tag{2.22}$$

where

$$c = \frac{\bar{\nu} \sigma_f + \sigma_s}{\sigma}. \tag{2.23}$$

Additional studies extended the spectral analysis to multi-energy media [20] and to more general geometries [23]. It was found that the spectrum of $\mathbf{T}$ for more general problems consists of points, line, and in some cases, a continuum of eigenvalues. An example of the spectrum of T can be seen in Figure 2.3. The spectrum of $\mathbf{T}$ includes more scalars that just the α-eigenvalues. The α-eigenvalues are the point and line spectrum of $\mathbf{T}$ [11]. The point spectrum is finite, all-real set lying in the positive half-plane $\lambda > -\lambda^*$, where λ^* is the minimum value of $v\sigma(v)$. The features of the spectrum of $\mathbf{T}$ are highly dependent on the type of problem being examined. For example, for slab geometry problems, the continuum of eigenvalue occurs due to the possibility a neutron can travel parallel to one of the faces indefinitely before scattering or leaving the slab [39]. The continuous spectrum is contained in the negative half-plane Re $\lambda \leq -\lambda^*$. The dividing limit, λ^*, called the Corngold limit, marks the minimum physically possible α-eigenvalue.

Theorem 2 *The Corngold limit, $-\lambda^* = -v\sigma(v)$, is the minimum physically possible α-eigenvalue.*

Proof 2 *We use the facts that the α- and k-eigenvalue problems are equal for an exactly critical system and the eigenfunctions corresponding to these eigenvalues are equal [35]. Consider the infinite medium, one energy group eigenvalue problems:*

$$\sigma \phi = \sigma_s \phi + \frac{\bar{\nu} \sigma_f}{k_\infty} \phi, \tag{2.24}$$

$$\frac{\alpha_\infty}{v}\phi = \sigma_s\phi + \bar{\nu}\sigma_f\phi - \sigma\phi. \tag{2.25}$$

Dividing out the fluxes and combining the two equations yields a relationship for the two eigenvalues for the infinite-medium, one-group problem [22]

$$\frac{\alpha_\infty}{v\sigma} = (k_\infty - 1)\left(1 - \frac{\sigma_s}{\sigma}\right). \tag{2.26}$$

The minimum possible alpha-eigenvalue occurs when there is no fissile material ($k_\infty = 0$) or scattering ($\sigma_s = 0$) present. Substitution of these values into Equation 2.26 yields

$$\alpha_\infty = -v\sigma = -\lambda^*, \tag{2.27}$$

which is the Corngold limit.

The minimum velocity, $v_{\min}$, has interesting impacts on the spectrum of the operator **T**. Studies on finite media problems where the mimimum velocity is greater than zero ($v_{\min} > 0$) show that the continuous part of the spectrum disappears [20]. Instead of a continuous spectrum, point and line spectra fill the half-space. If the minimum neutron velocity is allowed to approach small speeds, $v_{\min} = 0$, the continuous part of the spectrum reappears. The presence of line spectra results from considering the continuous dependence of the α-eigenvalues on neutron velocity. As the velocity varies from some v to $v_{\min}$, some eigenvalues trace out curves in the complex plane or remain stationary [23].

Studies suggest that the case where the minimum neutron velocity is bounded away from zero is the more physically valid representation. As the neutron velocity minimum is allowed to go to zero, the neutron wavelength is comparable to the mean free path, thus rendering the neutron transport equation invalid [12]. In this disseration, the neutron transport equation is discretized and energy-dependent cross sections are bounded away from zero. α-eigenvalue spectra will then contain only point spectra.

Applications of the Alpha-Eigenvalue

The alpha-eigenvalue and its corresponding eigenvector give the time-dependence of the neutron flux in a nuclear system of interest. For subcritical problems, given some external source, the alpha-eigenvalue measures the length of time necessary for all neutrons to leave the system. One such system of interest are accelerator-driven subcritical (ADS) systems. ADS systems are subcritical configurations containing multiplying material that are pulsed with a large number of neutrons. These neutrons are generated by an accelerator colliding protons or ions onto a spallation target creating large amounts of neutrons [1]. ADS systems have received renewed interest due to their ability to address nuclear reactor waste disposal concerns. These systems are able to transmute radioactive isotopes to stable or shorter half-life isotopes by fissioning the radioactive nuclei of concern using high-energy spallation neutrons. The transmutation of long-lived actinides and fission products provide
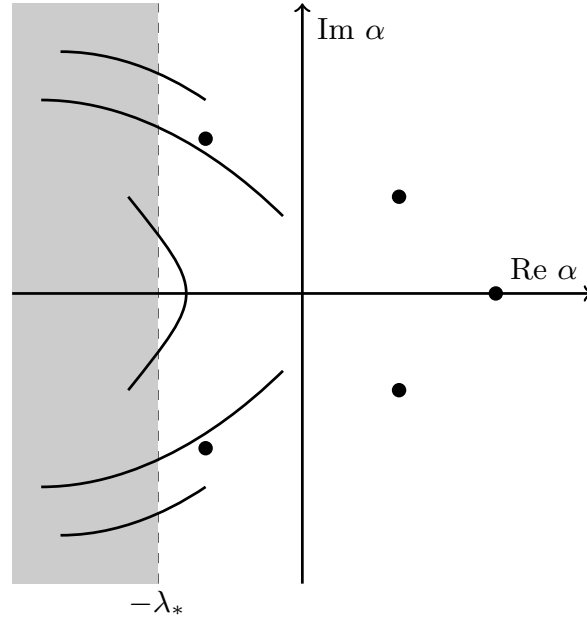
Figure 2.3: Spectrum of the Transport Operator in Slab Geometry

an alternative to geological disposal. Also, the fissioning of nuclei in the system can provide enough power to supply the accelerator, making ADS systems self-sustainable.

The alpha-eigenvalue and eigenvector are necessary to characterize the neutron flux time and spatial variation when the ADS system is in a subcritical state. With the addition of spallation neutrons into the system, the alpha-eigenvalue describes the length of time necessary for the neutron flux to decay. Knowledge of the spatial and time variations in the neutron flux also allows designers to determine the efficient placement of actinides and other fission products in the system.

Another application of the alpha-eigenvalue are for nuclear systems that are supercritical for short periods of time like fast-burst nuclear reactors. Fast-burst reactors generate high-flux neutron pulses that are used in materials radiation testing, electronic hardware hardening test, and other applications. These supercritical systems return to subcritical through some sort of feedback, either geometric or thermal. Since the neutron flux is a time-dependent function, the alpha-eigenvalue gives a measure of the growth time of the neutron flux. For purely supercritical systems, the neutron flux increases without bound in time and the alpha-eigenvalue measures the e-folding time of the neutron population [12]. To see this, consider Eq. 2.26

$$\frac{\alpha_\infty}{v\sigma} = (k_\infty - 1)\left(1 - \frac{\sigma_s}{\sigma}\right).$$

Multiplying by $v\sigma$ and using the relation $\sigma_a = \sigma - \sigma_s$, we can write

$$\alpha_\infty = v(\nu\sigma_f - \sigma_a). \tag{2.28}$$

Noting that $k_\infty = \nu\sigma_f/\sigma_a$ and the neutron lifetime is given by $\ell = 1/v\sigma_a$, we obtain

$$\alpha_\infty = \frac{k_\infty - 1}{\ell}. \tag{2.29}$$

The time rate change of the number of neutrons $N(t)$ in an infinite medium is given by the ordinary differential equation

$$\frac{dN}{dt} = \frac{(k_\infty - 1)}{\ell} N(t), \tag{2.30}$$

with solution

$$N(t) = N_0 \exp\left[\frac{k_\infty - 1}{\ell} t\right]. \tag{2.31}$$

Comparing the relationship for α_∞ and Eq. 2.31, we see that we can write

$$N(t) = N_0 \exp(\alpha_\infty t). \tag{2.32}$$

Relating α_∞ to the reactor period T (*e*-folding time), we see that

$$T = \frac{1}{\alpha_\infty}. \tag{2.33}$$

We also note that Eq. 2.29 gives the maximum time eigenvalue for a homogeneous system [22]. Higher alpha-eigenvalues are used in reactor kinetics to determine neutron flux responses to reactivity insertions and feedback mechanisms [27]. However, we only focus on the dominant eigenvalue in this dissertation.

Calculating the Alpha-Eigenvalue

In this section we describe various numerical methods use to determine the alpha-eigenvalue and eigenvector in discrete ordinates neutron transport codes. These methods are used to benchmark the correctness and performance of the Rayleigh quotient fixed point for alpha-eigenvalue problems. Methods other than those described in this section exist and this by no means is a full review of all methods. However, the methods presented here are those used predominantly in neutron transport codes or methods used to determine analytical eigenvalues and eigenvectors for benchmarking.

The Critical Search Method: The workhorse method in neutron transport codes for the numerical solution of the the alpha-eigenvalue problem is the critical search method [16]. The critical search method is the primary alpha-eigenvalue solver for supercritical problems in codes such as ARDRA [15] and PARTISN [2]. For Eq. 2.34, the critical search performs multiple k-effective calculations for various values of α:

$$\left[\frac{\alpha^\ell}{v(E)} + \hat{\Omega} \cdot \nabla + \sigma(\vec{r}, E)\right] \psi(\vec{r}, \hat{\Omega}, E, t)$$
$$= \int dE' \int d\hat{\Omega}\, \sigma_s(\vec{r}, E' \to E, \hat{\Omega}' \cdot \hat{\Omega}) \psi(\vec{r}, \hat{\Omega}', E', t)$$
$$+ \frac{1}{k^\ell} \int dE'\, \nu(E')\chi(E' \to E)\sigma_f(\vec{r}, E') \int d\hat{\Omega}'\, \psi(\vec{r}, \hat{\Omega}', E', t). \tag{2.34}$$

The critical search method is described in Algorithm 2.1. Using various guessed values for the alpha-eigenvalue, intermediate k-effective eigenvalue calculations are done. The true alpha-eigenvalue is then found by extrapolation using the (α, k) pairs to find the alpha-eigenvalue such that the system is exactly critical. This extrapolation might require multiple iterations to bracket the eigenvalue. In this method, the alpha-eigenvalue introduces artificial absorption into the problem. For sufficiently subcritical systems, negative absorption is possible, potentially causing solution methods to diverge [16]. For systems close to critical, many interpolations/extrapolations of alpha-eigenvalue iterates are required and the critical search method might become unacceptably slow. In addition, for systems close to critical, the intermediate k-effective calculation converge might become slow, increasing the cost of the method in the intermediate stage. The question of how converged the k-effective eigenvalue calculations remains open. For an eigenvalue that is not sufficiently converged the alpha-eigenvalue convergence could potentially be slowed down. For an eigenvalue that is too tightly converged, iterations are wasted and the method becomes inefficient.

Algorithm 2.1 Critical Search Method [16]

1: Make an initial guess for α^0.
2: Solve Eq. 2.34 for k^0.
3: Obtain a second guess α^1 by adjusting α^0 by some eigenvalue modifier value: $\alpha^1 = \alpha^0 + \text{EMV}$.
4: Solve Eq. 2.34 for k^1.
5: Using (α^ℓ, k^ℓ) and $(\alpha^{\ell-1}, k^{\ell-1})$, perform a linear extrapolation of $k(\alpha)$ to find $\alpha^{\ell+1}$ such that $k^{\ell+1}(\alpha^{\ell+1}) = 1$.
6: Solve Eq. 2.34 for $k^{\ell+1}$.
7: Repeat until $k^{\ell+1} = 1$.

Green's Function Method (GFM): Green's Function Method [22] uses Green's functions to model one-speed, multiplying, multi-region slabs and obtain boundary flux values for an eigenvalue search. The one-group neutron transport equation for a homogeneous material with isotropic scattering is

$$\left[\mu\frac{\partial}{\partial x} + \sigma + \frac{\alpha}{v}\right]\psi(x,\mu) = \frac{\nu\sigma_f + \sigma_s}{2}\int_{-1}^{-1} d\mu'\,\psi(x,\mu'). \tag{2.35}$$

Dividing by the total cross section we obtain

$$\left[\mu\frac{\partial}{\partial x} + \alpha'\right]\psi(x,\mu) = \frac{c}{2}\int_{-1}^{1} d\mu'\,\psi(x,\mu'), \tag{2.36}$$

where

$$\alpha' = 1 + \frac{\alpha}{v\sigma} \quad\text{and}\quad c = \frac{\nu\sigma_f + \sigma_s}{\sigma}. \tag{2.37}$$

Eq. 2.36 is measured in mean free paths. For infinite medium problems, $\alpha' \geq 0$. This can be seen by allowing α to be the Corngold limit, the smallest possible alpha-eigenvalue, and evaluating for α'.

The GFM is useful for multi-region systems because of Placzek's lemma [9]. Placzek's lemma states that the angular flux solution in a finite slab can be expressed in terms of a solution in an infinite medium by converting boundary angular flux sources into equivalent volumetric sources. Using the lemma, each slab region can be treated as an infinite homogeneous medium with a specified source based on the angular flux boundary conditions. For an infinite medium, the angular flux can be expressed by the Green's function

$$\psi(x,\mu) = \int_{-\infty}^{\infty} dx' \int_{-1}^{1} d\mu' \left[\mu'\psi(0,\mu')\delta(x') - \mu'\psi(\Delta,\mu')\delta(x'-\Delta,\mu')\right] G(x-x',\mu|\mu'), \quad (2.38)$$

where the Green's function satisfies the integro-differential equation

$$\left[\mu\frac{\partial}{\partial x} + \alpha'\right] G(x,\mu \mid \mu') = \frac{c}{2}\int_{-1}^{1} d\mu'' \, G(x,\mu'' \mid \mu') + \delta(x)\delta(\mu-\mu'). \quad (2.39)$$

The solution, $G(x,\mu \mid \mu')$, to Eq. 2.39 is in the form of the solution to the anisotropic plane source emitting particles in direction μ' for an infinite homogeneous medium problem with scattering parameter c. Taking a Fourier transform of Eq. 2.39, integrating over the scattering angle μ, inverting the transform, and using Placzek's lemma to connect individual slab regions through boundary angular fluxes, an integral equation for the angular flux in the multi-region medium is found:

$$\psi_i(0^+,-\mu) + \int_0^1 d\mu' \, \mu'\psi_i(0^+,-\mu')\left[G_c(0^-,\mu \mid \mu') \pm G_c(-\Delta_i,-\mu' \mid \mu')\right]$$

$$\pm \psi_i(\Delta_i^-,\mu) \pm \int_0^1 d\mu' \, \mu'\psi_i(\Delta_i^-,\mu')\left[G_c(0^-,\mu \mid \mu') \pm G_c(-\Delta_i,-\mu \mid \mu')\right]$$

$$\mp \psi_{i-1}(\Delta_{i-1}^-,\mu)\exp\left(\frac{-\alpha'\Delta_i}{\mu}\right) - \int_0^1 d\mu' \, \mu'\psi_{i-1}(\Delta_{i-1}^-,\mu')\left[G_c(0^+,-\mu \mid \mu')\right. \quad (2.40)$$

$$\left. \pm G_c(\Delta_i^-,\mu \mid \mu')\right] - \psi_{i+1}(0^+,-\mu)\exp\left(\frac{-\alpha'\Delta_i}{\mu}\right)$$

$$\mp \int_0^1 d\mu' \, \mu'\psi_{i+1}(0^+,-\mu')\left[G_c(0^+,-\mu \mid \mu') \pm G_c(\Delta_i^-,\mu \mid \mu')\right] = 0,$$

where

$$G_c(x,\mu \mid \mu') = \frac{c}{2\alpha'}\frac{1}{\mu'-\mu}\left[h(x,\mu') - h(x,\mu)\right], \quad (2.41)$$

$$h(x,\mu) = \frac{\mu}{2\pi}\int_{-\infty}^{\infty} dk \, \frac{e^{ikx}}{\alpha'+ik\mu}\frac{1}{1-\frac{c}{\alpha'}L\left(\frac{k}{\alpha'}\right)}, \quad (2.42)$$

and

$$L(z) = \frac{1}{2} \int_{-1}^{1} d\mu \, \frac{1}{1 + iz\mu} = \frac{\tan^{-1} z}{z}. \tag{2.43}$$

The eigenvalue problem is formulated by construction of a matrix of the interactions of slab boundary angular fluxes for each region as given by Eq. 2.40. The matrix consists of submatrices for each region where the integrals are approximated using numerical quadrature. Eigenvalues are then determined using a brute force search routine where all possible values for the eigenvalue within some search space are tested until a value is found such that the real and imaginary parts of the matrix determinant is zero. This value is then the eigenvalue of the system. GFM allows for the calculation of higher eigenvalues and eigenmodes. GFM provides benchmark-quality calculations for the alpha-eigenvalues in heterogeneous media slab problems.

The increase of computational difficulty increases with the number of regions present in the system. In addition, the search space might become large, especially if there is no estimate of the eigenvalue. The numerical quadrature of the integrals also present another cost, as improper integrals must be approximated in each region of the problem to some tolerance. Determination of the matrix determinant requires a complex LU decomposition routine. Further, the scope of GFM is limited to slab geometry, though using the slab-spherical equivalence [9], the eigenvalues of one-dimensional spherical systems can be determined by solving an equivalent slab geometry problem when certain conditions are met.

Direct Evaluation: Another numerical method capable of obtaining the alpha-eigenvalue and higher eigenvalues involves forming the matrix problem from the discretized form of the one-speed, one-dimensional transport equation [28] using discrete ordinates in angle and finite differences in space. Using a process similar to the one described in Chapter **??** with M directions in angle and N cells in space yields a generalized eigenvalue problem of the form

$$\mathbf{A}\psi = \alpha\mathbf{B}\psi. \tag{2.44}$$

Using standard eigenvalue solvers, the method gives NM eigenpairs. Given the discretization of the problem, the method gives far more eigenvalues than expected from theory. The spectrum is composed of the real eigenvalue spectrum and additional eigenvalues which are a product of the discretization of the problem. An example spectrum can be seen in Figure 2.4. Also, if only the dominant eigenvalue and vector are required, the formation of the matrices and the eigenvalue solver could be too costly. The method works well for homogeneous and multi-region slabs with isotropic scattering. However, the method quickly becomes complicated and expensive for problems involving complex geometries, anisotropic scattering, and multiple energy groups.

2.3.2 The k-Eigenvalue

In the k-eigenvalue problem, the time-dependence of the problem is eliminated and it is assumed there is no external source present [3]. Instead, a time-independent solution is
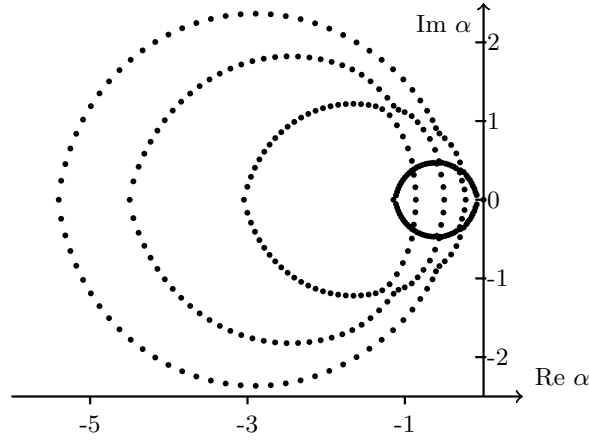
Figure 2.4: Discretized Alpha-Eigenvalue Spectrum for a Subcritical System

obtained by varying ν by a parameter k, which expresses the deviation from critical. Substituting ν/k for ν yields the k-eigenvalue problem:

$$\left[\hat{\Omega} \cdot \nabla + \sigma(\vec{r}, E)\right]\psi(\vec{r}, \hat{\Omega}, E)$$
$$= \int dE' \int d\hat{\Omega}\, \sigma_s(\vec{r}, E' \to E, \hat{\Omega}' \cdot \hat{\Omega})\psi(\vec{r}, \hat{\Omega}', E')$$
$$+ \frac{1}{k} \int dE'\, \nu(E')\chi(E' \to E)\sigma_f(\vec{r}, E') \int d\hat{\Omega}'\, \psi(\vec{r}, \hat{\Omega}', E'). \quad (2.45)$$

We define the operator form of Eq. 2.45 as

$$\mathcal{H}\psi = \left(\mathcal{S} + \frac{1}{k}\mathcal{F}\right)\psi. \quad (2.46)$$

There exists a spectrum of eigenvalues but the only the positive eigenvector corresponds to the largest real eigenvalue, k. The k-eigenvalue exists for any system containing fissile material and corresponding to the eigenvalue is a non-negative eigenvector. For a system containing no fissile material, the k-eigenvalue is zero. The criticality of a system can be defined by the value of k:

$$k \begin{cases} > 1, & \text{supercritical,} \\ = 1, & \text{critical,} \\ < 1, & \text{subcritical.} \end{cases}$$

The spectrum of eigenvalues for the k-eigenvalue problem is real and positive. The spectrum is ordered

$$k_0 > k_1 > k_2 > \ldots k_i, \quad (2.47)$$

where $k_0 = k$ is the dominant eigenvalue. An example of a k-effective eigenvalue spectrum can be seen in Figure 2.5. The full set of k-eigenvalues and eigenvectors have applications
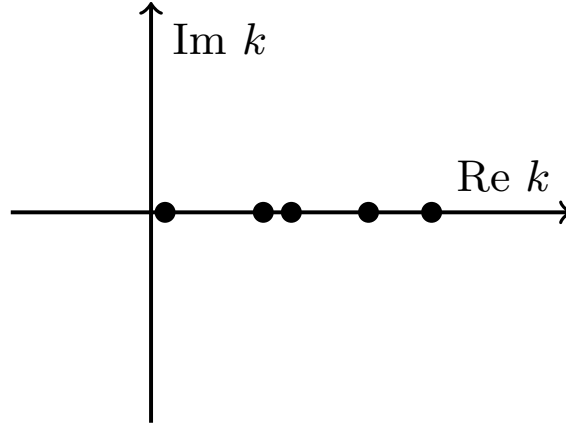
Figure 2.5: Example Spectrum for k-Effective Eigenvalue

in perturbation theory and provide a measure of numerical convergence for methods like the power method [25]. The dominance ratio, the ratio k_1/k_0, provides a measure of convergence for the power method [25]. If a designer is interested in how far a system is from a critical configuration, the k-eigenvalue is a good measure as it represents the ratio between the fission source and losses due to leakage and absorption. For an exactly critical system, the eigenvector corresponding to k is the flux shape within the reactor. For systems close to critical, the eigenvector is a good approximation of the flux shape. The k-eigenvalue has another simple physical interpretation: it is the ratio of neutrons in the next generation to those in the current generation [32].

Iterative Methods for the k-Effective Eigenvalue

In this section we describe two standard iterative methods used to calculate the k-effective eigenvalue of a nuclear system, the power method and shifted inverse iteration. As discussed in Section 2.3.2, the criticality of the nuclear system is given by the largest real eigenvalue and corresponding to this eigenvalue is the only positive eigenvector. This positive eigenvector is the neutron angular flux of the nuclear system. Discretization of Eq. 2.45 leads to large sparse linear systems which makes the use of *direct* eigenvalue solvers (such as the QR method) too expensive or unfeasible. In addition, most transport codes apply the discretized operators of Eq. 2.45 through matrix-vector multiplication or transport sweeps to invert operators and do not construct the large sparse matrices. Given that determining the criticality and fundamental flux mode only requires the dominant eigenvalue, it is instead preferably to use iterative eigenvalue methods.

Power Method with Fission Norm Update: The most basic method for solving for the k-effective eigenvalue is the power method [25]. To apply the method, we write the k-effective criticality problem as the standard eigenvalue problem

$$k\psi = (\mathcal{H} - \mathcal{S})^{-1}\mathcal{F}\psi. \tag{2.48}$$

The power method, described in Algorithm 2.2, consists of iteratively applying the operator on the right of Eq. 2.48 to some eigenfunction approximation ψ^{i+1}. The eigenfunction is then usually normalized by some norm of the angular flux.

Algorithm 2.2 Power Method [25]

1: Make initial guess $\psi^{(0)}, k^{(0)}$.
2: **for** $i = 0, 1, 2, \cdots$, **do**
3:     Compute $\psi^{(i+1)} = \frac{1}{k^{(i)}}(\mathcal{H} - \mathcal{S})^{-1}\mathcal{F}\psi^{(i)}$.
4:     Normalize $\psi^{(i+1)}$ by some norm, compute $k^{(i+1)}$.
5: **end for**

There are various ways to compute the eigenvalue iterate. One simple estimate of the eigenvalue is given by the expression

$$k^{(i+1)} = k^{(i)}\frac{\left\|\psi^{(i+1)}\right\|}{\left\|\psi^{(i)}\right\|}, \tag{2.49}$$

where $\|\psi\|$ is some discrete norm taken over the problem domain. In many implementations the norm takes into account only the isotropic scalar flux component as this is usually the required unknown [37]. However, there is no mathematical justification for this norm and any consistent norm can be used. Traditionally, in neutron transport codes, the eigenvalue is estimated using the total fission rate in the problem [37] which is given by

$$\|\phi\| \equiv \|\phi\|_F = \sum_{g=1}^{G}\sum_{s\in\mathcal{D}}\nu\sigma_{f,g,s}\phi_{0,g,s} \tag{2.50}$$

where the summation is over all energy group and over all spatial cells in the problem domain, $\mathcal{D}$. Another possible eigenvalue update is the Rayleigh quotient. It has been observed that using the Rayleigh quotient can at times improve the efficiency of the power iteration by providing a better estimate of the eigenvalue earlier in the iterative process [37].

The power method converges to the eigenvector corresponding to the largest eigenvalue in modulus provided that the eigenvalue is simple and the initial eigenvector guess contains a component in the eigendirection [13]. It has been shown that k is the largest eigenvalue in modulus for various type of problems in nuclear engineering [29]. However, it is possible the power iteration will not converge. For instance, for multigroup energy problems, it is not known if the dominant eigenvalue is always real and given an all real initial eigenvector guess, it is possible the method will not converge. In addition, the power method converges with rate equal to the dominance ratio, k_1/k_0, and for problems with dominance ratios close to one, convergence can be unacceptably slow. Problems with dominance ratios close to one include highly scattering nuclear reactor problems such as heavy water reactors and boiling water reactors. Despite these limitations, the simplicity of the power method makes it the default eigenvalue solver method of choice in neutron transport codes [12].

The Wielandt Method: Another method to calculate the k-effective eigenvalue is the Wielandt method or Wielandt acceleration (Algorithm 2.3) [40]. The Wielandt method, as it is known in the neutron transport community, is a shifted inverse iteration method [19] applied to the k-effective eigenvalue problem. In the shifted inverse iteration method, the power method is applied to the shifted problem of the form

$$(\mathcal{H} - \mathcal{S} - \beta\mathcal{F})\psi = (\lambda - \beta)\mathcal{F}\psi, \tag{2.51}$$

where $\lambda = 1/k$ and the shift β is selected such that $0 < |\lambda_1 - \beta| < |\lambda_2 - \beta| \leq |\lambda_j - \beta|$, $j > 2$. It can be shown that this yields a method with speed of convergence determined by $|\lambda_1 - \beta|/|\lambda_2 - \beta|$ [19]. For an appropriately selected shift β, the method can be faster than the power method. For criticality problems in nuclear engineering, the systems are expected to be close to critical and the shift can be selected to be $\beta = 1$. Alternatively, a variable shift can be used with the Rayleigh quotient being a standard choice. The power method can be considered a special case of the shifted inverse iteration method with no shift. Despite its improved theoretical convergence rate, the shifted inverse iteration shift requires *a priori* knowledge of the dominant eigenvalue magnitude. Given a poor shift, convergence of the method may be delayed.

Algorithm 2.3 Shifted Inverse Iteration [19]

1: Make initial guess $\psi^{(0)}$.
2: **for** $i = 0, 1, 2, \cdots$, **do**
3:    Define shift $\beta^{(i)}$.
4:    Compute $\psi^{(i+1)}$ such that $(\mathcal{H} - \mathcal{S} - \beta^{(i)}\mathcal{F}) = \mathcal{F}\psi^{(i)}$.
5:    Normalize $\psi^{(i+1)}$ by some norm.
6: **end for**

2.4 Review of Linear Algebra Fundamentals

We review and introduce some definitions of linear algebra concepts used in this dissertation. Of particular interest are the concepts of positivity and primitivity, which guide the derivation of the method later in this disseration. Definitions and theorems are from [18], [38], [34]. The theory of Perron-Frobenius for positive, irreducible, and primitive matrices is discussed and its results are used heavily throughout this dissertation.

2.4.1 Nonnegativity, Positivity, and the Spectral Radius of a Matrix

Definition 1 *A real matrix* $\mathbf{A}$ *is nonnegative (or positive) if all entries of* $\mathbf{A}$ *are nonnegative (or positive). We write* $\mathbf{A} \geq 0$ *or* $\mathbf{A} > 0$.

Definition 2 *Let* $\mathbf{A} = (a_{i,j})$ *be an* $n \times n$ *matrix with eigenvalues* $\lambda_i, 1 \leq i \leq n$. *Then*

$$\rho(\mathbf{A}) \equiv \max_{1 \leq i \leq n} |\lambda_i|$$

is called the spectral radius of the matrix $\mathbf{A}$.

2.4.2   Irreducible and Reducible Matrices

Definition 3 *For* $n \geq 2$, *an* $n \times n$ *real matrix* $\mathbf{A}$ *is reducible if there exists an* $n \times n$ *permutation matrix* $\mathbf{P}$ *such that*

$$\mathbf{P}\mathbf{A}\mathbf{P}^T = \begin{bmatrix} \mathbf{A}_{1,1} & \mathbf{A}_{1,2} \\ \mathbf{0} & \mathbf{A}_{2,2} \end{bmatrix}$$

Definition 4 *A matrix* $\mathbf{A}$ *that is not reducible is said to be irreducible.*

2.4.3   Primitive and Cyclic Matrices

Definition 5 *Let* $\mathbf{A} \geq \mathbf{0}$ *be an irreducible* $n \times n$ *matrix, and let* k *be the number of eigenvalues of* $\mathbf{A}$ *with modulus* $\rho(\mathbf{A})$. *If* $k = 1$, *then* $\mathbf{A}$ *is primitive.*

Definition 6 *Let* $\mathbf{A} \geq \mathbf{0}$ *be an irreducible* $n \times n$ *matrix, and let* k *be the number of eigenvalues of* $\mathbf{A}$ *with modulus* $\rho(\mathbf{A})$. *If* $k > 1$, *then* $\mathbf{A}$ *is cyclic of index* k.

2.4.4   Perron-Froebenius Theorem for Irreducible Matrices

Theorem 3 *Let* $\mathbf{A} \geq \mathbf{0}$ *be an irreducible* $n \times n$ *matrix. Then,*

1. $\mathbf{A}$ *has a positive real eigenvalue,* λ_1, *equal to its spectral radius, and which is greater than or equal to (in absolute value) all other eigenvalues.*

2. *For* $\rho(\mathbf{A})$ *there is a corresponding eigenvector* $x > 0$.

3. $\rho(\mathbf{A})$ *is a simple eigenvalue of* $\mathbf{A}$.

2.4.5   Perron-Froebenius Theorem for Primitive Matrices

Theorem 4 *Let* $\mathbf{A} \geq \mathbf{0}$ *be a primitive* $n \times n$ *matrix. Then,*

1. $\mathbf{A}$ *has a positive real eigenvalue,* λ_1, *equal to its spectral radius, and which is greater than (in absolute value) all other eigenvalues.*

2. *For* $\rho(\mathbf{A})$ *there is a corresponding eigenvector* $x > 0$.

3. $\rho(\mathbf{A})$ *is a simple eigenvalue of* $\mathbf{A}$.

2.4.6 Kronecker (Tensor) Product

Throughout this dissertation we use the *Kronecker (tensor) product* to simplify various matrix operations and forms required to discretize the neutron transport eigenvalue equations. We review some of the properties [17] of this product in this section.

For matrices $\mathbf{A} \in \mathbb{R}^{m \times n}$ and $\mathbf{B} \in \mathbb{R}^{k \times l}$, the Kronecker product of $\mathbf{A}$ and $\mathbf{B}$ is the $mk \times nl$ matrix denoted by

$$\mathbf{A} \otimes \mathbf{B} \equiv \begin{pmatrix} a_{11}\mathbf{B} & \dots & a_{1n}\mathbf{B} \\ \vdots & \ddots & \vdots \\ a_{m1}\mathbf{B} & \dots & a_{mn}\mathbf{B} \end{pmatrix}, \tag{2.52}$$

where $\mathbf{A} = (a_{ij})$. More explicitly:

$$\mathbf{A} \otimes \mathbf{B} = \begin{pmatrix} a_{11}b_{11} & a_{11}b_{12} & \cdots & a_{11}b_{1l} & \cdots & \cdots & a_{1n}b_{11} & a_{1n}b_{12} & \cdots & a_{1n}b_{1l} \\ a_{11}b_{21} & a_{11}b_{22} & \cdots & a_{11}b_{2l} & \cdots & \cdots & a_{1n}b_{21} & a_{1n}b_{22} & \cdots & a_{1n}b_{2l} \\ \vdots & \vdots & \ddots & \vdots & & & \vdots & \vdots & \ddots & \vdots \\ a_{11}b_{k1} & a_{11}b_{k2} & \cdots & a_{11}b_{kl} & \cdots & \cdots & a_{1n}b_{k1} & a_{1n}b_{k2} & \cdots & a_{1n}b_{kl} \\ \vdots & \vdots & & \vdots & \ddots & & \vdots & \vdots & & \vdots \\ \vdots & \vdots & & \vdots & & \ddots & \vdots & \vdots & & \vdots \\ a_{m1}b_{11} & a_{m1}b_{12} & \cdots & a_{m1}b_{1l} & \cdots & \cdots & a_{mn}b_{11} & a_{mn}b_{12} & \cdots & a_{mn}b_{1l} \\ a_{m1}b_{21} & a_{m1}b_{22} & \cdots & a_{m1}b_{2l} & \cdots & \cdots & a_{mn}b_{21} & a_{mn}b_{22} & \cdots & a_{mn}b_{2l} \\ \vdots & \vdots & \ddots & \vdots & & & \vdots & \vdots & \ddots & \vdots \\ a_{m1}b_{k1} & a_{m1}b_{k2} & \cdots & a_{m1}b_{kl} & \cdots & \cdots & a_{mn}b_{k1} & a_{mn}b_{k2} & \cdots & a_{mn}b_{kl} \end{pmatrix}. \tag{2.53}$$

Kronecker products have various interesting properties. We list the ones relevant to this dissertation:

- If $\mathbf{A}$ and $\mathbf{B}$ are nonsingular, then $\mathbf{A} \otimes \mathbf{B}$ is nonsingular with $(\mathbf{A} \otimes \mathbf{B})^{-1} = \mathbf{A}^{-1} \otimes \mathbf{B}^{-1}$,

- $(\mathbf{A} \otimes \mathbf{B})^T = \mathbf{A}^T \otimes \mathbf{B}^T$,

- Given matrices $\mathbf{A}$, $\mathbf{B}$, $\mathbf{C}$, and $\mathbf{D}$, $(\mathbf{A} \otimes \mathbf{B}) \cdot (\mathbf{C} \otimes \mathbf{D}) = \mathbf{AC} \otimes \mathbf{BD}$, as long as both sides of the equation make sense,

- $(\mathbf{A} + \mathbf{B}) \otimes \mathbf{C} = \mathbf{A} \otimes \mathbf{C} + \mathbf{B} \otimes \mathbf{C}$, and

- $\mathbf{A} \otimes (\mathbf{B} + \mathbf{C}) = \mathbf{A} \otimes \mathbf{B} + \mathbf{A} \otimes \mathbf{C}$.

2.5 Review of Fixed Point Iteration

In this section we review fixed point iteration methods. We begin by defining a *fixed point* of some equation $g(x)$:

Definition 7 *A point x_0 is called a fixed point of $g(x)$ if it satisfies*

$$x_0 = g(x_0). \tag{2.54}$$

Next, we define an *attractive fixed point* of a function $g(x)$:

Definition 8 *A point x_0 is an attractive fixed point of $g(x)$ if for any value of x in the domain that is sufficiently close to x_0, the iterated function sequence*

$$x, f(x), f(f(x)), f(f(f(x))), \dots \tag{2.55}$$

converges to x_0.

Given these two definitions, we can define an iterative method to find the fixed point of some function $g(x)$ as

$$x_{n+1} = g(x_n). \tag{2.56}$$

The convergence of this fixed point iteration method depends on the existence and uniqueness of the fixed point in the domain of the function $g(x)$. We introduce and prove the following theorem

Theorem 5 *Existence and Uniqueness of Fixed Point*

1. *Existence: If $g \in C[a,b]$ and $g(x) \in [a,b]$ for all $x \in [a,b]$, then g has a fixed point in $[a,b]$.*

2. *Uniqueness: If, in addition, $g'(x)$ exists on (a,b) and a positive constant $k < 1$ exists with*

$$|g'(x)| \le k, \quad \text{for all } x \in (a,b),$$

then there is exactly one fixed point in $[a,b]$.

Proof 3 *We note the following:*

- *$g \in C[a,b] - g$ is continuous in $[a,b]$.*

- *$g(x) \in C[a,b] - g$ takes values in $[a,b]$.*

1. *Existence: If $g(a) = a$ or $g(b) = b$, then g has a fixed point at that endpoint. Otherwise, $g(a) > a$ and $g(b) < b$. We define a new function $h(x) = g(x) - x$ such that $h(a) = g(a) - a > 0$, $h(b) = g(b) - b < 0$, and $h(x)$ is continuous. By the intermediate value theorem, there exists $p \in (a,b)$ for which $h(p) = p$ which implies $g(p) = p$.*

2. *Uniqueness: Assume $|g'(x)| \leq k < 1$. Suppose there are two fixed points p and q. By the mean value theorem, there is a number ξ between p and q such that*

$$g'(\xi) = \frac{g(p) - g(q)}{p - q}. \qquad (2.57)$$

This implies

$$|p - q| = |g(p) - g(q)| = |g'(\xi)||p - q| \leq k|p - q| < |p - q|, \qquad (2.58)$$

which is a contradiction. This implies there is only one fixed point and it is unique.

The previous concepts extend to vector valued functions. Given a vector valued function $F : \mathbb{R}^n \to \mathbb{R}^n$, a fixed point iteration method of the form

$$x_{n+1} = F(x_n) \qquad (2.59)$$

converges to the fixed point x_* if $\rho(J(x_*)) < 1$ where $J(x_*)$ is the Jacobian of the vector valued function F evaluated at the fixed point x_* [31].

Chapter 3

Discretization and Primitivity of the Neutron Transport Criticality Eigenvalue Problems

In this section we describe the discretization of the neutron transport criticality eigenvalue equations for three-dimensional Cartesian geometry. The discretization follows a similar approach to that of [5] [6] [7]. First, we derive semi-discretized forms of the eigenvalue equations by applying the *multigroup* in energy approximation and a spherical harmonics expansion for the scattering integral. We then discretize the spatial and angular variables using step differencing and the discrete ordinates approach. Finally, we write down the discretized matrix forms of the criticality eigenvalue equations for three-dimensional Cartesian geometry. For the one-dimensional slab geometry discretized alpha-eigenvalue problem, we show by example the fixed point matrix is primitive. A similar result can be shown for the two-dimensional and three-dimensional Cartesian discretized eigenvalue equations.

We begin with the linear alpha-eigenvalue neutron transport equation in a three-dimensional box geometry with scattering. The spatial domain is the box $\mathcal{D} \equiv \{\vec{r} = (x, y, z) \mid a_x \leq x \leq b_x, a_y \leq y \leq b_y, \text{ and } a_z \leq z \leq b_z\}$, the direction variable is $\hat{\Omega} \in \mathcal{S}^2$, the unit sphere in $\mathbb{R}^3$, the energy variable is $E \in (0, \infty)$, and the equation for the angular flux $\psi(\vec{r}, \hat{\Omega}, E)$ is given by

$$
\left[\frac{\alpha}{v(E)} + \hat{\Omega} \cdot \nabla + \sigma(\vec{r}, E) \right] \psi(\vec{r}, \hat{\Omega}, E)
$$
$$
= \int_0^\infty dE' \int_{4\pi} d\hat{\Omega} \, \sigma_s(\vec{r}, E' \to E, \hat{\Omega}' \cdot \hat{\Omega}) \psi(\vec{r}, \hat{\Omega}', E')
$$
$$
+ \int_0^\infty dE' \, \nu(E') \chi(E' \to E) \sigma_f(\vec{r}, E') \int_{4\pi} d\hat{\Omega}' \, \psi(\vec{r}, \hat{\Omega}', E'), \quad (3.1)
$$

where

$$\nabla \psi \equiv \left(\frac{\partial \psi}{\partial x}, \frac{\partial \psi}{\partial y}, \frac{\partial \psi}{\partial z} \right), \tag{3.2}$$

and

$$\int_{4\pi} d\hat{\Omega} = 1. \tag{3.3}$$

Boundary conditions must be specified to make Eq. 3.1 well-posed. Various boundary conditions can be specified such as a reflecting condition on a face or a Dirichlet condition where an incident flux is specified on a face. We consider vacuum boundary conditions in this dissertation, a special case of the Dirichlet boundary condition where no incident flux is imposed:

$$\psi(\vec{r}, \hat{\Omega}, E) = 0 \text{ for all } \vec{r} \in \partial\mathcal{D} \text{ and } \hat{\Omega} \in \mathcal{S}^2 \text{ with } \vec{n}(\vec{r}) \cdot \hat{\Omega} < 0, \tag{3.4}$$

where $\vec{n}(\vec{r})$ is the outward pointing unit normal at $\vec{r} \in \partial\mathcal{D}$.

3.1 Discretization of the Alpha-Eigenvalue and k-Effective Eigenvalue Equations

3.1.1 The Multigroup in Energy Discretization and Spherical Harmonics Expansion of the Angular Flux

The Multigroup in Energy Approximation

We begin by discretizing Eq. 3.1 in energy using the *multigroup* approximation [12]. We restrict the energy E to a finite interval and partition the interval into groups:

$$E_{max} = E_0 > E_1 > \cdots > E_G = E_{min}.$$

The eigenvalue equation is then averaged over each group $E_g < E < E_{g-1}$ and the cross sections are approximated by a flux-weighted average over each energy group to yield the following semi-discretization of Eq. 3.1:

$$\left[\frac{\alpha}{v_g} + \hat{\Omega} \cdot \nabla + \sigma_g(\vec{r}) \right] \psi_g(\vec{r}, \hat{\Omega}) = \sum_{g'=1}^{G} \int_{4\pi} d\hat{\Omega} \, \sigma_{s,g,g'}(\vec{r}, \hat{\Omega}' \cdot \hat{\Omega}) \psi_{g'}(\vec{r}, \hat{\Omega}')$$

$$+ \chi_g \sum_{g'=1}^{G} \nu_{g'} \sigma_{f,g'}(\vec{r}) \int_{4\pi} d\hat{\Omega}' \, \psi_{g'}(\vec{r}, \hat{\Omega}'), \quad (3.5)$$

for $g = 1, \ldots, G$, where

$$\psi_g(\vec{r}, \hat{\Omega}) \equiv \int_g dE \, \psi(\vec{r}, \hat{\Omega}, E), \tag{3.6}$$

with

$$\int_g dE = \int_{E_g}^{E_{g-1}} dE. \tag{3.7}$$

The Spherical Harmonics Expansion of the Angular Flux

For each flux $\psi_g(\vec{r}, \hat{\Omega})$, the flux is expanded in surface harmonics according to

$$\psi_g(\vec{r}, \hat{\Omega}) = \sum_{n=0}^{\infty} \sum_{m=-n}^{\infty} \phi_{g,n,m}(\vec{r}) Y_n^m(\hat{\Omega}), \tag{3.8}$$

where $Y_n^m(\hat{\Omega})$ is a surface harmonic defined as

$$Y_n^m(\hat{\Omega}) = a_n^m P_n^{|m|}(\xi) \tau_m(\varphi), \tag{3.9}$$

$$\hat{\Omega} = (\sin\theta\cos\varphi, \sin\theta\sin\varphi, \cos\theta), \tag{3.10}$$

$$\tau_m(\varphi) = \begin{cases} \cos m\varphi, & \text{if } m \geq 0, \\ \sin|m|\varphi & \text{if } m < 0, \end{cases} \tag{3.11}$$

and $P_n^{|m|}$ is an *associated Legendre polynomial*. The constants a_n^m are defined by

$$a_n^m = \left[\frac{2(2n+1)(n-|m|)!}{(1+\delta_{m0})(n+|m|)!} \right]^{1/2}. \tag{3.12}$$

where $\delta_{n,n'}$ is the *Kronecker delta*. The $(n,m)^{\text{th}}$ moment of $\psi(\vec{r}, \hat{\Omega})$, ϕ_n^m is given by

$$\phi_n^m(\vec{r}) = \int_{4\pi} d\hat{\Omega}\, \psi(\vec{r}, \hat{\Omega}) Y_n^m(\hat{\Omega}). \tag{3.13}$$

From the properties of the surface harmonics, we have

$$\int_{4\pi} d\hat{\Omega}\, Y_n^m(\hat{\Omega}) Y_{n'}^{m'}(\hat{\Omega}) = \delta_{n,n'}\delta_{m,m'}, \text{ for all } n, n' = 0, 1, \ldots, |m| \leq |n|, |m'| \leq |n'|. \tag{3.14}$$

The scattering integral can be then be written in the form

$$\int_{4\pi} d\hat{\Omega}\, \sigma_{s,g,g'}(\vec{r}, \hat{\Omega}' \cdot \hat{\Omega}) \psi_{g'}(\vec{r}, \hat{\Omega}') = \sum_{n=0}^{\infty} \sigma_{s,g,g',n}(\vec{r}) \sum_{m=-n}^{n} \phi_{g',n,m}(\vec{r}) Y_n^m(\hat{\Omega}), \tag{3.15}$$

where

$$\sigma_{s,g,g',n}(\vec{r}) \equiv \frac{1}{2} \int_{-1}^{1} d\mu_0\, \sigma_{s,g,g'}(\vec{r}, \mu_0) P_n(\mu_0), \tag{3.16}$$

and μ_0 is the cosine of the scattering angle. The infinite series in Eq. 3.15 is truncated to a finite number of terms N_s, where N_s is the maximum value for n. The fission integral can be written similarly. The multigroup equations can then be written as

$$\left[\frac{\alpha}{v_g} + \hat{\Omega} \cdot \nabla + \sigma_g(\vec{r})\right]\psi_g(\vec{r}, \hat{\Omega}) = \sum_{g'=1}^{G}\sum_{n=0}^{N_s}\sigma_{s,g,g',n}(\vec{r})\sum_{m=-n}^{n}\phi_{g',n,m}(\vec{r})Y_n^m(\hat{\Omega})$$

$$+ \chi_g\sum_{g'=1}^{G}\sum_{n=0}^{N_s}\nu_{g'}\sigma_{f,g',n}(\vec{r})\sum_{m=-n}^{n}\phi_{g',n,m}(\vec{r})Y_n^m(\hat{\Omega}), \quad (3.17)$$

for $g = 1, \ldots, G$.

3.1.2 Step Differencing and Discrete Ordinates in Angle

Step Differencing

We continue the discretization of Eq .3.17 by using a Step differencing method [25] for the spatial variable $\vec{r}$. We start with the three-dimensional mono-energetic alpha-eigenvalue equation for group g with scattering and fission source f:

$$\begin{cases} \frac{\alpha}{v}\psi + \hat{\Omega} \cdot \nabla\psi + \sigma\psi = f \text{ in } \mathcal{D} \\ \psi(\vec{r}) = 0 \text{ for all } \vec{r} \in \partial\mathcal{D} \text{ with } \vec{n}(\vec{r}) \cdot \hat{\Omega} < 0. \end{cases} \quad (3.18)$$

We discretize the domain $\mathcal{D}$ into zones and define

$$\Delta x_i = x_i - x_{i-1}, \text{ for } i = 1, \ldots, M, \quad (3.19)$$

$$\Delta y_i = y_j - y_{j-1}, \text{ for } j = 1, \ldots, J, \quad (3.20)$$

$$\Delta z_i = z_k - z_{k-1}, \text{ for } k = 1, \ldots, K. \quad (3.21)$$

We define the nodes $r_{ijk} = (x_i, y_j, z_k)$ and the zone volume $\Delta r_{ijk} = \Delta x_i \Delta y_j \Delta z_k$. The function values at the set of nodes, $\{r_{ijk}\}$ are called *nodal values*. We assume that σ and f have constant values, denoted as σ_{ijk} and f_{ijk} respectively, on each *zone* defined as

$$\mathcal{Z}_{ijk} \equiv \{r | x_{i-1} < x < x_i, y_{j-1} < y < y_j, z_{k-1} < z < z_k\}. \quad (3.22)$$

We define ψ_{ijk} to denote the approximation to $\psi(r_{ijk})$, the true solution at the point r_{ijk}. For a direction in the positive orthant, $\hat{\Omega} = (\mu, \eta, \xi) > 0$, the Step differencing equation for the zone $\mathcal{Z}_{ijk}$ is

$$\frac{\alpha}{v}\psi_{ijk} + \mu\frac{\psi_{ijk} - \psi_{i-1,jk}}{\Delta x_i} + \eta\frac{\psi_{ijk} - \psi_{i,j-1,k}}{\Delta y_j} + \xi\frac{\psi_{ijk} - \psi_{ij,k-1}}{\Delta z_k} + \sigma_{ijk}\psi_{ijk} = f_{ijk}. \quad (3.23)$$

For Eq. 3.23, we have $(M+1)(J+1)(K+1)$ unknowns ψ_{ijk}. There are MJK zonal equations with $JM + JK + M + J + K + 1$ boundary equations.

To write the discretized system in matrix form, we define the discrete angular flux vector

$$\Psi \in \mathbb{R}^{(M+1)(J+1)(K+1)}, \tag{3.24}$$

defined for all nodes ordered by i first, then j, and finally k. We define the diagonal matrices

$$\Delta x \equiv \mathrm{diag}(\Delta x_1, \ldots, \Delta x_M), \tag{3.25}$$

$$\Delta y \equiv \mathrm{diag}(\Delta y_1, \ldots, \Delta y_J), \tag{3.26}$$

$$\Delta z \equiv \mathrm{diag}(\Delta z_1, \ldots, \Delta z_K), \tag{3.27}$$

and the matrices expressing the discretized spatial derivatives

$$D_M \in \mathbb{R}^{M \times (M+1)} \equiv \begin{pmatrix} -1 & 1 & & \\ & \ddots & \ddots & \\ & & -1 & 1 \end{pmatrix}, S_{M,+} \in \mathbb{R}^{M \times (M+1)} \equiv \begin{pmatrix} 0 & 1 & & \\ & \ddots & \ddots & \\ & & 0 & 1 \end{pmatrix}, \tag{3.28}$$

$$D_J \in \mathbb{R}^{J \times (J+1)} \equiv \begin{pmatrix} -1 & 1 & & \\ & \ddots & \ddots & \\ & & -1 & 1 \end{pmatrix}, S_{J,+} \in \mathbb{R}^{J \times (J+1)} \equiv \begin{pmatrix} 0 & 1 & & \\ & \ddots & \ddots & \\ & & 0 & 1 \end{pmatrix}, \tag{3.29}$$

$$D_K \in \mathbb{R}^{K \times (K+1)} \equiv \begin{pmatrix} -1 & 1 & & \\ & \ddots & \ddots & \\ & & -1 & 1 \end{pmatrix}, S_{K,+} \in \mathbb{R}^{K \times (K+1)} \equiv \begin{pmatrix} 0 & 1 & & \\ & \ddots & \ddots & \\ & & 0 & 1 \end{pmatrix}. \tag{3.30}$$

We define the total cross section matrix as

$$\Sigma \equiv \mathrm{diag}(\sigma_{111}, \ldots, \sigma_{MJK}), \tag{3.31}$$

and the inverse neutron velocity matrix as

$$V^{-1} \equiv \mathrm{diag}(1/v_{111}, \ldots, 1/v_{MJK}). \tag{3.32}$$

The matrices describing the spatial derivatives with respect to a spatial variable C_x, C_y, and C_z are defined by

$$C_x \equiv S_{K,+} \otimes S_{J,+} \otimes \Delta x^{-1} D_M, \tag{3.33}$$

$$C_y \equiv S_{K,+} \otimes \Delta y^{-1} D_J \otimes S_{M,+}, \tag{3.34}$$

$$C_z \equiv \Delta z^{-1} D_K \otimes S_{J,+} \otimes S_{M,+}, \tag{3.35}$$

while the matrix associating the correct total cross section to each cell is defined as

$$S \equiv S_{K,+} \otimes S_{J,+} \otimes S_{M,+}. \tag{3.36}$$

With these matrices defined, we can write the MJK zone-centered equations for the unknown vector Ψ as

$$(\alpha V^{-1} + C + \Sigma S)\Psi = F, \tag{3.37}$$

where

$$C \equiv \mu C_x + \eta C_y + \xi C_z, \tag{3.38}$$

and

$$F \equiv (f_{ijk}) \in \mathbb{R}^{MJK}. \tag{3.39}$$

Boundary values are isolated by noting that for a positive direction vector $\hat{\Omega}$, ψ satisfies the Dirichlet condition for all $\vec{r} = r_{0jk}, r_{i0k}$, or r_{ij0}. These locations correspond to one of the three faces with coordinate $x = x_0, y_0$, or z_0 of the box. For a positive direction vector $\hat{\Omega}$, we define the vector Ψ_B with length equal to the length of Ψ. The vector Ψ_B is nonzero at all indices corresponding to boundary points where there is some incoming angular flux. The discrete boundary conditions can be written

$$E_{000}(\Psi - \Psi_B) = 0, \tag{3.40}$$

where we define E_{000} as

$$E_{000} = \begin{pmatrix} e_{0K}^T \otimes I_{J+1} \otimes I_{M+1} \\ (0, I_K) \otimes e_{0J}^T \otimes I_{M+1} \\ (0, I_K) \otimes (0, I_J) \otimes e_{0M}^T \end{pmatrix}, \tag{3.41}$$

where the vectors e_{0J} and e_{0K} are unit vectors. There are different E matrices for other directions. For three-dimensional Cartesian geometry, there are eight different matrices, E_{ijk}, corresponding to boundary points $i = 0, M$, $j = 0, L$, and $k = 0, K$.

Equation 3.37 is the discretized equation for quadrature point $\hat{\Omega}$ and energy group g. We generalize for multiple quadrature points and energy groups by introducing the indices ℓ and g, where ℓ is the index of quadrature point $\hat{\Omega} = \hat{\Omega}_\ell$ and g is the energy group index. The vectors Ψ and Ψ_B and matrix C of Eq. 3.37 become $\Psi_{g,\ell}$, $\Psi_{B,g,\ell}$, and C_ℓ.

We define the matrices Z and Z_b by

$$Z \equiv \begin{pmatrix} I_{MJK} \\ 0 \end{pmatrix} \in \mathbb{R}^{(M+1)(J+1)(K+1) \times MJK} \tag{3.42}$$

and

$$Z_b \equiv \begin{pmatrix} 0 \\ I_{(M+1)(J+1)(K+1)-MJK} \end{pmatrix} \in \mathbb{R}^{(M+1)(J+1)(K+1) \times (M+1)(J+1)(K+1)-MJK}. \tag{3.43}$$

The matrices Z and Z_b inject zone-centered vectors into the nodal vector space. We note the following properties:

$$Z^T Z = I_{MJK}, \tag{3.44}$$

$$Z_b^T Z_b = I_{(M+1)(J+1)(K+1)-MJK}, \tag{3.45}$$

and

$$Z^T Z_b = 0. \tag{3.46}$$

Then the matrix representation of Eq. 3.18 for energy group g and direction ℓ can be written as

$$(\alpha V_{g,\ell}^{-1} + H_{g,\ell})\Psi_{g,\ell} = ZF_{g,\ell} + Z_b B_\ell \Psi_{B,g,\ell}, \tag{3.47}$$

where

$$H_{g,\ell} \equiv Z(C_\ell + \Sigma_g S) + Z_b B_\ell, \tag{3.48}$$

and

$$V_{g,\ell}^{-1} \equiv ZV_g^{-1}S, \tag{3.49}$$

with $B_\ell = E_{ijk}$ for the appropriate choice of i, j, and k and C_ℓ is defined as

$$C_\ell \equiv \mu_\ell C_x + \eta_\ell C_y + \xi_\ell C_z. \tag{3.50}$$

The matrix $H_{g,\ell}$ operates on nodal vectors. We define the angular quadrature scheme in the next section.

The Discrete Ordinates Method

To integrate functions on the unit sphere, we consider symmetric quadrature rules of the form [8]:

$$\int_{4\pi} d\hat{\Omega}\, \psi(\hat{\Omega}) \approx \sum_{\ell=1}^{L} w_\ell \psi(\hat{\Omega}_\ell), \tag{3.51}$$

where $\hat{\Omega} \equiv (\mu_\ell, \eta_\ell, \xi_\ell)$, for all $\ell = 1, \ldots, L$, with $L = \nu(\nu+2)$ and ν is the number of direction cosines ($\nu = 2, 4, 6, \ldots$). It is assumed that $w_\ell > 0$ for all ℓ. We note that

$$\sum_{\ell=1}^{L} w_\ell = 1, \tag{3.52}$$

since

$$\int_{4\pi} d\hat{\Omega} = 1. \tag{3.53}$$

The symmetry requirement is met using symmetry through the origin. Namely, if $\hat{\Omega}_\ell$ is a quadrature point with corresponding weight, w_ℓ, then $-\hat{\Omega}_\ell$ is also a quadrature point. Letting ℓ^- denote the index, we can write $\hat{\Omega}_{-\ell} = -\hat{\Omega}_\ell$. It is also true that $w_{-\ell} = w_\ell$ [8].

We define discretized representations of angular flux moment operators in Eq. 3.18. These operators operate on zone-centered vectors and are easily seen to be given by $MJK \times LMJK$ size matrices

$$L_{n,m} \equiv (l_{n,m}W) \otimes I_{MJK}, \tag{3.54}$$

where

$$l_{n,m} \equiv \left(Y_n^m(\hat{\Omega}_1), Y_n^m(\hat{\Omega}_2), \ldots, Y_n^m(\hat{\Omega}_L)\right), \tag{3.55}$$

and

$$W \equiv \text{diag}(w_1, w_2, \ldots, w_L). \tag{3.56}$$

If the vector Ψ_g approximates $\psi_g(\vec{r}, \hat{\Omega})$, then $L_{n,m}\Psi_g$ approximates the $(n,m)^{\text{th}}$ moment of $\psi_g(\vec{r}, \hat{\Omega})$, $\phi_{g,n,m}(\vec{r})$. Similarly, we define $LMJK \times MJK$ size matrices

$$L_{n,m}^{+} \equiv l_{n,m}^{T} \otimes I_{MJK}. \tag{3.57}$$

If a vector Φ approximates $\phi(\vec{r})$, then $L_{n,m}^{+}\Phi$ approximates $Y_n^m(\hat{\Omega})\phi(\vec{r})$. We define the grouped matrices L_n and L_n^+, where

$$L_n = \begin{pmatrix} L_{n,-n} \\ \vdots \\ L_{n,n} \end{pmatrix} \quad \text{and} \quad L_n^+ = \begin{pmatrix} L_{n,-n}^+, \ldots, L_{n,n}^+ \end{pmatrix} \tag{3.58}$$

and the further grouped block matrices

$$L^N = \begin{pmatrix} L_0 \\ \vdots \\ L_N \end{pmatrix} \quad \text{and} \quad L^{N,+} = \begin{pmatrix} L_0^+, \ldots, L_N^+ \end{pmatrix}. \tag{3.59}$$

Given $N = N_s$, the number of terms in the scattering kernel, it is assumed that the symmetric quadrature rule is such that the spherical harmonics of order N_s and less satisfy

$$\sum_{\ell=1}^{L} Y_n^m(\hat{\Omega}_\ell) Y_{n'}^{m'}(\hat{\Omega}_\ell) = \delta_{n,n'}\delta_{m,m'}, \text{ for all } 0 \leq n, n' \leq N_s, |m| \leq n, |m'| \leq n'. \tag{3.60}$$

In matrix form, this can be written more compactly as

$$L^{N_s} L^{N_s,+} = I_{(N_s+1)^2} \otimes I_{MJK}. \tag{3.61}$$

For boundary terms, we define the block diagonal matrices B and C by

$$B \equiv \text{diag}(B_1, B_2, \ldots, B_L) \tag{3.62}$$

and

$$C \equiv \text{diag}(C_1, C_2, \ldots, C_L). \tag{3.63}$$

The scattering kernel matrix is defined by letting

$$\Sigma_{s,g,g',n} \equiv I_{2n+1} \otimes \hat{\Sigma}_{s,g,g',n}, \tag{3.64}$$

where

$$\hat{\Sigma}_{s,g,g',n} \equiv \text{diag}(\sigma_{s,g,g',n,111}, \ldots, \sigma_{s,g,g',n,MJK}), \quad n = 0, 1, \ldots \tag{3.65}$$

The fission matrix is defined by letting

$$\Sigma_{f,g,g',n} \equiv I_{2n+1} \otimes \hat{\Sigma}_{f,g,g',n}, \tag{3.66}$$

where

$$\hat{\Sigma}_{f,g,g',n} \equiv \mathrm{diag}(\chi_g \nu \sigma_{f,g',n,111}, \ldots, \chi_g \nu \sigma_{f,g',n,MJK}), \quad n = 0, 1, \ldots \tag{3.67}$$

We define the matrix $\bar{Z}$, which injects zone-centered vectors into the nodal vector space, as

$$\bar{Z} \equiv I_L \otimes Z, \tag{3.68}$$

along with the matrix $\bar{Z}_B$

$$\bar{Z}_B \equiv I_L \otimes Z_b. \tag{3.69}$$

We note that properties of Z and Z_b remain true for the matrices $\bar{Z}$ and $\bar{Z}_B$. We define the matrix $\bar{S}$, which averages nodal vectors to obtain zone-centered vectors, as

$$\bar{S} \equiv I_L \otimes S. \tag{3.70}$$

Finally, we define the total cross section matrix for all quadrature points $\bar{\Sigma}$ as

$$\bar{\Sigma} \equiv I_L \otimes \Sigma, \tag{3.71}$$

and the inverse velocity matrix $\bar{V}^{-1}$ as

$$\bar{V}^{-1} \equiv I_L \otimes V^{-1}. \tag{3.72}$$

Using the previously defined matrices, we can define the matrix H_g, the leakage and total cross section matrix for energy group g as

$$H_g \equiv \mathrm{diag}(H_{g,1}, H_{g,2}, \ldots, H_{g,L}) = \bar{Z}(C + \bar{\Sigma}_g \bar{S}) + \bar{Z}_B B, \tag{3.73}$$

along with the matrix V_g^{-1}

$$V_g^{-1} \equiv \mathrm{diag}(V_{g,1}^{-1}, V_{g,2}^{-1}, \ldots, V_{g,L}^{-1}) = \bar{Z}\bar{V}^{-1}\bar{S}. \tag{3.74}$$

The matrices $\bar{Z}$ and $\bar{Z}_B$ are necessary since H_g operates on nodal vectors while the matrices $\Sigma_{s,g,g',n}$ and $\Sigma_{f,g,g',n}$ operate on zone-centered vectors. Assuming only $N_s + 1$ terms in the scattering operator, then the complete discretization of Eq. 3.18 can be written as

$$\left(\alpha V_g^{-1} + H_g\right)\Psi_g = \bar{Z}\sum_{g'=1}^{G}\sum_{n=0}^{N_s} L_n^+ \Sigma_{s,g,g',n} L_n \bar{S}\Psi_{g'}$$

$$+ \bar{Z}\sum_{g'=1}^{G}\sum_{n=0}^{N_s} L_n^+ \Sigma_{f,g,g',n} L_n \bar{S}\Psi_{g'}, g = 1, \ldots, G. \tag{3.75}$$

Finally, we can write the fully discretized in space, angle, and energy matrix equation analog of Eq. 3.1. We first define the complex multigroup scattering and fission matrices

$$\boldsymbol{\Sigma_s} \equiv \begin{pmatrix} \Sigma_{s,11}^{N_s} & \cdots & \Sigma_{s,1G}^{N_s} \\ \vdots & \ddots & \vdots \\ \Sigma_{s,G1}^{N_s} & \cdots & \Sigma_{s,GG}^{N_s} \end{pmatrix}, \tag{3.76}$$

where

$$\Sigma_{s,gg'}^{N_s} \equiv \mathrm{diag}\big(\Sigma_{s,g,g',0}, \ldots, \Sigma_{s,g,g',N_s}\big), \tag{3.77}$$

and

$$\boldsymbol{\Sigma_f} \equiv \begin{pmatrix} \Sigma_{f,11}^{N_s} & \cdots & \Sigma_{f,1G}^{N_s} \\ \vdots & \ddots & \vdots \\ \Sigma_{f,G1}^{N_s} & \cdots & \Sigma_{f,GG}^{N_s} \end{pmatrix}, \tag{3.78}$$

where

$$\Sigma_{f,gg'}^{N_s} \equiv \mathrm{diag}\big(\Sigma_{f,g,g',0}, \ldots, \Sigma_{f,g,g',N_s}\big). \tag{3.79}$$

We define the following matrices

$$\mathbf{S} \equiv I_G \otimes \bar{S}, \tag{3.80}$$

$$\mathbf{Z} \equiv I_G \otimes \bar{Z}, \tag{3.81}$$

$$\mathbf{Z_B} \equiv I_G \otimes \bar{Z}_B, \tag{3.82}$$

$$\mathbf{L}^+ \equiv I_G \otimes L^{N_s,+}, \tag{3.83}$$

$$\mathbf{L} \equiv I_G \otimes L^{N_s}, \tag{3.84}$$

and

$$\mathbf{B} \equiv I_G \otimes B. \tag{3.85}$$

Finally, we define the matrices $\mathbf{H}$ and $\mathbf{V}^{-1}$ as

$$\mathbf{H} \equiv \mathrm{diag}\big(H_1, H_2, \ldots, H_G\big), \tag{3.86}$$

and

$$\mathbf{V}^{-1} \equiv \mathrm{diag}\big(V_1^{-1}, V_2^{-1}, \ldots, V_G^{-1}\big). \tag{3.87}$$

With these matrices defined, we can write Eq. 3.1 as the matrix equation

$$\big(\alpha \mathbf{V}^{-1} + \mathbf{H}\big)\boldsymbol{\Psi} = \mathbf{Z}\mathbf{L}^+\big(\boldsymbol{\Sigma_s} + \boldsymbol{\Sigma_f}\big)\mathbf{L}\mathbf{S}\boldsymbol{\Psi}, \tag{3.88}$$

where the angular flux vector, $\boldsymbol{\Psi}$, is defined as

$$\boldsymbol{\Psi} \equiv \begin{pmatrix} \Psi_1 \\ \Psi_2 \\ \vdots \\ \Psi_G \end{pmatrix}. \tag{3.89}$$

Equation 3.88 is the discretized alpha-eigenvalue neutron transport problem in matrix form for the node-centered angular flux. Similarly, the k-effective eigenvalue problem can be written as

$$\mathbf{H}\boldsymbol{\Psi} = \mathbf{Z}\mathbf{L}^{+}\left(\boldsymbol{\Sigma}_{\mathbf{s}} + \frac{1}{k}\boldsymbol{\Sigma}_{\mathbf{f}}\right)\mathbf{L}\mathbf{S}\boldsymbol{\Psi}. \tag{3.90}$$

Equations 3.88 and 3.90 are eigenvalue equations for the criticality eigenvalue and the node-centered angular flux eigenvector. In the derivation of the Rayleigh quotient fixed point method, we require an inner product. However, the inner product is defined for zone-centered vectors, whereas the unknown angular flux eigenvectors in Eqns. 3.88 and 3.90 are node-centered. To satisfy this requirement, we write Eqns. 3.88 and 3.90 using zone-centered angular flux eigenvectors. We denote $\boldsymbol{\Psi}_{\mathbf{z}}$ as the zone-centered unknown and $\mathbf{H}_{\mathbf{z}}$ as the zone-centered version of $\mathbf{H}$. To write Eqns. 3.88 and 3.90, we use the following lemma.

Lemma 1 *For all $\ell = 1, 2, \ldots, L$,*

$$B_\ell(ZS + Z_bB_\ell)^{-1}Z = 0 \cdot I_{MJK} \text{ and } S(ZS + Z_bB_\ell)^{-1}Z = I_{MJK}. \tag{3.91}$$

Proof 4 *The matrix $ZS + Z_bB_\ell$ is nonsingular for all $\ell = 1, 2, \ldots, L$. [5]. Therefore,*

$$I_{MJK} = ZS(ZS + Z_bB_\ell)^{-1} + Z_bB_\ell(ZS + Z_bB_\ell)^{-1}. \tag{3.92}$$

Multiplying by Z_b^T and using the fact $Z^TZ_b = 0$ gives

$$Z_b^T = B_\ell(ZS + Z_bB_\ell)^{-1}. \tag{3.93}$$

Multiplying on the right by Z gives the first assertion in Eq. 3.91. Using the fact $Z^TZ = I_{MJK}$ and $Z^TZ_b = 0$, multiplying Eq. 3.92 on the left by Z^T gives

$$Z^T = S(ZS + Z_bB_\ell)^{-1}. \tag{3.94}$$

Multiplying on the right by Z gives the second assertion in Eq. 3.91.

Given a zone-centered angular flux vector $\boldsymbol{\Psi}_{\mathbf{z}}$, the nodal angular flux vector $\boldsymbol{\Psi}$ defined by

$$\Psi_{g,\ell} \equiv (ZS + Z_bB_\ell)^{-1}Z\Psi_{z,g,\ell} \text{ for all } g = 1, 2, \ldots, G \text{ and } \ell = 1, 2, \ldots, L, \tag{3.95}$$

satisfies $B_\ell\Psi_{g,\ell} = 0$ and $S\Psi_{g,\ell} = \Psi_{z,g,\ell}$ for all g and ℓ. Defining the matrices

$$\mathbf{C} \equiv I_G \otimes C, \tag{3.96}$$

$$\mathbf{B} \equiv I_G \otimes B, \tag{3.97}$$

$$\mathbf{Z_B} \equiv I_G \otimes \bar{Z}_B, \tag{3.98}$$

and

$$\boldsymbol{\Sigma} \equiv \mathrm{diag}(\bar{\Sigma}_1, \bar{\Sigma}_2, \ldots, \bar{\Sigma}_G), \tag{3.99}$$

then $\mathbf{H}$ and $\mathbf{V}^{-1}$ can be rewritten as

$$\mathbf{H} = \mathbf{Z}(\mathbf{C} + \boldsymbol{\Sigma}\mathbf{S}) + \mathbf{Z_B}\mathbf{B}, \tag{3.100}$$

and

$$\mathbf{V}^{-1} = \mathbf{Z}\mathbf{V}^{-1}\mathbf{S}. \tag{3.101}$$

For the nodal-centered angular flux $\boldsymbol{\Psi}$, we have from Lemma 1 that

$$\boldsymbol{\Psi} = (\mathbf{ZS} + \mathbf{Z_B}\mathbf{B})^{-1}\mathbf{Z}\boldsymbol{\Psi_z}. \tag{3.102}$$

Substituting Eq. 3.102 into Eq. 3.88 and 3.90 and multiplying on the left by $\mathbf{Z}^T$ gives

$$\left(\alpha\mathbf{V_z}^{-1} + \mathbf{H_z}\right)\boldsymbol{\Psi_z} = \mathbf{L}^+(\boldsymbol{\Sigma_s} + \boldsymbol{\Sigma_f})\mathbf{L}\boldsymbol{\Psi_z}, \tag{3.103}$$

and

$$\mathbf{H_z}\boldsymbol{\Psi_z} = \mathbf{L}^+\left(\boldsymbol{\Sigma_s} + \frac{1}{k}\boldsymbol{\Sigma_f}\right)\mathbf{L}\boldsymbol{\Psi_z}, \tag{3.104}$$

where

$$\mathbf{H_z} \equiv \mathbf{C}(\mathbf{ZS} + \mathbf{Z_B}\mathbf{B})^{-1}\mathbf{Z} + \boldsymbol{\Sigma}, \tag{3.105}$$

and

$$\mathbf{V_z}^{-1} \equiv \mathbf{V}^{-1}\mathbf{S}(\mathbf{ZS} + \mathbf{Z_B}\mathbf{B})^{-1}\mathbf{Z}. \tag{3.106}$$

We consider Eqns. 3.103 and 3.104 in the derivation of the Rayleigh quotient fixed point method.

3.2 Primitivity of the Discretized Eigenvalue Equations

Assuming isotropic fission and scattering, we show by example that the matrix $\mathbf{A}(\alpha)$ is a primitive matrix. A primitive matrix is a matrix $\mathbf{B} \geq 0$ for which there exists some n such that $\mathbf{B}^n > 0$ [18]. Consider a two energy group problem with discrete ordinates S_2 angular quadrature from [25] and two spatial cells $(G, L, M = 2)$. The scattering matrix is then

$$\mathbf{L}^+\boldsymbol{\Sigma_s}\mathbf{L} = \begin{pmatrix} L^{0,+} & 0 \\ 0 & L^{0,+} \end{pmatrix} \begin{pmatrix} \Sigma^0_{s,11} & \Sigma^0_{s,12} \\ \Sigma^0_{s,21} & \Sigma^0_{s,22} \end{pmatrix} \begin{pmatrix} L^0 & 0 \\ 0 & L^0 \end{pmatrix}$$

$$= \begin{pmatrix} L^{0,+}\Sigma^0_{s,11}L^0 & L^{0,+}\Sigma^0_{s,12}L^0 \\ L^{0,+}\Sigma^0_{s,21}L^0 & L^{+,0}\Sigma^0_{s,22}L^0 \end{pmatrix}. \tag{3.107}$$

Each block matrix can be written as

$$L^{0,+}\Sigma^0_{s,11}L = (\ell_0^T \otimes I_M)\Sigma_{s,11,0}(\ell_0 W \otimes I_M)$$

$$= \begin{pmatrix} 1 & 0 \\ 0 & 1 \\ 1 & 0 \\ 0 & 1 \end{pmatrix} \begin{pmatrix} \sigma_{s,1,1,0,1} & 0 \\ 0 & \sigma_{s,1,1,0,2} \end{pmatrix} \begin{pmatrix} 1/2 & 0 & 1/2 & 0 \\ 0 & 1/2 & 0 & 1/2 \end{pmatrix}$$

$$= \begin{pmatrix} \frac{1}{2}\sigma_{s,1,1,0,1} & 0 & \frac{1}{2}\sigma_{s,1,1,0,1} & 0 \\ 0 & \frac{1}{2}\sigma_{s,1,1,0,2} & 0 & \frac{1}{2}\sigma_{s,1,1,0,2} \\ \frac{1}{2}\sigma_{s,1,1,0,1} & 0 & \frac{1}{2}\sigma_{s,1,1,0,1} & 0 \\ 0 & \frac{1}{2}\sigma_{s,1,1,0,2} & 0 & \frac{1}{2}\sigma_{s,1,1,0,2} \end{pmatrix}. \qquad (3.108)$$

Similarly, for $L^{0,+}\Sigma^0_{f,11}L$ we have

$$L^{0,+}\Sigma^0_{f,11}L = \begin{pmatrix} \frac{1}{2}\chi_1\nu\sigma_{f,1,1} & 0 & \chi_1\frac{1}{2}\nu\sigma_{f,1,1} & 0 \\ 0 & \frac{1}{2}\chi_1\nu\sigma_{f,1,2} & 0 & \frac{1}{2}\chi_1\nu\sigma_{f,1,2} \\ \frac{1}{2}\chi_1\nu\sigma_{f,1,1} & 0 & \frac{1}{2}\chi_1\nu\sigma_{f,1,1} & 0 \\ 0 & \frac{1}{2}\chi_1\nu\sigma_{f,1,2} & 0 & \frac{1}{2}\chi_1\nu\sigma_{f,1,2} \end{pmatrix}. \qquad (3.109)$$

For our model problem, $\mathbf{H_z^{-1}} \geq 0$ and has the form [14]

$$\mathbf{H_z^{-1}} = \begin{pmatrix} \begin{pmatrix} x & 0 \\ x & x \end{pmatrix} & \mathbf{0} & \mathbf{0} & \mathbf{0} \\ \mathbf{0} & \begin{pmatrix} x & x \\ 0 & x \end{pmatrix} & \mathbf{0} & \mathbf{0} \\ \mathbf{0} & \mathbf{0} & \begin{pmatrix} x & 0 \\ x & x \end{pmatrix} & \mathbf{0} \\ \mathbf{0} & \mathbf{0} & \mathbf{0} & \begin{pmatrix} x & x \\ 0 & x \end{pmatrix} \end{pmatrix}, \qquad (3.110)$$

and $\mathbf{L^+\Sigma_f L}$ has the form

$$\mathbf{L^+\Sigma_f L} = \frac{1}{2} \begin{pmatrix} \chi_1\nu\sigma_{f,1}I_L & \chi_1\nu\sigma_{f,1}I_L & \chi_1\nu\sigma_{f,2}I_L & \chi_1\nu\sigma_{f,2}I_L \\ \chi_1\nu\sigma_{f,1}I_L & \chi_1\nu\sigma_{f,1}I_L & \chi_1\nu\sigma_{f,2}I_L & \chi_1\nu\sigma_{f,2}I_L \\ \chi_2\nu\sigma_{f,1}I_L & \chi_2\nu\sigma_{f,1}I_L & \chi_2\nu\sigma_{f,2}I_L & \chi_2\nu\sigma_{f,2}I_L \\ \chi_2\nu\sigma_{f,1}I_L & \chi_2\nu\sigma_{f,1}I_L & \chi_2\nu\sigma_{f,2}I_L & \chi_2\nu\sigma_{f,2}I_L \end{pmatrix}. \qquad (3.111)$$

Therefore, the matrix $\mathbf{H_z^{-1}L^+\Sigma_f L}$ has the form

$$\mathbf{H_z^{-1}L^+\Sigma_f L} = \begin{pmatrix} \begin{pmatrix} x & 0 \\ x & x \end{pmatrix} & \begin{pmatrix} x & 0 \\ x & x \end{pmatrix} & \begin{pmatrix} x & 0 \\ x & x \end{pmatrix} & \begin{pmatrix} x & 0 \\ x & x \end{pmatrix} \\ \begin{pmatrix} x & x \\ 0 & x \end{pmatrix} & \begin{pmatrix} x & x \\ 0 & x \end{pmatrix} & \begin{pmatrix} x & x \\ 0 & x \end{pmatrix} & \begin{pmatrix} x & x \\ 0 & x \end{pmatrix} \\ \begin{pmatrix} x & 0 \\ x & x \end{pmatrix} & \begin{pmatrix} x & 0 \\ x & x \end{pmatrix} & \begin{pmatrix} x & 0 \\ x & x \end{pmatrix} & \begin{pmatrix} x & 0 \\ x & x \end{pmatrix} \\ \begin{pmatrix} x & x \\ 0 & x \end{pmatrix} & \begin{pmatrix} x & x \\ 0 & x \end{pmatrix} & \begin{pmatrix} x & x \\ 0 & x \end{pmatrix} & \begin{pmatrix} x & x \\ 0 & x \end{pmatrix} \end{pmatrix}, \qquad (3.112)$$

where I_L is the identity matrix of size L. It follows that each block of the matrix $(\mathbf{H_z^{-1}L^+\Sigma_f L})^2$ is

$$\begin{pmatrix} x & 0 \\ x & x \end{pmatrix} \begin{pmatrix} x & x \\ 0 & x \end{pmatrix} = \begin{pmatrix} x^2 & x^2 \\ x^2 & x^2 \end{pmatrix} > 0 \text{ because } \begin{pmatrix} \chi_1 \nu \sigma_{f,1} & \chi_1 \nu \sigma_{f,2} \\ \chi_2 \nu \sigma_{f,1} & \chi_2 \nu \sigma_{f,2} \end{pmatrix} > 0 \qquad (3.113)$$

and $\mathbf{H_z^{-1}} \geq 0$. Therefore, $\mathbf{H_z^{-1}L^+\Sigma_f L}$ is primitive and it follows that $\mathbf{A}(\alpha)$ is primitive since $\mathbf{L^+\Sigma_s L} \geq 0$. When the system is subcritical, $\alpha < 0$ and the matrix $\mathbf{A}(\alpha)$ is primitive. For supercritical systems, $\alpha > 0$ and there is an upper limit $\alpha_{\max}$ such that the matrix $\mathbf{A}(\alpha)$ remains primitive. For k-effective eigenvalue problems, k is always positive and therefore the matrix $\mathbf{T}(k)$ is primitive.

Chapter 4

The Rayleigh Quotient Fixed Point Method

In this chapter we derive the Rayleigh Quotient Fixed Point (RQFP) method for alpha- and k-effective eigenvalue problems. We begin with the matrix form of the eigenvalue equations and proceed to develop a fixed point method for the angular flux eigenvector. Since the eigenvector corresponds to the alpha- or k-effective eigenvalue, we require an update for the eigenvalue at each iteration. We derive an eigenvalue update that is optimal in the least squares sense by relating the alpha- or k-effective eigenvalue to the dominant eigenvalue of a primitive matrix (see Section 2.4). This primitive matrix serves as the fixed point function to determine the solution of the eigenvalue problem. Since the dominant eigenvalue of a primitive matrix corresponds to the only positive eigenvector of the matrix, this eigenvector also solves the discretized criticality eigenvalue neutron transport problem. We end this chapter with a discussion of the primitivity of the discretized alpha- and k-effective eigenvalue matrix equations.

4.1 Derivation of the Rayleigh Quotient Fixed Point Method for Alpha-Eigenvalue Problems

We begin with the discretized alpha-eigenvalue matrix equation:

$$\left(\alpha \mathbf{V_z}^{-1} + \mathbf{H_z}\right)\mathbf{\Psi_z} = \mathbf{L}^+\left(\mathbf{\Sigma_s} + \mathbf{\Sigma_f}\right)\mathbf{L}\mathbf{\Psi_z}. \tag{4.1}$$

Solution of Eq. 4.1 consists of finding the eigenpair $(\alpha, \mathbf{\Psi})$ that satisfies the equation with α a real number and the vector $\mathbf{\Psi}$ positive. We write a fixed point equation for Eq. 4.1 in the form

$$\mathbf{\Psi_z} = \mathbf{H_z}^{-1}\left(-\alpha \mathbf{V_z}^{-1} + \mathbf{L}^+\left(\mathbf{\Sigma_s} + \mathbf{\Sigma_f}\right)\mathbf{L}\right)\mathbf{\Psi} \equiv \mathbf{A}(\alpha)\mathbf{\Psi_z}. \tag{4.2}$$

For all subcritical and critical systems, the righthand side of Eq. 4.2 is nonnegative since for isotropic scattering the scattering matrix is nonnegative. For supercritical systems, there is

an $\alpha_{\max}$ such that the righthand side is still nonnegative. Various fixed point equations can be written for the angular flux eigenvector $\mathbf{\Psi_z}$. However, this form was selected as it only requires the inversion of the matrix $\mathbf{H_z}$. In standard neutron transport codes [15] [2], the matrix $\mathbf{H_z}$ is inverted without being formed by sweeping across the domain in space and angle. The updated eigenvector iterate is obtained by the action of the inverted operator on the source. By writing the fixed point in this way, the Rayleigh quotient fixed point method can be implemented easily in production neutron transport codes.

We define an iterative method to find the fixed point (see Section **??**) of Eq. 4.2 as

$$\mathbf{\Psi_z}^{(i+1)} = \mathbf{A}(\alpha^{(i)})\mathbf{\Psi_z}^{(i)}. \tag{4.3}$$

From some initial positive starting vector $\mathbf{\Psi_z}^{(0)}$, the subsequent eigenvector iterate is determined by the action of inversion of the matrix $\mathbf{H_z}$ on the scattering and fission source adjusted by the alpha-eigenvalue. At each iteration, an update for the eigenvalue is required. A natural choice of update is that the eigenvalue be a function of the eigenvector iterate. Given an eigenpair, $(\alpha_*, \mathbf{\Psi_z^*})$ to Eq. 4.1, it follows that

$$\mathbf{\Psi_z^*} = \mathbf{A}(\alpha_*)\mathbf{\Psi_z^*} \tag{4.4}$$

is also an eigenvalue problem for the fixed matrix $\mathbf{A}(\alpha_*)$ with eigenvector $\mathbf{\Psi_z^*}$ and eigenvalue one.

If the matrix $\mathbf{A}(\alpha)$ is a primitive matrix, it follows from the Perron-Froebenius Theorem for Primitive Matrices that there is only one unique positive eigenvector of $\mathbf{A}(\alpha)$ corresponding to the dominant eigenvalue. This fact allows us to derive an update for the alpha-eigenvalue at each iteration.

If $(\mathbf{\Psi_z^*}, \lambda)$ is an eigenpair of the matrix $\mathbf{A}(\alpha_*)$, then

$$\|\mathbf{A}(\alpha_*)\mathbf{\Psi_z^*} - \lambda\mathbf{\Psi_z^*}\|_2^2 = 0. \tag{4.5}$$

However, suppose $\mathbf{\Psi}_{(i)}$ is an approximate eigenvector and we seek to find the best approximate eigenvalue $\hat{\lambda}$ such that

$$\hat{\lambda} = \arg\min_{\mu} \left\|\mathbf{A}\left(\alpha_{(i)}\right)\mathbf{\Psi}_{(i)} - \mu\mathbf{\Psi}_{(i)}\right\|_2^2. \tag{4.6}$$

This is a linear least squares problem in the variable μ. It is found that [18]

$$\hat{\lambda} = \frac{\mathbf{\Psi}_{(i)}^T \mathbf{A}\left(\alpha_{(i)}\right)\mathbf{\Psi}_{(i)}}{\mathbf{\Psi}_{(i)}^T \mathbf{\Psi}_{(i)}}, \tag{4.7}$$

the Rayleigh quotient, minimizes the residual in the least squares sense. Setting the Rayleigh quotient to one and solving for the approximate alpha-eigenvalue $\alpha_{(i)}$, we obtain the alpha-eigenvalue update for an approximate eigenvector $\mathbf{\Psi}_{(i)}$

$$\alpha_{(i)} = \frac{\mathbf{\Psi}_{(i)}^T \mathbf{H_z}^{-1} \mathbf{L}^+\left(\mathbf{\Sigma_s} + \mathbf{\Sigma_f}\right)\mathbf{L}\mathbf{\Psi}_{(i)} - \mathbf{\Psi}_{(i)}^T \mathbf{\Psi}_{(i)}}{\mathbf{\Psi}_{(i)}^T \mathbf{H_z}^{-1} \mathbf{V_z}^{-1} \mathbf{\Psi}_{(i)}}. \tag{4.8}$$

Algorithm 4.1 Rayleigh Quotient Fixed Point Method for the Alpha-Eigenvalue Problem

while residual > tolerance **do**

$$\alpha_{(i)} = \frac{\mathbf{\Psi}_{(i)}^T \mathbf{H_z}^{-1} \mathbf{L}^+ \big(\mathbf{\Sigma_s} + \mathbf{\Sigma_f}\big) \mathbf{L} \mathbf{\Psi}_{(i)} - \mathbf{\Psi}_{(i)}^T \mathbf{\Psi}_{(i)}}{\mathbf{\Psi}_{(i)}^T \mathbf{H_z}^{-1} \mathbf{V_z}^{-1} \mathbf{\Psi}_{(i)}}$$

$$\mathbf{\Psi}_{(i+1)} = \mathbf{H_z}^{-1} \bigg(- \alpha_{(i)} \mathbf{V_z}^{-1} + \mathbf{L}^+ \big(\mathbf{\Sigma_s} + \mathbf{\Sigma_f}\big) \mathbf{L} \bigg) \mathbf{\Psi}_{(i)}$$

$$\text{residual} = \frac{\big\|\mathbf{\Psi}_{(i+1)} - \mathbf{\Psi}_{(i)}\big\|_2}{\big\|\mathbf{\Psi}_{(i+1)}\big\|_2}$$

end while

Given Eq. 4.8, we introduce Algorithm 4.1, an iterative scheme to determine the alpha-eigenvalue and its corresponding eigenvector. The eigenvalue update is optimal in the least squares sense. For alpha-eigenvalue problems, whereas traditional techniques have focused on supercritical problems and were limited in subcritical cases [16], this method allows for the solution of both subcritical and supercritical systems.

For each iteration in Algorithm 4.1 two transport sweeps (inversions of $\mathbf{H_z}$) are required. To reduce the number of transport sweeps required, we note that Eq. 4.8 can be written as

$$\alpha_{(i)} = \frac{\mathbf{\Psi}_{(i)}^T \mathbf{L}^+ \big(\mathbf{\Sigma_s} + \mathbf{\Sigma_f}\big) \mathbf{L} \mathbf{\Psi}_{(i)} - \mathbf{\Psi}_{(i)}^T \mathbf{H_z} \mathbf{\Psi}_{(i)}}{\mathbf{\Psi}_{(i)}^T \mathbf{V_z}^{-1} \mathbf{\Psi}_{(i)}}. \tag{4.9}$$

Using the fact that

$$\mathbf{H_z} \mathbf{\Psi}_{(i)} = \bigg(- \alpha_{(i-1)} \mathbf{V_z}^{-1} + \mathbf{L}^+ \big(\mathbf{\Sigma_s} + \mathbf{\Sigma_f}\big) \mathbf{L} \bigg) \mathbf{\Psi}_{(i-1)} \equiv \mathbf{q}_{(i-1)}, \tag{4.10}$$

where $\mathbf{q}$ is the scattering and fission source vector, we can write Eq. 3 as

$$\alpha_{(i)} = \frac{\mathbf{\Psi}_{(i)}^T \mathbf{L}^+ \big(\mathbf{\Sigma_s} + \mathbf{\Sigma_f}\big) \mathbf{L} \mathbf{\Psi}_{(i)} - \mathbf{\Psi}_{(i)}^T \mathbf{q}_{(i-1)}}{\mathbf{\Psi}_{(i)}^T \mathbf{V_z}^{-1} \mathbf{\Psi}_{(i)}}. \tag{4.11}$$

We introduce a one-sweep variant of Algorithm 4.1 in Algorithm 4.2. For the first iteration $(i = 0)$, the source $\mathbf{q}_{(-1)} = \mathbf{0}$ where $\mathbf{0}$ is the zero vector. Algorithm 4.2 requires only one transport sweep per iteration of the method. However, the method requires two vectors per iteration, one to store the angular flux vector and another to store the previous fission and scattering source vector.

Algorithm 4.2 One-Sweep Rayleigh Quotient Fixed Point Method for the Alpha-Eigenvalue Problem

---

while residual > tolerance **do**

   if $i = 0$ **then**

$$\alpha_{(i)} = \frac{\mathbf{\Psi}_{(i)}^T \mathbf{L}^+ \left(\Sigma_{\mathbf{s}} + \Sigma_{\mathbf{f}} \right) \mathbf{L} \mathbf{\Psi}_{(i)}}{\mathbf{\Psi}_{(i)}^T \mathbf{V}_{\mathbf{z}}^{-1} \mathbf{\Psi}_{(i)}}.$$

$$\mathbf{q}_{(i)} = \left(-\alpha_{(i)} \mathbf{V}_{\mathbf{z}}^{-1} + \mathbf{L}^+ \left(\Sigma_{\mathbf{s}} + \Sigma_{\mathbf{f}} \right) \mathbf{L} \right) \mathbf{\Psi}_{(i)}$$

$$\mathbf{\Psi}_{(i+1)} = \mathbf{H}_{\mathbf{z}}^{-1} \mathbf{q}_{(i)}$$

   else

$$\alpha_{(i)} = \frac{\mathbf{\Psi}_{(i)}^T \mathbf{L}^+ \left(\Sigma_{\mathbf{s}} + \Sigma_{\mathbf{f}} \right) \mathbf{L} \mathbf{\Psi}_{(i)} - \mathbf{\Psi}_{(i)}^T \mathbf{q}_{(i-1)}}{\mathbf{\Psi}_{(i)}^T \mathbf{V}_{\mathbf{z}}^{-1} \mathbf{\Psi}_{(i)}}.$$

$$\mathbf{q}_{(i)} = \left(-\alpha_{(i)} \mathbf{V}_{\mathbf{z}}^{-1} + \mathbf{L}^+ \left(\Sigma_{\mathbf{s}} + \Sigma_{\mathbf{f}} \right) \mathbf{L} \right) \mathbf{\Psi}_{(i)}$$

$$\mathbf{\Psi}_{(i+1)} = \mathbf{H}_{\mathbf{z}}^{-1} \mathbf{q}_{(i)}$$

   end if

$$\text{residual} = \frac{\left\| \mathbf{\Psi}_{(i+1)} - \mathbf{\Psi}_{(i)} \right\|_2}{\left\| \mathbf{\Psi}_{(i+1)} \right\|_2}$$

  end while

4.2 Derivation of the Rayleigh Quotient Fixed Point Method for k-Effective Problems

Derivation of the k-effective Rayleigh Quotient Fixed Point Method follows a similar procedure as the alpha-eigenvalue RQFP. We begin with the discretized k-effective eigenvalue matrix equation:

$$\mathbf{H}_{\mathbf{z}} \mathbf{\Psi}_{\mathbf{z}} = \mathbf{L}^+ \left(\Sigma_{\mathbf{s}} + \frac{1}{k} \Sigma_{\mathbf{f}} \right) \mathbf{L} \mathbf{\Psi}_{\mathbf{z}}, \tag{4.12}$$

Once again, we search for the eigenpair $(k, \mathbf{\Psi})$ that satisfies Eq. 4.12. We write Eq. 4.12 in the fixed point form

$$\mathbf{\Psi}_{\mathbf{z}} = \mathbf{H}_{\mathbf{z}}^{-1} \left[\mathbf{L}^+ \left(\Sigma_{\mathbf{s}} + \frac{1}{k} \Sigma_{\mathbf{f}} \right) \mathbf{L} \right] \mathbf{\Psi} \equiv \mathbf{T}(k) \mathbf{\Psi}_{\mathbf{z}}. \tag{4.13}$$

For all systems, the righthand side of Eq. 4.13 is nonnegative for isotropic scattering and k is nonnegative [37]. The fixed point form is selected to only require the inversion of the matrix $\mathbf{H_z}$. We define an iterative method to find the fixed point of Eq. 4.13 as

$$\mathbf{\Psi_z}^{(i+1)} = \mathbf{T}(k^{(i)})\mathbf{\Psi_z}^{(i)}. \tag{4.14}$$

From some initial positive starting vector $\mathbf{\Psi_z}^{(0)}$, the subsequent eigenvector iterate is determined by the action of inversion of the matrix $\mathbf{H_z}$ on the scattering and fission source where the fission source is adjusted by the k-effective eigenvalue. At each iteration, an update for the eigenvalue is required. If $(k_*, \mathbf{\Psi_z^*})$ is an eigenpair of Eq. 4.14, it follows that

$$\mathbf{\Psi_z}^* = \mathbf{T}(k_*)\mathbf{\Psi_z^*} \tag{4.15}$$

is also an eigenvalue problem with eigenpair $(\mathbf{1}, \mathbf{\Psi_z^*})$.

Similar to the alpha-eigenvalue matrix $\mathbf{A}(\alpha)$, if the matrix $\mathbf{T}(k)$ is a primitive matrix, it follows from the Perron-Froebenius Theorem for Primitive Matrices that there is only one unique positive eigenvector of $\mathbf{T}(k)$ corresponding to the dominant eigenvalue. This fact allows us to derive an update for the k-effective eigenvalue at each iteration.

Suppose $\mathbf{\Psi}_{(i)}$ is an approximate eigenvector and we seek to find the best approximate eigenvalue $\hat{\lambda}$ such that

$$\hat{\lambda} = \arg\min_{\mu} \left\| \mathbf{T}(k_{(i)})\mathbf{\Psi}_{(i)} - \mu\mathbf{\Psi}_{(i)} \right\|_2^2. \tag{4.16}$$

This is, once again, a linear least squares problem in the variable μ. From before, it is found that the Rayleigh quotient given by

$$\hat{\lambda} = \frac{\mathbf{\Psi}_{(i)}^T \mathbf{T}(k_{(i)})\mathbf{\Psi}_{(i)}}{\mathbf{\Psi}_{(i)}^T \mathbf{\Psi}_{(i)}}, \tag{4.17}$$

minimizes the residual in the least square sense. Setting the Rayleigh quotient to one and solving for the k-effective eigenvalue $k_{(i)}$, we obtain the k-effective eigenvalue update for eigenvector iterate $\mathbf{\Psi}_{(i)}$

$$k_{(i)} = \frac{\mathbf{\Psi}_{(i)}^T \mathbf{H_z}^{-1}\mathbf{L}\mathbf{\Sigma_f}\mathbf{L}^+\mathbf{\Psi}_{(i)}}{\mathbf{\Psi}_{(i)}^T \mathbf{\Psi}_{(i)} - \mathbf{\Psi}_{(i)}^T \mathbf{H_z}^{-1}\mathbf{L}\mathbf{\Sigma_s}\mathbf{L}^+\mathbf{\Psi}_{(i)}}. \tag{4.18}$$

Given Eq. 4.18, we introduce Algorithm 4.3, an iterative scheme to determine the k-effective eigenvalue and its corresponding eigenvector. The eigenvalue update is optimal in the least squares sense.

For each iteration of Algorithm 4.3, two transport sweeps are required to determine the transported fission and scattering terms. To require only one transport sweep, we rewrite Eq. 4.18 as

$$k_{(i)} = \frac{\mathbf{\Psi}_{(i)}^T \mathbf{L}\mathbf{\Sigma_f}\mathbf{L}^+\mathbf{\Psi}_{(i)}}{\mathbf{\Psi}_{(i)}^T \mathbf{H_z}\mathbf{\Psi}_{(i)} - \mathbf{\Psi}_{(i)}^T \mathbf{L}\mathbf{\Sigma_s}\mathbf{L}^+\mathbf{\Psi}_{(i)}}. \tag{4.19}$$

Algorithm 4.3 Rayleigh Quotient Fixed Point Method for the k-Effective Eigenvalue Problem

---

while residual > tolerance **do**

$$k_{(i)} = \frac{\mathbf{\Psi}_{(i)}^T \mathbf{H_z}^{-1} \mathbf{L} \mathbf{\Sigma_f} \mathbf{L}^+ \mathbf{\Psi}_{(i)}}{\mathbf{\Psi}_{(i)}^T \mathbf{\Psi}_{(i)} - \mathbf{\Psi}_{(i)}^T \mathbf{H_z}^{-1} \mathbf{L} \mathbf{\Sigma_s} \mathbf{L}^+ \mathbf{\Psi}_{(i)}}$$

$$\mathbf{\Psi}_{(i+1)} = \mathbf{H_z}^{-1} \left[\mathbf{L}^+ \left(\mathbf{\Sigma_s} + \frac{1}{k_{(i)}} \mathbf{\Sigma_f} \right) \mathbf{L} \right] \mathbf{\Psi}_{(i)}$$

$$\text{residual} = \frac{\left\| \mathbf{\Psi}_{(i+1)} - \mathbf{\Psi}_{(i)} \right\|_2}{\left\| \mathbf{\Psi}_{(i+1)} \right\|_2}$$

end while

Using the fact that

$$\mathbf{H_z}\mathbf{\Psi}_{(i)} = \left[\mathbf{L}^+ \left(\mathbf{\Sigma_s} + \frac{1}{k} \mathbf{\Sigma_f} \right) \mathbf{L} \right] \mathbf{\Psi}_{(i-1)} \equiv \mathbf{q}_{(i-1)}, \tag{4.20}$$

we can write the update, Eq. 4.21 as

$$k_{(i)} = \frac{\mathbf{\Psi}_{(i)}^T \mathbf{L} \mathbf{\Sigma_f} \mathbf{L}^+ \mathbf{\Psi}_{(i)}}{\mathbf{\Psi}_{(i)}^T \mathbf{q}_{(i-1)} - \mathbf{\Psi}_{(i)}^T \mathbf{L} \mathbf{\Sigma_s} \mathbf{L}^+ \mathbf{\Psi}_{(i)}}. \tag{4.21}$$

We introduce Algorithm 4.4, a one-sweep variant of Algorithm 4.3. For the initial iteration, $k_{(0)} = 1$. Algorithm 4.4 requires only one transport sweep per iteration of the method. However, it requires three vectors to store the angular flux and fission and scattering sources. For some angular flux iterates, it has been observed that the k-effective eigenvalue iterate can be negative for some iterations. However, in practice, this has not prevented convergence of the method to a positive eigenvalue.

Algorithm 4.4 One-Sweep Rayleigh Quotient Fixed Point Method for the k-Effective Eigenvalue Problem

---

$\quad$ **while** residual $>$ tolerance **do**

$\qquad$ **if** $i = 0$ **then**

$$\mathbf{q}_{(i)} = \left[\mathbf{L}^{+}\left(\mathbf{\Sigma_s} + \mathbf{\Sigma_f}\right)\mathbf{L}\right]\mathbf{\Psi}_{(i)}$$

$$\mathbf{\Psi}_{(i+1)} = \mathbf{H_z}^{-1}\mathbf{q}_{(i)}$$

$\qquad$ **else**

$$k_{(i)} = \frac{\mathbf{\Psi}_{(i)}^{T}\mathbf{L}\mathbf{\Sigma_f}\mathbf{L}^{+}\mathbf{\Psi}_{(i)}}{\mathbf{\Psi}_{(i)}^{T}\mathbf{q}_{(i-1)} - \mathbf{\Psi}_{(i)}^{T}\mathbf{L}\mathbf{\Sigma_s}\mathbf{L}^{+}\mathbf{\Psi}_{(i)}}.$$

$$\mathbf{q}_{(i)} = \left[\mathbf{L}^{+}\left(\mathbf{\Sigma_s} + \frac{1}{k_{(i)}}\mathbf{\Sigma_f}\right)\mathbf{L}\right]\mathbf{\Psi}_{(i)}$$

$$\mathbf{\Psi}_{(i+1)} = \mathbf{H_z}^{-1}\mathbf{q}_{(i)}$$

$\qquad$ **end if**

$$\text{residual} = \frac{\left\|\mathbf{\Psi}_{(i+1)} - \mathbf{\Psi}_{(i)}\right\|_2}{\left\|\mathbf{\Psi}_{(i+1)}\right\|_2}$$

$\quad$ **end while**

Chapter 5

Eigenvalues for Infinite Medium Problems

In this section we describe the performance of the Rayleigh quotient methods for various infinite medium problem selected from the *Analytical Benchmark Test Set for Criticality Code Verification* [33] or analytical benchmark solutions. Some problems were selected that did not meet the assumptions used in deriving the methods to test the general applicability of the Rayleigh quotient methods. The Rayleigh quotient method was compared to the critical search method [16] for alpha-eigenvalue problems and to standard power iteration for k-effective eigenvalue problems. The total number of transport sweeps was compared for each method as they represent the majority of computational expensive in standard transport codes. The methods were implemented in ARDRA, a 1D, 2D, and 3D deterministic discrete ordinates neutron and gamma transport code developed and maintained by Lawrence Livermore National Laboratory [15].

5.1 Criticality Benchmark One-Speed Verification for Various Critical and Supercritical Problems

A set of six infinite medium supercritical problems were selected from the *Analytical Benchmark Test Set for Criticality Code Verification* [33] to test the Rayleigh quotient fixed point method for both alpha-eigenvalue and k-effective eigenvalue problems. These problems were selected as they contained cross sections of commonly used fissile isotopes in nuclear engineering applications such as plutonium-239 and uranium-235 (Table 5.1). The reference eigenvalues for these problems can be seen in Table 5.2. For one-speed problems, the velocity was set to 1 cm/s unless otherwise noted.

For the supercritical one-speed criticality benchmark problems, the alpha-eigenvalue Rayleigh quotient fixed point method performed substantially better than the critical search method, reducing the number of transport sweeps by a factor of 10-20 (Table 5.2a). Due to the critical search method requiring at least two k-effective eigenvalue calculations to bracket

Table 5.1: Plutonium and Uranium Cross Sections for Infinite Medium Problems (cm^{-1}) [33]

Cross Section Set	σ	$\nu\sigma_f$	σ_s	v [cm/s]
PUa	0.32640	0.264384	0.225216	1.0
PUb	0.231744	0.264384	0.225216	1.0

(a) PU Cross Section Sets

Cross Section Set	σ	$\nu\sigma_f$	σ_s	v [cm/s]
Ua	0.32640	0.176256	0.248064	1.0
Ub	0.32640	0.18259475328	0.248064	1.0
Uc	0.32640	0.17673306624	0.248064	1.0
Ud	0.32640	0.17489804544	0.248064	1.0

(b) U Cross Section Sets

the alpha-eigenvalue, the number of sweeps increases rapidly. The computation expense of one iteration of the RQFP method is the same as one iteration of the k-effective eigenvalue calculation. During the k-effective eigenvalue calculation, the alpha-eigenvalue iterate is held constant. Since there is no need for any intermediate calculations, the Rayleigh quotient fixed point method can calculate the eigenvalue/eigenvector pair directly, avoiding this drawback of the critical search method and drastically reducing the number of total sweeps necessary. Convergence behavior of the alpha-eigenvalue RQFP for an infinite medium problem can be seen in Figure 5.1. For these very supercritical systems, the Rayleigh quotient fixed point method was able to calculate the supercritical alpha-eigenvalues without issue.

The RQFP for the k-effective eigenvalue reduces the number of sweeps by a factor of three (Table 5.2b) as compared to the power method with the fission source norm update. In these particular problems, all cells contain fissile material and the angular flux is exactly equal to the fission source to some constant. The rapid convergence of the angular flux by the Rayleigh quotient fixed point method as compared to the power method with fission source norm update results in a substantial reduction in the number of transport sweeps necessary to converge the eigenvector/eigenvalue. While the convergence of the method is linear, it appears in practice to have a lower asymptotic constant coefficient than the power method as seen in Figure 5.2.

Table 5.2: Reference Eigenvalues and Transport Sweep Comparisons for Infinite Medium Problems in [33]

Cross Section Set	Reference α_∞	Transport Sweeps	
		RQFP	Critical Search
PUa	0.1632	33	432
PUb	0.1306	21	391
Ua	0.1265	24	472
Ub	0.1347	24	464
Uc	0.1271	24	474
Ud	0.1247	24	472

(a) Alpha-Eigenvalue: Comparison of RQFP and Critical Search Transport Sweeps

Cross Section Set	Reference k_∞	Transport Sweeps	
		RQFP	Power Method
PUa	2.612903	41	111
PUb	2.290323	34	96
Ua	2.25	29	130
Ub	2.330917	30	132
Uc	2.256083	27	131
Ud	2.232667	33	131

(b) k-Effective: Comparison of RQFP and Power Method Transport Sweeps

PUa-1-0-IN (Infinite Medium)
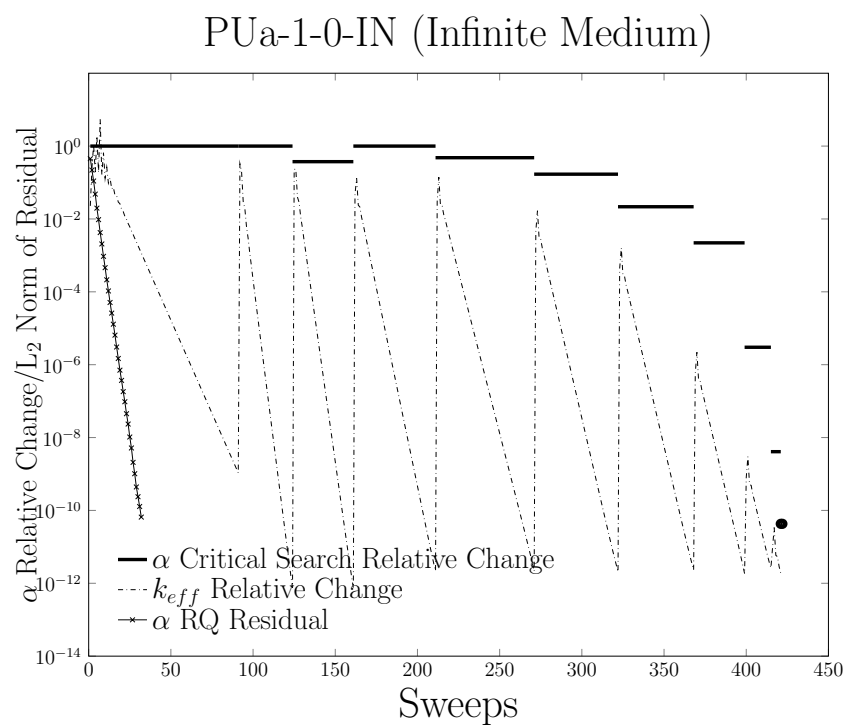
Figure 5.1: Convergence of Rayleigh Quotient Fixed Point and Critical Search Methods for Plutonium Infinite Medium Problem
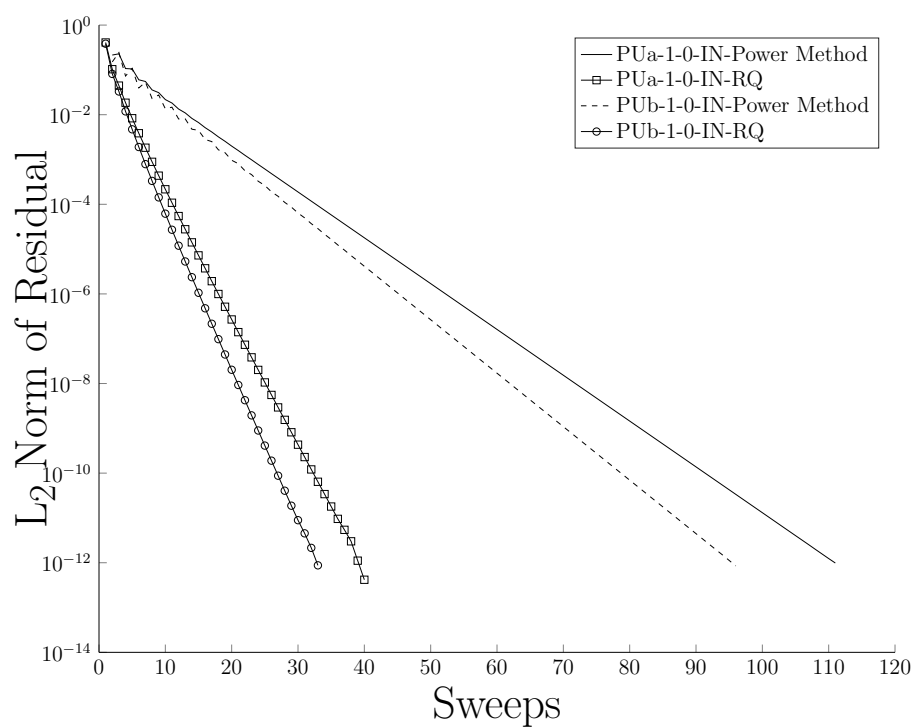
Figure 5.2: Eigenvector Residual as a Function of Sweeps for Two Infinite Medium k-Effective Eigenvalue Problems

5.2 Infinite Medium Multigroup Problems

5.2.1 Infinite Medium Subcritical/Critical Problems

Problem 5.2.1.1: We consider a three energy group problem with cross sections shown in Table 5.3. The problem only has fissions in energy group $g = 3$ emitting $\bar{\nu}$ neutrons in energy group $g = 1$. There is no upscatter and downscatter only occurs into the next group. We vary $\bar{\nu}$ from zero neutrons emitted in fission to $\bar{\nu} = 3$ to create various subcritical systems. The analytic k-eigenvalue is given by

$$k = \frac{\bar{\nu}\sigma_{f,1}\sigma_{s12}\sigma_{s23}}{\sigma_1\sigma_2\sigma_3}, \tag{5.1}$$

and the analytical alpha-eigenvalue can be calculated from the system

$$\begin{pmatrix} -v_1\sigma_1 & v_1\sigma_{s12} & 0 \\ 0 & -v_2\sigma_2 & v_2\sigma_{s23} \\ v_1\bar{\nu}\sigma_{f1} & 0 & -v_3\sigma_3 \end{pmatrix} \begin{pmatrix} \phi_1 \\ \phi_2 \\ \phi_3 \end{pmatrix} = \alpha \begin{pmatrix} \phi_1 \\ \phi_2 \\ \phi_3 \end{pmatrix}. \tag{5.2}$$

The reference eigenvalues and the number of transport sweeps needed to converge the eigenvector residuals to a value of 10^{-8} are seen in Table 5.4.

For alpha-eigenvalue problems, the Rayleigh quotient fixed point method is able to converge the various subcritical problems to the correct eigenvalue. The number of sweeps necessary varies with the most subcritical and closest to critical problems requiring more sweeps to converge the angular flux. The critical search method is unable to converge these problems as the sum of the total cross section and the negative eigenvalue introduces negative absorption into the system (Table 5.4a). This pseudo-absorption term causes instabilities in the transport sweep algorithm and forces the method to terminate before convergence. We see that for even simple, three energy group, subcritical problems, the Rayleigh quotient fixed point method is able to converge very subcritical problems and critical problems without difficulty.

For k-effective eigenvalue problems, the Rayleigh quotient fixed point method requires a similar number of sweeps for all values of k_∞. It requires approximately 40% more iterations as compared to the traditional power method (Table 5.4b). One reason for this is that the fission source of Problem 5.1.1 is simple with fissions only occurring in the highest energy group and neutrons are only born in the lowest energy group. Using the fission distribution as the norm is better in this particular case because it does not require all energy group scalar fluxes to converge.

5.2.2 Analytical Infinite Medium Supercritical Problems

Problem 5.2.2.1: We consider a $G = 81$ energy group medium with cross sections shown in Table 5.5. Neutrons can only downscatter to the next energy group and prompt fissions in energy group $g = 81$ emit $\bar{\nu} = 2.5$ neutrons per fission into energy group $g = 1$.

Table 5.3: Infinite Medium Subcritical Problem Cross Sections (cm^{-1})

g	σ	σ_f	$\sigma_{sg,g+1}$	χ	v_g [cm/s]
1	6.0	0.0	5.0	1.0	4.0
2	5.0	0.0	4.0	0.0	2.0
3	4.0	2.0	0.0	0.0	1.0

Table 5.4: Reference Eigenvalues/Transport Sweeps for Convergence for Problem 5.1.1

$\bar{\nu}$	α_∞	Transport Sweeps		$\bar{\nu}$	α_∞	Transport Sweeps	
		RQFP	Critical Search			RQFP	Critical Search
0.30	-3.30687	89	*	1.80	-1.15114	48	*
0.60	-2.75305	48	*	2.10	-0.83485	56	*
0.90	-2.28186	35	*	2.40	-0.53965	66	*
1.20	-1.86682	38	*	2.70	-0.26222	77	*
1.50	-1.49303	43	*	3.00	0.00000	91	*

*Did Not Converge

(a) Alpha-Eigenvalue: Comparison of RQFP and Critical Search Transport Sweeps

$\bar{\nu}$	k_∞	Transport Sweeps		$\bar{\nu}$	k_∞	Transport Sweeps	
		RQFP	Power Method			RQFP	Power Method
0.30	0.10	76	53	1.80	0.60	74	50
0.60	0.20	74	49	2.10	0.70	74	51
0.90	0.30	74	40	2.40	0.80	72	51
1.20	0.40	74	48	2.70	0.90	72	51
1.50	0.50	74	50	3.00	1.00	72	52

(b) k-Effective Eigenvalue: Comparison of RQFP and Power Method Transport Sweeps

The total cross sections σ_g, neutron speeds v_g, and neutron removal cross sections are the same for all groups. With these cross sections, this unphysical problem yields an analytical solution for both k-effective and alpha-eigenvalues. The k-effective eigenvalue is given by

$$k = \frac{\bar{\nu}\sigma_f(\sigma_{sg,g+1})^{G-1}}{(\sigma_g)^G} = 1.11663. \tag{5.3}$$

Using the multigroup equations, the analytical expression for the alpha-eigenvalues is found to be

$$\frac{\alpha_n}{v} = -(\sigma_g - \sigma_f) + \sigma_{sg,g+1}\left[\bar{\nu}^{G-1}\exp\left(\frac{2\pi in}{G}\right) - 1\right], \text{ for } n = 0, \ldots, G-1. \tag{5.4}$$

The alpha-eigenvalues are located along a circle in the complex plane centered on the real axis at $\text{Re}(\alpha) = -(\sigma_g - \sigma_f)$ with radius $r = \bar{\nu}^{G-1}\sigma_{gs,s+1}$. Using this expression, the fundamental alpha-eigenvalue is found to be $\alpha_0 = 0.13765$ s^{-1}.

The number of transport sweep needed to converge to a eigenvalue residual of 10^{-8} for Problem 2 can be seen in Table 5.6. We note that the alpha-eigenvalue Rayleigh quotient fixed point method does not converge for this problem. The failure to converge for this problem can be explained as follows. The alpha-eigenvalue spectrum for Problem 5.2 can be seen in Figure 5.3 and shows that all eigenvalue lie on a circle. Therefore, all eigenvalues are equal in magnitude. Since the Rayleigh quotient fixed point method is looking for the positive eigenvector corresponding to the dominant eigenvalue, it is unable to find the unique eigenvalue corresponding to the positive eigenvector. The spectral radius of the Jacobian matrix of the Rayleigh quotient fixed point method at the fixed point was found to be larger than one, implying the method will not converge as seen in practice. It is interesting to note the method cycles with period 81, indicating that it goes through every single eigenvalue unsuccessfully before failing to converge.

Both the k-effective eigenvalue Rayleigh quotient fixed point method and the power method converge for this particular problem requiring a similar number of iterations. The fact that the k-effective eigenvalue is the dominant eigenvalue with a corresponding positive eigenvector allows the Rayleigh quotient method fixed method to converge to the right eigenvalue and eigenvector. In this particular problem, all other eigenvalues except for the dominant eigenvalue are zero. Both methods require a large amount of iterations, reflecting the unphysical nature of the problem cross sections.

Table 5.5: Infinite Medium 81-Group Problem Cross Sections (cm^{-1})

g	σ	σ_f	$\sigma_{sg,g+1}$	χ	v_g [cm/s]
1	101.0	0.0	100.0	1.0	1.0
2-80	101.0	0.0	100.0	0.0	1.0
81	101.0	100.0	0.0	0.0	1.0
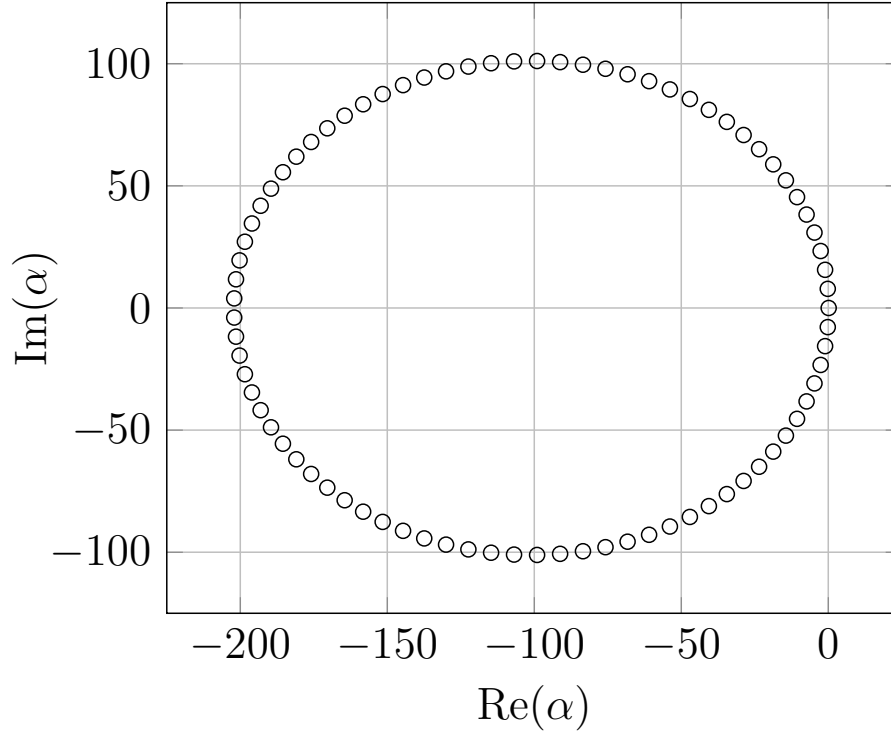
Figure 5.3: Alpha-Eigenvalue Spectrum for Problem 5.2.2.1

Table 5.6: Transport Sweeps for Convergence for Problem 5.2.2.1

Transport Sweeps			
kRQ	kPM	αRQ	αCS
6701	6707	*	63843

*Did Not Converge

Problem 5.2.2.2: We consider a problem similar to Problem 5.2.1.1 where the energy group velocities are group-dependent. The velocity of each group is given by $v_g = 82 - g$ and the cross sections are the same as Problem 5.2.1.1 (Table 5.7). The k-effective eigenvalue remains 1.11663 as only the velocity terms have been modified. The problem no longer has an analytical expression for the alpha-eigenvalue spectrum. The dominant alpha-eigenvalue is found to be 2.2464 s^{-1} from numerical eigenvalue solvers. With the change in the velocity, the alpha-eigenvalue spectrum eigenvalues are no longer on a circle (Figure 5.4). Instead, the eigenvalues are along elliptical shapes with very negative real eigenvalues now existing. We also note that there are complex eigenvalues whose real parts are larger than zero, a phenomenon unexpected for alpha-eigenvalue problems where only the dominant eigenvalue has real part larger than zero for supercritical systems.

Similar to Problem 5.2.2.1, the alpha-eigenvalue Rayleigh quotient method does not converge for this method. The spectral radius of the Jacobian matrix for the fixed point formulation evaluated at the fixed point is found to be larger than one, implying the method will not converge for this problem. The critical search method is able to converge the alpha-eigenvalue. However, it requires a large number of iterations (Table 5.8).

Also similar to Problem 5.2.2.1, both the Rayleigh quotient fixed point method and power method were able to converge the k-effective eigenvalue. This is expected as the only change from Problem 5.2.2.1 was in the group velocities which do not matter in the k-effective eigenvalue problem. The number of transport sweeps required to converge the problem did not change.

Table 5.7: Infinite Medium 81-Group Problem Cross Sections (cm^{-1}), Velocity Modification

| g	σ	σ_f	$\sigma_{sg,g+1}$	χ	v_g [cm/s]
1	101.0	0.0	100.0	1.0	1.0
2-80	101.0	0.0	100.0	0.0	2.0-80.0
81	101.0	100.0	0.0	0.0	81.0
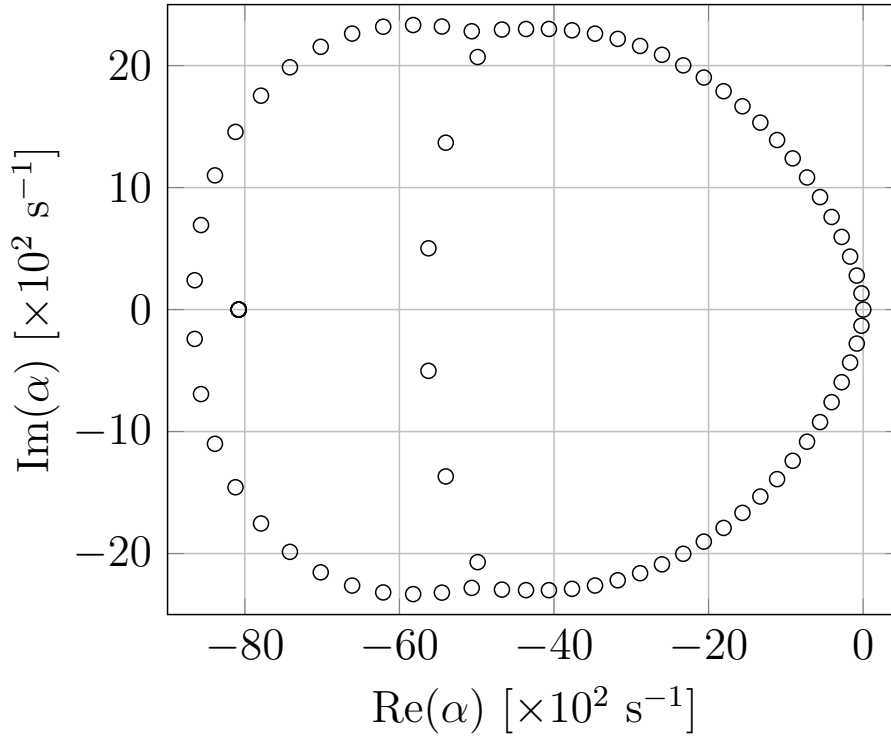
Figure 5.4: Alpha-Eigenvalue Spectrum for Problem 5.2.2.2

Table 5.8: Transport Sweeps for Convergence for Problem 5.2.2.2

	Transport Sweeps		
kRQ	kPM	αRQ	αCS
6701	6707	*	50773

*Did Not Converge

Problem 5.2.2.3: We consider another problem similar to Problem 5.2.1.1 where we now allow downscattering from energy group $g \to g'$ over several energy groups with equal probability where $g + 1 \leq g' \leq g + 5$. For the last five energy groups, the downscattering cross section is equally distributed among the remaining groups where $g + 1 \leq g' \leq G$. The total scattering cross section remains unchanged. The k-effective eigenvalue is 1.8853 and the alpha-eigenvalue is 2.2914 s^{-1}.

The alpha-eigenvalue spectrum seen in Figure 5.5 is significantly different to that of Problem 5.2.2.1. The spectrum contains more eigenvalues with large real negative parts. This is due to neutrons being able to downscatter quickly by skipping several energy groups.

The alpha-eigenvalue Rayleigh quotient method was able to converge on the analytical alpha-eigenvalue. By allowing downscattering to more energy groups, the Jacobian of the fixed point method at the fixed point is now less than one, allowing the convergence of the method. In this particular problem, the alpha-eigenvalue Rayleigh quotient method vastly outperforms the critical search method. The critical search method requires 20 times the number of sweeps than the Rayleigh quotient fixed point method. This is caused by the need for multiple k-effective eigenvalue calculations to bracket the alpha-eigenvalue.

Both the Rayleigh quotient fixed point and power method were able to converge the eigenvalue and eigenvector for the k-effective eigenvalue problem requiring a similar number of iterations.

Table 5.9: Transport Sweeps for Convergence for Problem 5.2.2.3

	Transport Sweeps		
kRQ	kPM	αRQ	αCS
5306	5080	5516	105570

*Did Not Converge

5.3 Conclusion

The RQFP method for alpha- and k-effective eigenvalues performs well for infinite medium problems, reducing in certain cases the number of iterations up to a factor of twenty. For the
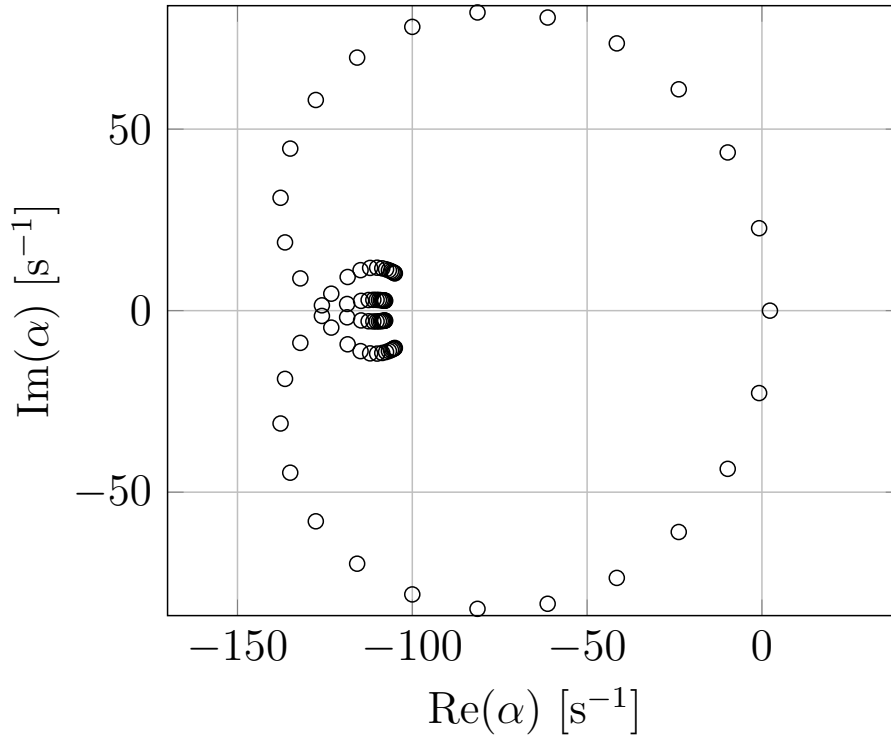
Figure 5.5: Alpha-Eigenvalue Spectrum for Problem 5.2.2.3

alpha-eigenvalue RQFP method, the method is able to converge subcritical systems without issue. For a certain class of problems with unphysical cross sections, the alpha-eigenvalue RQFP method fails to converge. This failure to converge is caused by the structure of the alpha-eigenvalue spectrum. However, these problems are special cases with unphysical data such as unit velocity in all energy groups. For this reason, we believe the alpha-eigenvalue RQFP method is robust for all infinite-medium problems of interest. The RQFP method for k-effective eigenvalue calculations performed better or similar to the power method with a fission norm update for the eigenvalue. For problems where only the number of neutrons emitted in fission was varied, the RQFP method took a similar number of iterations to converge for all problems, no matter the criticality of the system. This suggests that the method's convergence is determined by the eigenvector shape rather than the eigenvalue.

Chapter 6

Eigenvalues of Slabs and Spheres

In this chapter we verify the correctness and examine the performance of the Rayleigh quotient fixed point methods for one-dimensional media such as slabs and one-dimensional spheres. In slab geometry, the phase space of the neutron transport equation is simplified with only one position variable x and one angular variable μ defined as the x-direction cosine. For slab geometry, the alpha- and k-effective eigenvalue neutron transport equations are given by Eq. 6.1 and Eq. 6.2, respectively:

$$
\left[\mu\frac{\partial}{\partial x} + \frac{\alpha}{v(E)} + \sigma(x, E)\right]\psi(x, \mu, E)
$$
$$
= \frac{\chi(E)}{2}\int_0^\infty dE'\,\nu(E')\sigma_f(x, E')\int_{-1}^1 d\mu'\,\psi(x, \mu', E)
$$
$$
+ \frac{1}{2}\int_0^\infty dE'\,\sigma_s(x, E' \to E)\int_{-1}^1 d\mu'\,\psi(x, \mu', E), \quad (6.1)
$$

$$
\left[\mu\frac{\partial}{\partial x} + \sigma(x, E)\right]\psi(x, \mu, E)
$$
$$
= \frac{1}{k}\frac{\chi(E)}{2}\int_0^\infty dE'\,\nu(E')\sigma_f(x, E')\int_{-1}^1 d\mu'\,\psi(x, \mu', E)
$$
$$
+ \frac{1}{2}\int_0^\infty dE'\,\sigma_s(x, E' \to E)\int_{-1}^1 d\mu'\,\psi(x, \mu', E). \quad (6.2)
$$

Various homogeneous and heterogeneous slab geometry problems with vacuum boundary conditions were modeled in ARDRA. These slab media problems consist of multiplying and non-multiplying materials with thicknesses Δ. Alpha- and k-effective eigenvalues were calculated and the number of transport sweeps compared to various methods such as the critical search method and the power method. To verify the correctness of the Rayleigh quotient fixed point method (RQFP), the method was compared to various methods such

as Green's Function Method (GFM) and Direct Evaluation (DE) and compared to other discrete ordinate neutron transport codes such as PARTISN/DANT.

In one-dimensional spherical geometry, there is only one position variable r, the radial position from the center of the sphere, and one angular variable μ defined as the direction cosine with respect to the radial direction. For spherical geometry, the alpha- and k-effective eigenvalue neutron transport equations are given by Eq. 6.3 and Eq. 6.4, respectively:

$$\frac{\mu}{r^2}\frac{\partial}{\partial r}\left[r^2\psi(r,\mu,E)\right] + \frac{1}{r}\frac{\partial}{\partial \mu}\left[(1-\mu^2)\psi(r,\mu,E)\right] + \sigma(x,E)\psi(r,\mu,E)$$
$$= \frac{1}{k}\frac{\chi(E)}{2}\int_0^\infty dE'\,\nu(E')\sigma_f(r,E')\int_{-1}^1 d\mu'\,\psi(r,\mu',E)$$
$$+ \frac{1}{2}\int_0^\infty dE'\,\sigma_s(r,E'\to E)\int_{-1}^1 d\mu'\,\psi(r,\mu',E), \quad (6.3)$$

$$\frac{\mu}{r^2}\frac{\partial}{\partial r}\left[r^2\psi(r,\mu,E)\right] + \frac{1}{r}\frac{\partial}{\partial \mu}\left[(1-\mu^2)\psi(r,\mu,E)\right] + \left[\frac{\alpha}{v(E)} + \sigma(x,E)\right]\psi(r,\mu,E)$$
$$= \frac{\chi(E)}{2}\int_0^\infty dE'\,\nu(E')\sigma_f(r,E')\int_{-1}^1 d\mu'\,\psi(r,\mu',E)$$
$$+ \frac{1}{2}\int_0^\infty dE'\,\sigma_s(r,E'\to E)\int_{-1}^1 d\mu'\,\psi(r,\mu',E). \quad (6.4)$$

For one-dimensional spherical geometry, various homogeneous and heterogeneous spherical problems with vacuum boundary conditions were modeled in ARDRA. Using the same cross-sections for multiplying and non-multiplying materials as the slab media problems, equivalent spherical systems were created using the Davison sphere-equivalence theorem [10] and the alpha-eigenvalue calculated. To verify the correctness of the RQFP for one-dimensional spherical geometry, the method was compared to GFM. Performance of the RQFP for one-dimensional spherical problems was measured by comparing the number of transport sweeps necessary for convergence as compared to the critical search method.

6.1 One-Speed Verification for Slab Geometry

For five one-speed non-multiplying slabs, calculated alpha-eigenvalues were benchmarked to the GFM [22], described in Section 2.3.1. For these sets of problems, the neutron speed was set to $v = 1$ cm/s and the total cross section set to unity $\sigma = 1$ cm^{-1}. The slabs were purely scattering (Table 6.1). Problem thicknesses Δ were in mean free paths (mfps).

Table 6.1: Non-Multiplying Homogeneous Slab Cross Sections (cm^{-1})

σ	$\nu\sigma_f$	σ_s	v [cm/s]
1.0	0.0	1.0	1.0

For multiplying media, 22 one-speed slabs of varying thickness Δ were examined and the Rayleigh quotient fixed point calculated alpha-eigenvalues were benchmarked to the GFM. The total cross section was set to unity and the slab neutron multiplication set to $\nu\sigma_f = 0.25$. The scattering cross section was set to $\sigma_s = 0.9$ cm^{-1} (Table 6.2).

Table 6.2: Multiplying Homogeneous Slab Cross Sections (cm^{-1})

σ	$\nu\sigma_f$	σ_s	v [cm/s]
1.0	0.25	0.9	1.0

Five one-speed heterogeneous slab problems consisting of two materials were examined and the Rayleigh quotient fixed point calculated alpha-eigenvalues compared to the GFM, direct evaluation (DE) [28], and DANT/PARTISN [2]. With a fixed maximum medium width, material slabs of thickness Δ with cross sections as seen in Table 6.3 were alternated until reaching the maximum fixed width. The impact of material widths on the alpha-eigenvalue was examined for this non-multiplying medium.

Table 6.3: Non-Multiplying Heterogeneous Slab Material Cross Sections (cm^{-1})

Material	σ	$\nu\sigma_f$	σ_s	v_g [cm/s]
1	10.0	0.0	10.0	1.0
2	10.0	0.0	9.0	1.0
Homogeneous	10.0	0.0	9.5	1.0

A two-region multiplying slab was examined with material properties as seen in Table 6.4. The problem consisted of a 1.5 mfp region on the right and a 1.0 mfp region to the left. Both materials were multiplying and the system was supercritical [21].

Table 6.4: Multiplying Heterogeneous Slab Material Cross Sections (cm^{-1})

Material	σ	$\nu\sigma_f$	σ_s	v_g [cm/s]
1	1.0	0.6	0.9	1.0
2	1.0	0.3	0.2	1.0

Four one-speed five region slab problems consisting of fuel, moderator, and absorber materials were examined and the Rayleigh quotient fixed point method alpha-eigenvalue compared to the GFM. The leftmost fuel pin width was allowed to vary (see Figure 6.5).The alpha-eigenvalue was calculated for different fuel width thicknesses with the fuel having $\nu\sigma_f = 0.3$ or 0.7. Cross sections for the three materials are seen in Table 6.5.

Table 6.5: Five Region Slab Material Cross Sections (cm^{-1})

Material	σ	$\nu\sigma_f$	σ_s	v_g [cm/s]
Fuel	1.0	0.3/0.7	0.8	1.0
Moderator	1.0	0.0	0.8	1.0
Absorber	1.0	0.0	0.1	1.0

6.1.1 Non-Multiplying Homogeneous Slab

For the one-speed, purely-scattering, homogeneous slabs of thicknesses $\Delta = 1.0$ to $\Delta = 25.0$ mfp with cross sections shown in Table 6.1, the Rayleigh quotient fixed point method showed good agreement with the GFM (Table 6.6). For diamond difference discretization ($M = 500$ cells) and S_{64} discrete ordinates quadrature ($L = 64$), the subcritical alpha-eigenvalues matched within less than 0.1% relative error. 500 spatial cells and 64 angular quadrature points were selected to guarantee the positivity of the flux solution for all slab widths. The greatest discrepancy between the two methods was for $\Delta = 1.0$ mfp. As the slab thickness gets smaller, the existence of a dominant alpha-eigenvalue is not assured and we begin to see this behavior. As the slab thickness increases, the number of transport sweeps necessary to converge the alpha-eigenvalue to a tolerance of 10^{-12} increases. However, the relative error between RQFP and the GFM decreases. For problems without any multiplication, the k-effective eigenvalue is not defined.

6.1.2 Multiplying Homogeneous Slab

For the material cross sections shown in Table 6.2, one-speed homogeneous multiplying slabs of thicknesses of thickness $\Delta = 1.0$ to $\Delta = 50.0$ mfp showed good agreement between RQFP and the GFM with the exception of thin slabs. For thin slabs of up to width $\Delta = 1.0$ mfp, percent relative error was substantial. This is caused by the difficulty of numerically determining the alpha-eigenvalues for thin slabs. If the slab is thin enough, the existence of an alpha-eigenvalue is not assured. As the slab thickness increase, agreement was substantially better (Table 6.7).

For supercritical systems, the RQFP was compared to the critical search method (Table 6.13a). The RQFP method substantially outperformed the critical search method in all cases. As the system became more supercritical, the number of transport sweeps necessary to converge increased for both methods. For the most supercritical slab ($\Delta = 50.0$ mfp), the

Table 6.6: Comparison of RQFP- and GFM-calculated alpha-eigenvalues for a homogeneous scattering slab

	Alpha-Eigenvalue/Percent Relative Error		
Δ	RQFP	GFM	% Relative Error
1	-6.08420×10^{-1}	-6.08072×10^{-1}	0.057189
5	-8.10966×10^{-2}	-8.10933×10^{-2}	0.004113
10	-2.53506×10^{-2}	-2.53500×10^{-2}	0.002349
20	-7.18015×10^{-3}	-7.17962×10^{-3}	0.007358
25	-4.71736×10^{-3}	-4.71722×10^{-3}	0.002966

$M = 500$, $L = 64$, Tolerance $= 10^{-12}$

number of sweeps necessary for the RQFP method to converge was less than the number of transport sweeps necessary for critical search to converge for the $\Delta = 4.0$ mfp case. Since the RQFP method requires no intermediate k-effective eigenvalue calculations, the method substantially reduced the number of transport sweeps necessary as there was no need to do multiple k-effective eigenvalue calculations to bracket the alpha-eigenvalue.

For the one-speed homogeneous multiplying slabs of varying thickness, the k-effective eigenvalue RQFP method was compared to the power method with the fission norm update (Table 6.13b). It was seen that the number of transport sweeps for convergence increased as the k-effective eigenvalue increased. The RQFP method required far more sweeps than the power method, up to a factor of five. Underperformance of the RQFP method for these particular k-effective problems is believed to be caused by flattening of the fundamental angular flux mode. As the system thickness is increases, the flux profile is flattened but higher flux modes take longer to decay.

Table 6.7: Comparison of RQFP- and GFM-calculated alpha-eigenvalues for a homogeneous scattering multiplying slab

	Alpha-Eigenvalue/Percent Relative Error		
Δ	RQFP	GFM	% Relative Error
0.25	-1.15480	-9.90300×10^{-1}	16.611352
0.30	-1.06633	-9.74300×10^{-1}	9.446240
0.35	-9.98584×10^{-1}	-9.49350×10^{-1}	5.186069
0.40	-9.42114×10^{-1}	-9.17000×10^{-1}	2.738758
0.45	-8.91833×10^{-1}	-8.79460×10^{-1}	1.406940
0.50	-8.44920×10^{-1}	-8.38790×10^{-1}	0.730822
0.75	-6.34756×10^{-1}	-6.34060×10^{-1}	0.109818
1	-4.69398×10^{-1}	-4.69160×10^{-1}	0.050762
2	-1.36335×10^{-1}	-1.36310×10^{-1}	0.018335
3	-1.39888×10^{-2}	-1.39790×10^{-2}	0.070397
4	4.36998×10^{-2}	4.37050×10^{-2}	0.011811
5	7.54667×10^{-2}	7.54690×10^{-2}	0.003096
6	9.48296×10^{-2}	9.48310×10^{-2}	0.001470
7	1.07508×10^{-1}	1.07510×10^{-1}	0.002137
8	1.16263×10^{-1}	1.16260×10^{-1}	0.002344
9	1.22563×10^{-1}	1.22560×10^{-1}	0.002390
10	1.27248×10^{-1}	1.27250×10^{-1}	0.001492
15	1.39126×10^{-1}	1.39130×10^{-1}	0.002605
20	1.43649×10^{-1}	1.43650×10^{-1}	0.000663
30	1.47066×10^{-1}	1.47070×10^{-1}	0.002483
40	1.48317×10^{-1}	1.48320×10^{-1}	0.001982
50	1.48910×10^{-1}	1.48910×10^{-1}	0.000004

$M = 500$, $L = 64$, Tolerance $= 10^{-12}$

Table 6.8: Transport Sweep Comparisons for Homogeneous Multiplying Slabs

	Transport Sweeps			Transport Sweeps	
Δ	RQFP	Critical Search	Δ	RQFP	Critical Search
0.25	x	*	5	70	33036
0.30	x	*	6	85	44655
0.35	x	*	7	103	55242
0.40	x	*	8	122	63851
0.45	x	*	9	143	71181
0.50	x	*	10	166	78002
0.75	x	*	15	308	89627
1	x	*	20	495	97267
2	x	*	30	1002	98087
3	x	*	40	1682	106055
4	56	21044	50	2530	113189

*Did Not Converge

(a) Alpha-Eigenvalue: Comparison of RQFP and Critical Search Sweeps

	Transport Sweeps			Transport Sweeps	
Δ	RQFP	Power Method	Δ	RQFP	Power Method
0.25	16	17	5	67	37
0.30	16	17	6	81	40
0.35	17	18	7	97	44
0.40	18	19	8	115	47
0.45	18	19	9	133	51
0.50	19	19	10	154	55
0.75	21	21	15	280	81
1	23	22	20	445	115
2	33	27	30	892	206
3	43	31	40	1490	238
4	54	34	50	2235	481

$M = 500$, $L = 64$, Tolerance $= 10^{-12}$

(b) k-Effective: Comparison of RQFP and Power Method Transport Sweeps

6.1.3 Heterogeneous Slabs

Problem 6.1.3.1-Non-multiplying Heterogeneous Slab: For the subcritical heterogeneous medium shown in Figure 6.1, five problems were constructed by varying the grain sizes of alternating slabs consisting of materials with the cross sections shown in Table 6.3. The maximum width of the domain was fixed at 10.0 mfp. Grain sizes of 0.5, 1, 2.5, and 5 mfp were examined and their alpha-eigenvalue calculated by the RQFP method and compared to the GFM. One last case consisting of a homogenized material was considered. In all cases, the RQFP method showed good agreement with DANT/PARTISN (Table 6.9a), Green's Function Method (Table 6.9b), and Direct Evaluation (Table 6.9c) with percent relative error within 0.15%. The number of transport sweeps required to obtain the eigenvalue and eigenvector increased as the problem approached critical and the number of regions increased. The scalar fluxes for the four heterogeneous region problems can be seen in Figure 6.2
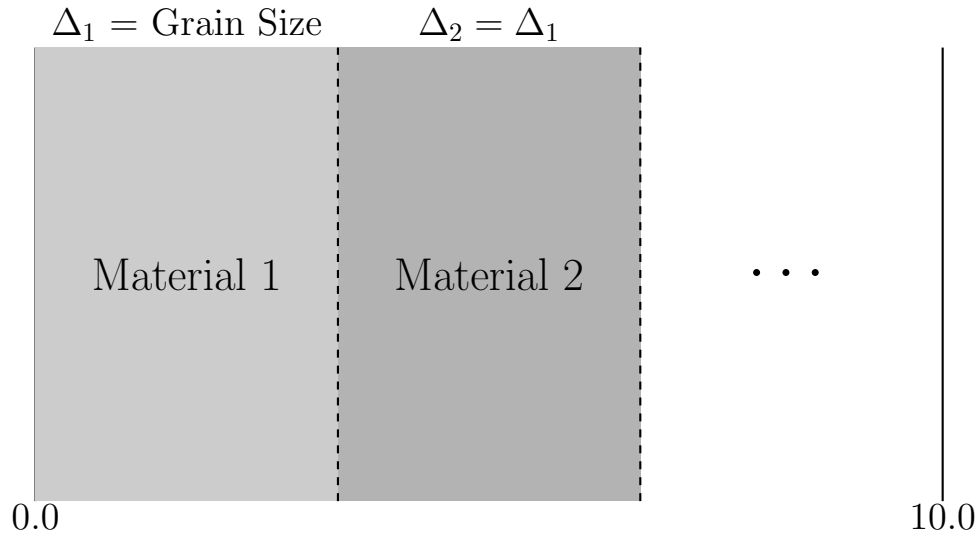
Figure 6.1: Heterogeneous Slab Benchmark Problem Domain [22]

Table 6.9: Comparison of RQFP-calculated eigenvalues to various methods for multi-region scattering slab ($M = 500$, $L = 64$, Tolerance $= 10^{-12}$)

Grain Size	Alpha-Eigenvalue/Percent Relative Error		
	RQFP	DANT/PARTISN	% Relative Error
5 (2 slabs)	-5.51528×10^{-1}	-5.50813×10^{-1}	0.129782
2.5 (4 slabs)	-7.03144×10^{-1}	-7.03134×10^{-1}	0.001470
1 (10 slabs)	-7.48808×10^{-1}	-7.48793×10^{-1}	0.001942
0.5 (20 slabs)	-7.57221×10^{-1}	-7.57199×10^{-1}	0.002882
0 (homogeneous)	-7.63513×10^{-1}	-7.63507×10^{-1}	0.000848

(a) Comparison of RQFP- and DANT/PARTISN-calculated alpha-eigenvalues

Grain Size	Alpha-Eigenvalue/Percent Relative Error		
	RQFP	GFM	% Relative Error
5 (2 slabs)	-5.51528×10^{-1}	-5.50812×10^{-1}	0.129964
2.5 (4 slabs)	-7.03144×10^{-1}	-7.03133×10^{-1}	0.001612
1 (10 slabs)	-7.48808×10^{-1}	-7.48792×10^{-1}	0.002075
0.5 (20 slabs)	-7.57221×10^{-1}	-7.57198×10^{-1}	0.003014
0 (homogeneous)	-7.63513×10^{-1}	-7.63507×10^{-1}	0.000848

(b) Comparison of RQFP- and GFM-calculated alpha-eigenvalues

Grain Size	Alpha-Eigenvalue/Percent Relative Error		
	RQFP	GFM	% Relative Error
5 (2 slabs)	-5.51528×10^{-1}	-5.50812×10^{-1}	0.129964
2.5 (4 slabs)	-7.03144×10^{-1}	-7.03133×10^{-1}	0.001612
1 (10 slabs)	-7.48808×10^{-1}	-7.48792×10^{-1}	0.002075
0.5 (20 slabs)	-7.57221×10^{-1}	-7.57198×10^{-1}	0.003014
0 (homogeneous)	-7.63513×10^{-1}	-7.63507×10^{-1}	0.000848

(c) Comparison of RQFP- and DE-calculated alpha-eigenvalues
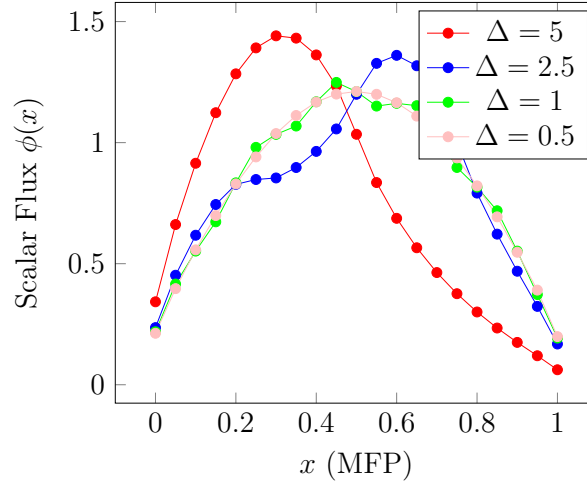
Figure 6.2: Scalar Flux Results for Alternating Slabs Grain Size Problems

Problem 6.1.3.2-Multiplying Two Region Heterogeneous Slab: For a supercritical two-region medium (Figure 6.3) consisting of two materials with cross sections given in Table 6.4, the calculated alpha-eigenvalue and scalar flux were compared to the Green's Function Method. The calculated alpha-eigenvalue $\alpha = 0.142475$ s^{-1} agreed with the GFM eigenvalue. The alpha-eigenvalue RQFP method required 50 iterations to converge the problems to a tolerance of 10^{-12}. The critical search method required 22076 iterations, requiring multiple bracketing attempts. The multiple bracketing attempts were required since the system was close to critical. To verify the correctness of the RQFP alpha-eigenvalue scalar flux, the scalar flux was compared to the GFM scalar flux. The fluxes were found to be in agreement within tolerance (Figure 6.4).

The k-effective eigenvalue of the supercritical two-region medium was found to be 1.28656. The RQFP method was found to require 46 transport sweeps to converge to a tolerance of 10^{-12}. The power method with fission norm update required 36 transport sweeps.
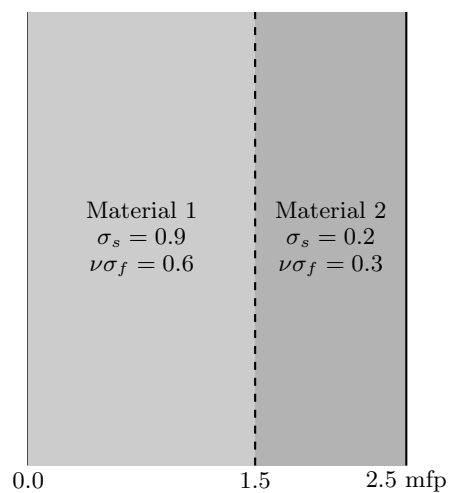
Figure 6.3: Heterogeneous Multiplying Slab Benchmark Problem Domain [21]
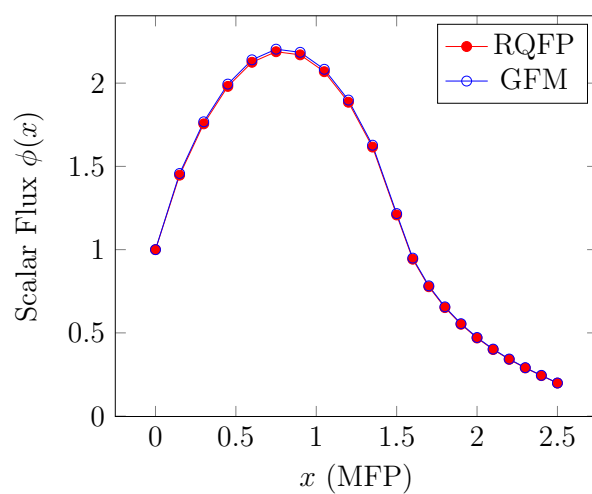
Figure 6.4: Alpha-Eigenvalue Scalar Flux Results for Two-Region Multiplying Slab

Problem 6.1.3.3-Multiplying Five Region Fuel-Pin:

A five region fuel-pin-like domain was modeled ($M = 1000$ and $L = 64$) and the alpha-eigenvalues compared to GFM for four cases. For case one and two, the fuel-pin domain consisted of five regions as seen in Figure 6.5, fuel, moderator, absorber, moderator, and fuel, with cross sections given in Table 6.5. The leftmost fuel pin had a one mean free path width. For case one and two, the fuel fission cross section was set to $\nu\sigma_f = 0.3$ or $\nu\sigma_f = 0.7$. The alpha-eigenvalues were $\alpha = -0.3196537 \text{ s}^{-1}$ and $\alpha = -0.006156369 \text{ s}^{-1}$ for the $\nu\sigma_f = 0.3$ and $\nu\sigma_f = 0.7$ cases, respectively. The RQFP method eigenvalues matched the GFM-calculated alpha-eigenvalues within tolerance. Convergence of the $\nu\sigma_f = 0.3$ and $\nu\sigma_f = 0.7$ cases for the RQFP method required 32 and 29 transport sweeps, respectively. The scalar fluxes for both cases matched GFM within tolerance and are seen in Figure 6.6. For cases three and four, the leftmost fuel pin width was set to 1.1. The alpha-eigenvalues for $\nu\sigma_f = 0.3$ and $\nu\sigma_f = 0.7$ were found to be -0.2932897 s^{-1} and 0.0375543 s^{-1}, respectively. The RQFP method eigenvalues matched the GFM-calculated alpha-eigenvalues within tolerance (Table 6.10).

For leftmost fuel pin width of one mean free path, the k-effective eigenvalue of the five region fuel-pin-like was determined to be 0.42428 and 0.98998 for the $\nu\sigma_f = 0.3$ and $\nu\sigma_f = 0.7$ cases, respectively. For the $\nu\sigma_f = 0.3$ fuel pin, the RQFP method required 29 transport sweeps while the power method with fission norm update required 22 transport sweeps. For the $\nu\sigma_f = 0.7$ fuel pin, the RQFP method required 28 transport sweeps while the power method with fission norm update required 21 transport sweeps. For leftmost fuel pin width of 1.1 mean free paths, the k-effective was determined to be 0.45554 and 1.06316, respectively, for $\nu\sigma_f = 0.3$ and $\nu\sigma_f = 0.7$. For the $\nu\sigma_f = 0.3$ fuel pin, the RQFP method required 514 transport sweeps while the power method with fission norm update required 355 transport sweeps. For the $\nu\sigma_f = 0.7$ fuel pin, the RQFP method required 513 transport sweeps while the power method with fission norm update required 355 transport sweeps.
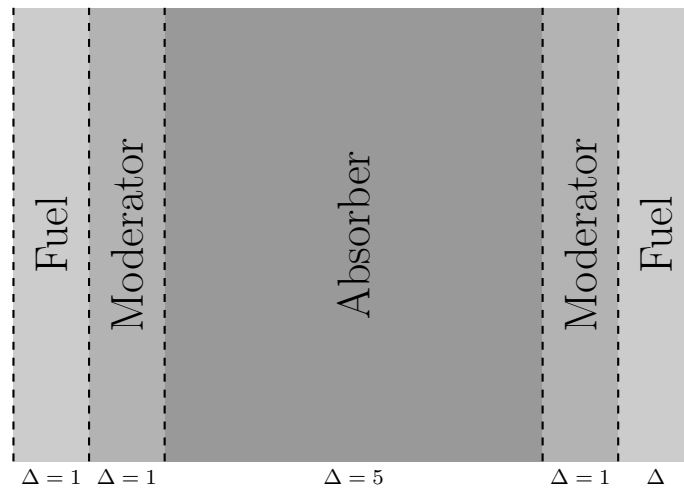
Figure 6.5: Five Region Heterogeneous Slab Benchmark Problem Domain [22]

Table 6.10: Comparison of RQFP- and GFM-calculated alpha-eigenvalues for a homogeneous scattering multiplying slab

		Alpha-Eigenvalue	
Δ	$\nu\sigma_f$	RQFP	GFM
1	0.3	-3.196537×10^{-1}	-3.196537×10^{-2}
1	0.7	-6.156369×10^{-2}	-6.156369×10^{-2}
1.1	0.3	-2.932897×10^{-1}	-2.93247×10^{-1}
1.1	0.7	3.75543×10^{-2}	3.759991×10^{-2}

$M = 1000$, $L = 64$, Tolerance $= 10^{-12}$
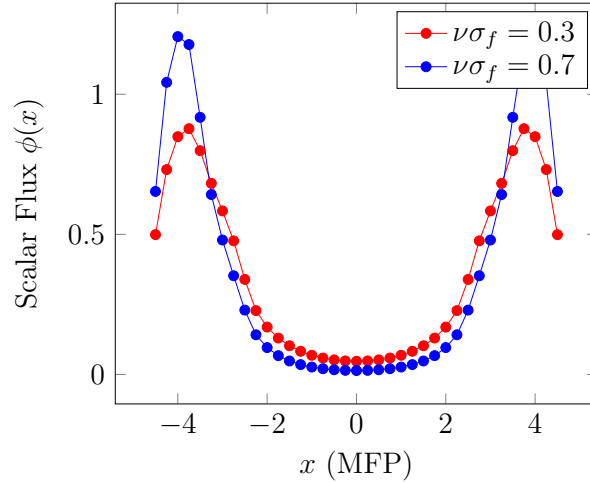
Figure 6.6: Case One and Two Scalar Flux Results for Five-Region Multiplying Slab-Two Cases

6.2   Multigroup Verification for Slab Geometry

6.3   One-Speed Verification for Spherical Geometry

In certain circumstances, alpha-eigenvalue results for slab geometry also apply to spherical geometry problems. This slab-sphere equivalence holds for isotropically scattering heterogeneous media where the total cross section is equal for all regions [10]. More generally, a convenient property of spherically symmetric systems is that if the mean free path in the system is independent of position and scattering is isotropic, then the determination of the spherically symmetric neutron distribution of these systems is reduced to the determination of these distributions in certain systems with plane symmetries. Thus, for all homogeneous

Table 6.11: Comparison of RQFP- and GFM-calculated alpha-eigenvalues for a homogeneous scattering sphere

	Alpha-Eigenvalue/Percent Relative Error		
Δ	RQFP	GFM	% Relative Error
5	-3.41177×10^{-1}	-3.41216×10^{-1}	0.0114
10	-1.02973×10^{-1}	-1.02978×10^{-1}	0.0049
20	-2.88443×10^{-2}	-2.88447×10^{-2}	0.0014
25	-1.89226×10^{-2}	-1.89228×10^{-2}	0.0011

$M = 500$, $L = 64$, Tolerance $= 10^{-12}$

slab and symmetric heterogeneous slab systems where each region has the same total cross section, it follows that there exists a spherical equivalent for the problems studied in the previous sections. Specifically, it can be shown that the second eigenvalue of a slab system is identical to the fundamental eigenvalue for the equivalent sphere. In this section, we examine the performance of the RQFP method for one-dimensional spherical problems which are equivalent to the slab problems from before. We verify the correctness of the method for this subset of problems and compare its performance to the critical search and power methods.

6.3.1 Non-Multiplying Homogeneous Spheres

6.3.2 Multiplying Homogeneous Spheres

6.4 Multigroup Verification for Spherical Geometry

6.5 Conclusion

Table 6.12: Comparison of RQFP- and GFM-calculated alpha-eigenvalues for a homogeneous scattering multiplying sphere

	Alpha-Eigenvalue/Percent Relative Error		
Δ	RQFP	GFM	% Relative Error
3	-5.68218×10^{-1}	-5.6833×10^{-1}	0.0197
4	-3.00486×10^{-1}	-3.0054×10^{-1}	0.0180
5	-1.60321×10^{-1}	-1.6035×10^{-1}	0.0181
6	-7.72739×10^{-2}	-7.7292×10^{-2}	0.0234
7	-2.38450×10^{-2}	-2.3857×10^{-2}	0.0503
8	1.26235×10^{-2}	1.2616×10^{-2}	0.0594
9	3.86541×10^{-2}	3.8649×10^{-2}	0.0132
10	5.78980×10^{-2}	5.7894×10^{-2}	0.0069
15	1.06258×10^{-1}	1.0626×10^{-1}	0.0019
20	1.24512×10^{-1}	1.2451×10^{-1}	0.0016
30	1.38248×10^{-1}	1.3825×10^{-1}	0.0014
40	1.43262×10^{-1}	1.4326×10^{-1}	0.0014
50	1.45638×10^{-1}	1.4564×10^{-1}	0.0014

$M = 500$, $L = 64$, Tolerance $= 10^{-12}$

Table 6.13: Transport Sweep Comparisons for Homogeneous Multiplying Spheres

	Transport Sweeps			Transport Sweeps	
Δ	RQFP	Critical Search	Δ	RQFP	Critical Search
3	x	*	10	130	29645
4	x	*	15	232	61303
5	x	*	20	364	84353
6	x	*	30	722	100433
7	x	*	40	1201	99135
8	98	10865	50	1799	97037
9	113	21555			

*Did Not Converge

(a) Alpha-Eigenvalue: Comparison of RQFP and Critical Search Sweeps

	Transport Sweeps			Transport Sweeps	
Δ	RQFP	Power Method	Δ	RQFP	Power Method
3	49	43	10	127	62
4	57	47	15	214	79
5	66	49	20	329	103
6	76	52	30	636	167
7	87	54	40	1049	253
8	99	56	50	1562	360
9	113	59			

$M = 500$, $L = 64$, Tolerance $= 10^{-12}$

(b) k-Effective: Comparison of RQFP and Power Method Transport Sweeps

Fuel

Moderator

Absorber
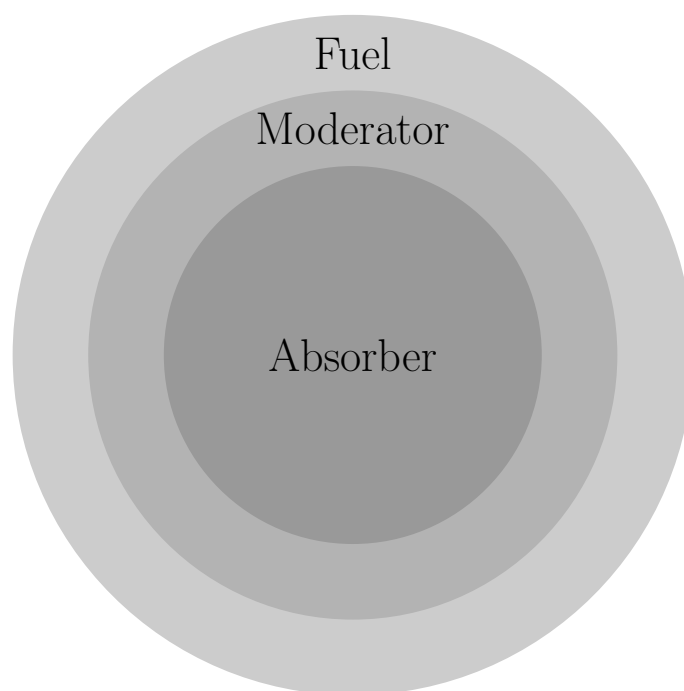
Figure 6.7: Five Region Fuel Pin Spherical Equivalent [22]

Chapter 7

Higher Dimensional Eigenvalues

In this chapter we verify the correctness and examine the performance of the Rayleigh quotient fixed point methods for higher-dimensional problems. We consider realistic two- and three-dimensional problems involving fuel rods and fuel assemblies. For higher dimensions, the phase space of the neutron transport equation is a function of two (x, y) or three (x, y, z) spatial variables x and two (μ, η) or three (μ, η, ξ) angular variables defined as the x-, y-, and z-direction cosines. For higher-dimensional Cartesian geometry, the two-dimensional and three-dimensional alpha-eigenvalue neutron transport equations are given by Eq. ?? and Eq. 7.2, respectively:

$$
\left[\mu \frac{\partial}{\partial x} + \eta \frac{\partial}{\partial y} + \frac{\alpha}{v(E)} + \sigma(x, y, E) \right] \psi(x, y, \mu, \eta, E)
$$
$$
= \frac{\chi(E)}{2} \int_0^\infty dE' \nu(E') \sigma_f(x, y, E') \int_{-1}^1 d\mu' \int_{-1}^1 d\eta' \psi(x, y, \mu', \eta', E)
$$
$$
+ \frac{1}{2\pi} \int_0^\infty dE' \sigma_s(x, y, E' \to E) \int_{-1}^1 d\mu' \int_{-1}^1 d\eta' \, \psi(x, y, \mu', \eta', E), \quad (7.1)
$$

$$
\left[\mu \frac{\partial}{\partial x} + \eta \frac{\partial}{\partial y} + \xi \frac{\partial}{\partial z} + \frac{\alpha}{v(E)} + \sigma(x, y, z, E) \right] \psi(x, y, z, \mu, \eta, \xi, E)
$$
$$
= \frac{\chi(E)}{2} \int_0^\infty dE' \nu(E') \sigma_f(x, y, z, E') \int_{-1}^1 d\mu' \int_{-1}^1 d\eta' \int_0^\pi d\xi' \psi(x, y, z, \mu', \eta', \xi', E)
$$
$$
+ \frac{1}{4\pi} \int_0^\infty dE' \sigma_s(x, y, z, E' \to E) \int_{-1}^1 d\mu' \int_{-1}^1 d\eta' \int_0^\pi d\xi' \, \psi(x, y, z, \mu', \eta', \xi', E), \quad (7.2)
$$

7.1 Conclusion

(a) UO$_2$ Fuel-Clad Cross Sections – (cm^{-1})

Energy Group g	σ_g	$\sigma_{g,tr}$	$\sigma_{a,g}$	$\sigma_{\gamma,g}$	$\sigma_{f,g}$	ν_g	χ_g
1	2.12450E-01	1.77949E-01	8.02480E-03	8.12740E-04	7.21206E-03	2.78145E+00	5.87910E-01
2	3.55470E-01	3.29805E-01	3.71740E-03	2.89810E-03	8.19301E-04	2.47443E+00	4.11760E-01
3	4.85540E-01	4.80388E-01	2.67690E-02	2.03158E-02	6.45320E-03	2.43383E+00	3.39060E-04
4	5.59400E-01	5.54367E-01	9.62360E-02	7.76712E-02	1.85648E-02	2.43380E+00	1.17610E-07
5	3.18030E-01	3.11801E-01	3.00200E-02	1.22116E-02	1.78084E-02	2.43380E+00	0.00000E+00
6	4.01460E-01	3.95168E-01	1.11260E-01	2.82252E-02	8.30348E-02	2.43380E+00	0.00000E+00
7	5.70610E-01	5.64406E-01	2.82780E-01	6.67760E-02	2.16004E-01	2.43380E+00	0.00000E+00

(b) UO$_2$ Fuel-Clad Scattering Block (cm^{-1})

g', g	1	2	3	4	5	6	7
1	1.27537E-01	4.23780E-02	9.43740E-06	5.51630E-09	0.00000E+00	0.00000E+00	0.00000E+00
2	0.00000E+00	3.24456E-01	1.63140E-03	3.14270E-09	0.00000E+00	0.00000E+00	0.00000E+00
3	0.00000E+00	0.00000E+00	4.50940E-01	2.67920E-03	0.00000E+00	0.00000E+00	0.00000E+00
4	0.00000E+00	0.00000E+00	0.00000E+00	4.52565E-01	5.56640E-03	0.00000E+00	0.00000E+00
5	0.00000E+00	0.00000E+00	0.00000E+00	1.25250E-04	2.71401E-01	1.02550E-02	1.00210E-08
6	0.00000E+00	0.00000E+00	0.00000E+00	0.00000E+00	1.29680E-03	2.65802E-01	1.68090E-02
7	0.00000E+00	0.00000E+00	0.00000E+00	0.00000E+00	0.00000E+00	8.54580E-03	2.73080E-01

Table 7.1: C5G7MOX Cross Sections - UO$_2$ Fuel-Clad

(a) 4.3% MOX Fuel – Clad Cross Sections (cm^{-1})

Energy Group g	σ_g	$\sigma_{g,tr}$	$\sigma_{a,g}$	$\sigma_{\gamma,g}$	$\sigma_{f,g}$	ν_g	χ_g
1	2.11920E-01	1.78731E-01	8.43390E-03	8.06860E-04	7.62704E-03	2.85209E+00	5.87910E-01
2	3.55810E-01	3.30849E-01	3.75770E-03	2.88080E-03	8.76898E-04	2.89099E+00	4.11760E-01
3	4.88900E-01	4.83772E-01	2.79700E-02	2.22717E-02	5.69835E-03	2.85486E+00	3.39060E-04
4	5.71940E-01	5.66922E-01	1.04210E-01	8.13228E-02	2.28872E-02	2.86073E+00	1.17610E-07
5	4.32390E-01	4.26227E-01	1.39940E-01	1.29177E-01	1.07635E-02	2.85447E+00	0.00000E+00
6	6.84950E-01	6.78997E-01	4.09180E-01	1.76423E-01	2.32757E-01	2.86415E+00	0.00000E+00
7	6.88910E-01	6.82852E-01	4.09350E-01	1.60382E-01	2.48968E-01	2.86780E+00	0.00000E+00

(b) 4.3% MOX Fuel Scattering Block (cm^{-1})

g', g	1	2	3	4	5	6	7
1	1.28876E-01	4.14130E-02	8.22900E-06	5.04050E-09	0.00000E+00	0.00000E+00	0.00000E+00
2	0.00000E+00	3.25452E-01	1.63950E-03	1.59820E-09	0.00000E+00	0.00000E+00	0.00000E+00
3	0.00000E+00	0.00000E+00	4.53188E-01	2.61420E-03	0.00000E+00	0.00000E+00	0.00000E+00
4	0.00000E+00	0.00000E+00	0.00000E+00	4.57173E-01	5.53940E-03	0.00000E+00	0.00000E+00
5	0.00000E+00	0.00000E+00	0.00000E+00	1.60460E-04	2.76814E-01	9.31270E-03	9.16560E-09
6	0.00000E+00	0.00000E+00	0.00000E+00	0.00000E+00	2.00510E-03	2.52962E-01	1.48500E-02
7	0.00000E+00	0.00000E+00	0.00000E+00	0.00000E+00	0.00000E+00	8.49480E-03	2.65007E-01

Table 7.2: C5G7MOX Cross Sections - 4.3% MOX Fuel

(a) 7.0% MOX Fuel – Clad Cross Sections (cm^{-1})

Energy Group g	σ_g	$\sigma_{g,tr}$	$\sigma_{a,g}$	$\sigma_{\gamma,g}$	$\sigma_{f,g}$	ν_g	χ_g
1	2.14540E-01	1.81323E-01	9.06570E-03	8.11240E-04	8.25446E-03	2.88498E+00	5.87910E-01
2	3.59350E-01	3.34368E-01	4.29670E-03	2.97105E-03	1.32565E-03	2.91079E+00	4.11760E-01
3	4.98910E-01	4.93785E-01	3.28810E-02	2.44594E-02	8.42156E-03	2.86574E+00	3.39060E-04
4	5.96220E-01	5.91216E-01	1.22030E-01	8.91570E-02	3.28730E-02	2.87063E+00	1.17610E-07
5	4.80350E-01	4.74198E-01	1.82980E-01	1.67016E-01	1.59636E-02	2.86714E+00	0.00000E+00
6	8.39360E-01	8.33601E-01	5.68460E-01	2.44666E-01	3.23794E-01	2.86658E+00	0.00000E+00
7	8.59480E-01	8.53603E-01	5.85210E-01	2.22407E-01	3.62803E-01	2.87539E+00	0.00000E+00

(b) 7.0% MOX Fuel Scattering Block (cm^{-1})

g', g	1	2	3	4	5	6	7
1	1.30457E-01	4.17920E-02	8.51050E-06	5.13290E-09	0.00000E+00	0.00000E+00	0.00000E+00
2	0.00000E+00	3.28428E-01	1.64360E-03	2.20170E-09	0.00000E+00	0.00000E+00	0.00000E+00
3	0.00000E+00	0.00000E+00	4.58371E-01	2.53310E-03	0.00000E+00	0.00000E+00	0.00000E+00
4	0.00000E+00	0.00000E+00	0.00000E+00	4.63709E-01	5.47660E-03	0.00000E+00	0.00000E+00
5	0.00000E+00	0.00000E+00	0.00000E+00	1.76190E-04	2.82313E-01	8.72890E-03	9.00160E-09
6	0.00000E+00	0.00000E+00	0.00000E+00	0.00000E+00	2.27600E-03	2.49751E-01	1.31140E-02
7	0.00000E+00	0.00000E+00	0.00000E+00	0.00000E+00	0.00000E+00	8.86450E-03	2.59529E-01

Table 7.3: C5G7MOX Cross Sections - 7.0% MOX Fuel

(a) 8.7% MOX Fuel – Clad Cross Sections (cm^{-1})

Energy Group g	σ_g	$\sigma_{g,tr}$	$\sigma_{a,g}$	$\sigma_{\gamma,g}$	$\sigma_{f,g}$	ν_g	χ_g
1	2.16280E-01	1.83045E-01	9.48620E-03	8.14110E-04	8.67209E-03	2.90426E+00	5.87910E-01
2	3.61700E-01	3.36705E-01	4.65560E-03	3.03134E-03	1.62426E-03	2.91795E+00	4.11760E-01
3	5.05630E-01	5.00507E-01	3.62400E-02	2.59684E-02	1.02716E-02	2.86986E+00	3.39060E-04
4	6.11170E-01	6.06174E-01	1.32720E-01	9.36753E-02	3.90447E-02	2.87491E+00	1.17610E-07
5	5.08900E-01	5.02754E-01	2.08400E-01	1.89142E-01	1.92576E-02	2.87175E+00	0.00000E+00
6	9.26670E-01	9.21028E-01	6.58700E-01	2.83812E-01	3.74888E-01	2.86752E+00	0.00000E+00
7	9.60990E-01	9.55231E-01	6.90170E-01	2.59571E-01	4.30599E-01	2.87808E+00	0.00000E+00

(b) 8.7% MOX Fuel Scattering Block (cm^{-1})

g', g	1	2	3	4	5	6	7
1	1.31504E-01	4.20460E-02	8.69720E-06	5.19380E-09	0.00000E+00	0.00000E+00	0.00000E+00
2	0.00000E+00	3.30403E-01	1.64630E-03	2.60060E-09	0.00000E+00	0.00000E+00	0.00000E+00
3	0.00000E+00	0.00000E+00	4.61792E-01	2.47490E-03	0.00000E+00	0.00000E+00	0.00000E+00
4	0.00000E+00	0.00000E+00	0.00000E+00	4.68021E-01	5.43300E-03	0.00000E+00	0.00000E+00
5	0.00000E+00	0.00000E+00	0.00000E+00	1.85970E-04	2.85771E-01	8.39730E-03	8.92800E-09
6	0.00000E+00	0.00000E+00	0.00000E+00	0.00000E+00	2.39160E-03	2.47614E-01	1.23220E-02
7	0.00000E+00	0.00000E+00	0.00000E+00	0.00000E+00	0.00000E+00	8.96810E-03	2.56093E-01

Table 7.4: C5G7MOX Cross Sections - 8.7% MOX Fuel

(a) Fission Chamber – Cross Sections (cm^{-1})

Energy Group g	σ_g	$\sigma_{g,tr}$	$\sigma_{a,g}$	$\sigma_{\gamma,g}$	$\sigma_{f,g}$	ν_g	χ_g
1	1.90730E-01	1.26032E-01	5.11320E-04	5.11315E-04	4.79002E-09	2.76283E+00	5.87910E-01
2	4.56520E-01	2.93160E-01	7.58130E-05	7.58072E-05	5.82564E-09	2.46239E+00	4.11760E-01
3	6.40700E-01	2.84250E-01	3.16430E-04	3.15966E-04	4.63719E-07	2.43380E+00	3.39060E-04
4	6.49840E-01	2.81020E-01	1.16750E-03	1.16226E-03	5.24406E-06	2.43380E+00	1.17610E-07
5	6.70630E-01	3.34460E-01	3.39770E-03	3.39755E-03	1.45390E-07	2.43380E+00	0.00000E+00
6	8.75060E-01	5.65640E-01	9.18860E-03	9.18789E-03	7.14972E-07	2.43380E+00	0.00000E+00
7	1.43450E+00	1.17214E+00	2.32440E-02	2.32419E-02	2.08041E-06	2.43380E+00	0.00000E+00

(b) Fission Chamber Scattering Block (cm^{-1})

g', g	1	2	3	4	5	6	7
1	6.61659E-02	5.90700E-02	2.83340E-04	1.46220E-06	2.06420E-08	0.00000E+00	0.00000E+00
2	0.00000E+00	2.40377E-01	5.24350E-02	2.49900E-04	1.92390E-05	2.98750E-06	4.21400E-07
3	0.00000E+00	0.00000E+00	1.83425E-01	9.22880E-02	6.93650E-03	1.07900E-03	2.05430E-04
4	0.00000E+00	0.00000E+00	0.00000E+00	7.90769E-02	1.69990E-01	2.58600E-02	4.92560E-03
5	0.00000E+00	0.00000E+00	0.00000E+00	3.73400E-05	9.97570E-02	2.06790E-01	2.44780E-02
6	0.00000E+00	0.00000E+00	0.00000E+00	0.00000E+00	9.17420E-04	3.16774E-01	2.38760E-01
7	0.00000E+00	0.00000E+00	0.00000E+00	0.00000E+00	0.00000E+00	4.97930E-02	1.09910E+00

Table 7.5: C5G7MOX Cross Sections - Fission Chamber

(a) Guide Tube Cross Sections (cm^{-1})

Energy Group g	σ_g	$\sigma_{g,tr}$	$\sigma_{a,g}$	$\sigma_{\gamma,g}$
1	1.90730E-01	1.26032E-01	5.11320E-04	5.11320E-04
2	4.56520E-01	2.93160E-01	7.58010E-05	7.58010E-05
3	6.40670E-01	2.84240E-01	3.15720E-04	3.15720E-04
4	6.49670E-01	2.80960E-01	1.15820E-03	1.15820E-03
5	6.70580E-01	3.34440E-01	3.39750E-03	3.39750E-03
6	8.75050E-01	5.65640E-01	9.18780E-03	9.18780E-03
7	1.43450E+00	1.17215E+00	2.32420E-02	2.32420E-02

(b) Guide Tube Scattering Block (cm^{-1})

g', g	1	2	3	4	5	6	7
1	6.61659E-02	5.90700E-02	2.83340E-04	1.46220E-06	2.06420E-08	0.00000E+00	0.00000E+00
2	0.00000E+00	2.40377E-01	5.24350E-02	2.49900E-04	1.92390E-05	2.98750E-06	4.21400E-07
3	0.00000E+00	0.00000E+00	1.83297E-01	9.23970E-02	6.94460E-03	1.08030E-03	2.05670E-04
4	0.00000E+00	0.00000E+00	0.00000E+00	7.88511E-02	1.70140E-01	2.58810E-02	4.92970E-03
5	0.00000E+00	0.00000E+00	0.00000E+00	3.73330E-05	9.97372E-02	2.06790E-01	2.44780E-02
6	0.00000E+00	0.00000E+00	0.00000E+00	0.00000E+00	9.17260E-04	3.16765E-01	2.38770E-01
7	0.00000E+00	0.00000E+00	0.00000E+00	0.00000E+00	0.00000E+00	4.97920E-02	1.09912E+00

Table 7.6: C5G7MOX Cross Sections - Guide Tube

(a) Moderator Cross Sections (cm^{-1})

Energy Group g	σ_g	$\sigma_{g,tr}$	$\sigma_{a,g}$	$\sigma_{\gamma,g}$
1	2.30070E-01	1.59206E-01	6.01050E-04	6.01050E-04
2	7.76460E-01	4.12970E-01	1.57930E-05	1.57930E-05
3	1.48420E+00	5.90310E-01	3.37160E-04	3.37160E-04
4	1.50520E+00	5.84350E-01	1.94060E-03	1.94060E-03
5	1.55920E+00	7.18000E-01	5.74160E-03	5.74160E-03
6	2.02540E+00	1.25445E+00	1.50010E-02	1.50010E-02
7	3.30570E+00	2.65038E+00	3.72390E-02	3.72390E-02

(b) Moderator Scattering Block (cm^{-1})

g', g	1	2	3	4	5	6	7
1	4.44777E-02	1.13400E-01	7.23470E-04	3.74990E-06	5.31840E-08	0.00000E+00	0.00000E+00
2	0.00000E+00	2.82334E-01	1.29940E-01	6.23400E-04	4.80020E-05	7.44860E-06	1.04550E-06
3	0.00000E+00	0.00000E+00	3.45256E-01	2.24570E-01	1.69990E-02	2.64430E-03	5.03440E-04
4	0.00000E+00	0.00000E+00	0.00000E+00	9.10284E-02	4.15510E-01	6.37320E-02	1.21390E-02
5	0.00000E+00	0.00000E+00	0.00000E+00	7.14370E-05	1.39138E-01	5.11820E-01	6.12290E-02
6	0.00000E+00	0.00000E+00	0.00000E+00	0.00000E+00	2.21570E-03	6.99913E-01	5.37320E-01
7	0.00000E+00	0.00000E+00	0.00000E+00	0.00000E+00	0.00000E+00	1.32440E-01	2.48070E+00

Table 7.7: C5G7MOX Cross Sections - Moderator

Appendix A

Discretization of the Alpha-Eigenvalue Problem For One-Dimensional Slab Geometry

In this Appendix, we describe the discretization of the alpha-eigenvalue problem for one-dimensional slab geometry using a matrix formalism similar to that of three-dimensional Cartesian geometry. In one dimension, the discretization of the continuous eigenvalue equation is substantially simpler and may be helpful to reader to study this case before analyzing the three-dimensional problem.

We begin with the alpha-eigenvalue transport equation in one-dimensional slab geometry with isotropic scattering. The spatial domain is the interval $[a, b]$ in x, μ is the angle cosine in $[-1, 1]$, the energy variable is $E \in [0, \infty)$, and the equations for the angular flux $\psi(x, \mu, E)$ are given by

$$
\left[\mu \frac{\partial}{\partial x} + \frac{\alpha}{v(E)} + \sigma(x, E) \right] \psi(x, \mu, E)
$$
$$
= \frac{\chi(E)}{2} \int_0^\infty dE' \nu(E') \sigma_f(x, E') \int_{-1}^1 d\mu' \psi(x, \mu', E)
$$
$$
+ \frac{1}{2} \int_0^\infty dE' \sigma_s(x, E' \to E) \int_{-1}^1 d\mu' \psi(x, \mu', E). \quad \text{(A.1)}
$$

We assume vacuum Dirichlet conditions

$$
\psi(a, \mu, E) = 0, \quad 0 < \mu \leq 1, \quad \text{(A.2)}
$$
$$
\psi(b, \mu, E) = 0, \quad -1 \leq \mu < 0. \quad \text{(A.3)}
$$

The discretization of Eqn A.1 is done using diamond differencing in space, multigroup in energy, and discrete ordinates collocation in angle.

A.1 Discretization of the One-Dimensional Slab Geometry Problem

We begin by discretizing Eq. A.1 in energy using the *multigroup* approximation. We restrict the energy E to a finite interval and partition the interval into groups:

$$E_{max} = E_0 > E_1 > \cdots > E_G = E_{min}. \tag{A.4}$$

The eigenvalue equation is then averaged over each group $E_g < E < E_{g-1}$ and the cross sections are approximated by a flux-weighted average over each energy group. In the spatial dimension, we introduce a spatial grid

$$a \equiv x_0 < \cdots < x_{i+1} < x_i < \cdots < x_M \equiv b, \tag{A.5}$$

and let

$$\Delta x_i = x_i - x_{i-1}. \tag{A.6}$$

We refer to the x_i as nodes and function values at the nodes are called nodal values. We assume that σ_g and $\sigma_{s,g,g'}$, the total and scattering cross sections for energy group g, are constant on the zone $x_{i-1} < x < x_i$ and denote these values by $\sigma_{g,i}$ and $\sigma_{s,g,g',i}$. We use a discrete ordinates collocation of Eq. A.1 at an even number of Gauss points μ_ℓ with

$$-1 < \mu_1 < \cdots < \mu_{L/2} < 0 < \mu_{L/2+1} < \cdots < \mu_L < 1, \mu_{L+1-\ell} = -\mu_\ell. \tag{A.7}$$

The integrals in angle in Eq. A.1 are then approximated by

$$\frac{1}{2} \int_{-1}^{1} d\mu \, \psi_g(x, \mu) \approx \sum_{\ell=1}^{L} w_\ell \psi_g(x, \mu_\ell). \tag{A.8}$$

Using diamond differencing in the spatial dimension [25], we obtain the fully discretized set of equations for the eigenvalue problems

$$\mu_\ell \frac{\psi_{g,\ell,i} - \psi_{g,\ell,i-1}}{\Delta x_i} + \frac{\alpha}{v_g} \frac{\psi_{g,\ell,i} + \psi_{g,\ell,i-1}}{2} + \sigma_{g,i} \frac{\psi_{g,\ell,i} + \psi_{g,\ell,i-1}}{2}$$

$$= \frac{\chi_g}{2} \sum_{g'=1}^{G} \frac{\nu_g \sigma_{f,g',i}}{2} \sum_{\ell'=1}^{L} w_{\ell'} \psi_{g',\ell',i} + \sum_{g'=1}^{G} \frac{\sigma_{s,g,g',i}}{2} \sum_{\ell'=1}^{L} w_{\ell'} \psi_{g',\ell',i}, \tag{A.9}$$

for $g = 1, \ldots, G$, $i = 1, \ldots, M$, and $\ell = 1, \ldots, L$. The discretized boundary conditions are given by

$$\psi_{g,\ell,M} = 0 \text{ for } \ell = 1, \ldots, L/2, \tag{A.10}$$

$$\psi_{g,\ell,0} = 0 \text{ for } \ell = L/2 + 1, \ldots, L. \tag{A.11}$$

Using cell-centered flux values, it follows that Eq. A.9 is a system of GLM equations for GLM unknowns.

To write Eq. A.9 in matrix form, we define the angular flux vector for a single energy group g as

$$\Psi_g \equiv \begin{pmatrix} \Psi_{g,1} \\ \vdots \\ \Psi_{g,L} \end{pmatrix} \in \mathbf{R}^{L(M+1)} \quad \text{with} \quad \Psi_{g,\ell} \equiv \begin{pmatrix} \Psi_{g,\ell,0} \\ \vdots \\ \Psi_{g,L,M} \end{pmatrix} \in \mathbf{R}^{M+1}. \tag{A.12}$$

To write the matrix form of the diamond difference discretized operator $\mu_\ell \partial/\partial x + 1/v_g + \sigma_g$, we define the block diagonal matrix

$$\bar{S} \equiv \operatorname{diag}(S_1, \ldots, S_L) \in \mathbf{R}^{LM \times L(M+1)} \tag{A.13}$$

with

$$S_\ell = S = \frac{1}{2} \begin{pmatrix} 1 & 1 & & \\ & \ddots & \ddots & \\ & & 1 & 1 \end{pmatrix} \in \mathbf{R}^{M \times (M+1)}, \tag{A.14}$$

for all ℓ. The matrix S interpolates nodal vectors into zone-centered vectors by averaging the nodal values. Now we define the total cross section and inverse velocity matrices for energy group g as

$$\Sigma_g \equiv \operatorname{diag}(\sigma_{g,1}, \ldots, \sigma_{g,M}) \in \mathbf{R}^{M \times M}, \tag{A.15}$$

$$V_g^{-1} \equiv \operatorname{diag}(1/v_{g,1}, \ldots, 1/v_{g,M}) \in \mathbf{R}^{M \times M}. \tag{A.16}$$

We define the following matrices to describe the discretized derivative term

$$\Delta x \equiv \operatorname{diag}(\Delta x_1, \ldots, \Delta x_M) \in \mathbf{R}^{M \times M} \tag{A.17}$$

and

$$D \equiv \begin{pmatrix} -1 & 1 & & \\ & \ddots & \ddots & \\ & & -1 & 1 \end{pmatrix} \in \mathbf{R}^{M \times (M+1)}. \tag{A.18}$$

Boundary values are isolated by defining the row vector

$$B_\ell \equiv \begin{cases} e_M^T & \text{if } \ell \leq L/2, \\ e_0^T & \text{if } \ell > L/2 \end{cases} \in \mathbf{R}^{M+1}, \tag{A.19}$$

where the indices on the standard basis vectors e_ℓ are from 0 to M. Finally, we define the matrices Z and Z_b as

$$Z \equiv \begin{pmatrix} I_M \\ 0 \end{pmatrix} \in \mathbf{R}^{(M+1) \times M} \quad \text{and} \quad Z_b \equiv e_M. \tag{A.20}$$

We can now define the matrix form of the diamond difference representation of $\mu_\ell \partial/\partial x + \alpha/v_g + \sigma_g$ as

$$H_g + \alpha V_g^{-1} \equiv \mathrm{diag}(H_{g,1}, \ldots, H_{g,L}) + \alpha \; \mathrm{diag}(V_{g,1}^{-1}, \ldots, V_{g,L}^{-1}) \in \mathbf{R}^{L(M+1)}, \qquad (A.21)$$

where

$$H_{g,\ell} + \alpha V_{g,\ell}^{-1} \equiv Z(\mu_\ell \Delta x^{-1} D + \Sigma_g S_\ell) + Z_b B_\ell + \alpha Z V_g^{-1} S_\ell. \qquad (A.22)$$

It can be shown that $H_g + \alpha V_g^{-1}$ is nonsingular for the diamond difference method if α is not too negative.

We now define discretized representations of angular flux moment operators. The matrices operate on zone-centered vectors and are in $\mathbf{R}^{M \times LM}$. We define the matrix

$$L_n \equiv (l_n W) \otimes I_M, \qquad (A.23)$$

where $l_n \equiv (P_n(\mu_1), P_n(\mu_2), \ldots, P_n(\mu_L))$ are the Legendre polynomials and the quadrature weights are given by $W \equiv \mathrm{diag}(w_1, \ldots, w_L)$. If the vector Ψ_g approximates $\psi_g(x, \mu)$, then $L_n \Psi_g$ approximates taking the nth moment of the angular flux $\phi_{g,n}(x)$. We also define the matrix

$$L_n^+ \equiv (2n+1) l_n^T \otimes I_M \in \mathbf{R}^{LM \times M}. \qquad (A.24)$$

If a vector Φ approximates $\phi(x)$, then $L_n^+ \Psi$ will approximate $P_n(\mu)\phi(x)$. We define the grouped matrices for N_s moments as

$$L^N = \begin{pmatrix} L_0 \\ \vdots \\ L_N \end{pmatrix} \quad \text{and} \quad L^{N,+} = (L_0^+, \ldots, L_N^+). \qquad (A.25)$$

We can define the scattering and fission matrices as

$$\Sigma_{s,g,g',n} \equiv \mathrm{diag}(\sigma_{s,g,g',n,1}, \ldots, \sigma_{s,g,g',n,M}) \in \mathbf{R}^{M \times M} \qquad (A.26)$$

and

$$\Sigma_{f,g,g',n} \equiv \mathrm{diag}(\chi_g \nu \sigma_{f,g',n,1}, \ldots, \chi_g \nu \sigma_{f,g',n,M}) \in \mathbf{R}^{M \times M}. \qquad (A.27)$$

We now define matrices that inject zone-centered vectors into nodal vector space and vice versa. We define the matrices

$$\bar{\Sigma}_g \equiv I_L \otimes \Sigma_g \in \mathbf{R}^{LM \times LM}, \qquad (A.28)$$

$$\bar{V^{-1}}_g \equiv I_L \otimes V_g^{-1} \in \mathbf{R}^{LM \times LM}, \qquad (A.29)$$

$$\bar{Z} = I_L \otimes Z \in \mathbf{R}^{L(M+1) \times LM}, \qquad (A.30)$$

$$\bar{Z}_B = I_L \otimes Z_b \in \mathbf{R}^{L(M+1) \times L}, \qquad (A.31)$$

$$B = \mathrm{diag}(B_1, \ldots, B_L) \in \mathbf{R}^{L \times L(M+1)}, \qquad (A.32)$$

and

$$C = \text{diag}(\mu_1 \Delta x^{-1} D, \ldots, \mu_L \Delta x^{-1} D) \in \mathbf{R}^{LM \times L(M+1)}. \tag{A.33}$$

Using the above matrices, we can write the matrix $H_g + V_g^{-1}$ as

$$H_g + V_g^{-1} \equiv \text{diag}(H_{g,1}, \ldots, H_{g,L}) + \text{diag}(V_{g,1}^{-1}, \ldots, V_{g,L}^{-1})$$
$$= \bar{Z}(C + \bar{\Sigma}_g \bar{S}) + \bar{Z}_B B + \bar{Z} \bar{V}^{-1} \bar{S}. \tag{A.34}$$

The discretized multigroup eigenvalue equations can then be written in the matrix form as

$$H_g \Psi_g + \alpha V_g^{-1} \Psi_g = \bar{Z} \sum_{g'=1}^{G} \sum_{n=0}^{N_s} L_n^+ \Sigma_{s,g,g',n} L_n \bar{S} \Psi_{g'} + \bar{Z} \sum_{g'=1}^{G} \sum_{n=0}^{N_s} L_n^+ \Sigma_{f,g,g',n} L_n \bar{S} \Psi_{g'}, \tag{A.35}$$

Finally, we can write the multigroup discretized eigenvalue equations if we define the matrices

$$\boldsymbol{\Psi} \equiv \begin{pmatrix} \Psi_1 \\ \Psi_2 \\ \vdots \\ \Psi_G \end{pmatrix}, \quad \boldsymbol{\Sigma_s} \equiv \begin{pmatrix} \Sigma_{s,11}^{N_s} & \cdots & \Sigma_{s,1G}^{N_s} \\ \vdots & \ddots & \vdots \\ \Sigma_{s,G1}^{N_s} & \cdots & \Sigma_{s,GG}^{N_s} \end{pmatrix}, \quad \boldsymbol{\Sigma_f} \equiv \begin{pmatrix} \Sigma_{f,11}^{N_s} & \cdots & \Sigma_{f,1G}^{N_s} \\ \vdots & \ddots & \vdots \\ \Sigma_{f,G1}^{N_s} & \cdots & \Sigma_{f,GG}^{N_s} \end{pmatrix}, \tag{A.36}$$

where

$$\Sigma_{s,gg'}^{N_s} \equiv \text{diag}(\Sigma_{s,g,g',0}, \ldots, \Sigma_{s,g,g',N_s}) \tag{A.37}$$

and

$$\Sigma_{f,gg'}^{N_s} \equiv \text{diag}(\Sigma_{f,g,g',0}, \ldots, \Sigma_{f,g,g',N_s}). \tag{A.38}$$

Defining the following matrices

$$\mathbf{S} \equiv I_G \otimes \bar{S}, \tag{A.39}$$

$$\mathbf{Z} \equiv I_G \otimes \bar{Z}, \tag{A.40}$$

$$\mathbf{H} + \mathbf{V}^{-1} \equiv \text{diag}(H_1 + V_1^{-1}, H_2 + V_2^{-1}, \ldots, H_G + V_G^{-1}), \tag{A.41}$$

$$\mathbf{L}^+ \equiv I_G \otimes L^{N_s,+}, \tag{A.42}$$

$$\mathbf{L} \equiv I_G \otimes L^{N_s}, \tag{A.43}$$

then Eq. A.35 can be written as

$$\mathbf{H}\boldsymbol{\Psi} + \alpha \mathbf{V}^{-1}\boldsymbol{\Psi} = \mathbf{Z}\mathbf{L}^+ \boldsymbol{\Sigma_s} \mathbf{L}\boldsymbol{\Psi} + \mathbf{Z}\mathbf{L}^+ \boldsymbol{\Sigma_f} \mathbf{L}\boldsymbol{\Psi}. \tag{A.44}$$

Similarly, the discretized k-eigenvalue problem can be written as

$$\mathbf{H}\boldsymbol{\Psi} = \mathbf{Z}\mathbf{L}^+ \boldsymbol{\Sigma_s} \mathbf{L}\boldsymbol{\Psi} + \frac{1}{k}\mathbf{Z}\mathbf{L}^+ \boldsymbol{\Sigma_f} \mathbf{L}\boldsymbol{\Psi}. \tag{A.45}$$

Bibliography

[1]   H Aıt Abderrahim et al. "MYRRHA: A multipurpose accelerator driven system for research & development". In: *Nuclear Instruments and Methods in Physics Research Section A: Accelerators, Spectrometers, Detectors and Associated Equipment* 463.3 (2001), pp. 487–494.

[2]   R. E. Alcouffe et al. *PARTISN: A Time-Dependent, Parallel Neutral Particle Transport Code System.* Tech. rep. LA-UR-05-3925. Los Alamos National Laboratory, 2005.

[3]   G. I. Bell and S. Glasstone. *Nuclear Reactor Theory.* English. Tech. rep. TID–25606. Division of Technical Information, US Atomic Energy Commission, Jan. 1970. URL: `https://www.osti.gov/scitech/biblio/4074688` (visited on 02/01/2017).

[4]   Garrett Birkhoff and Richard S. Varga. "Reactor criticality and nonnegative matrices". In: *Journal of the Society for Industrial and Applied Mathematics* 6.4 (1958), pp. 354–377. URL: `http://epubs.siam.org/doi/pdf/10.1137/0106025` (visited on 07/07/2016).

[5]   P. Brown. "A Linear Algebraic Development of Diffusion Synthetic Acceleration for Three-Dimensional Transport Equations". In: *SIAM Journal on Numerical Analysis* 32.1 (Feb. 1995), pp. 179–214. ISSN: 0036-1429. DOI: `10.1137/0732006`. URL: `https://epubs.siam.org/doi/abs/10.1137/0732006` (visited on 03/21/2019).

[6]   Peter N. Brown. *On the Probability of Initiation for Neutron Transport Calculations.* Tech. rep. LLNL-JRNL-401245. Lawrence Livermore National Laboratory, 2008.

[7]   Peter N. Brown. *Probability of Initiation for Neutron Transport.* Tech. rep. LLNL-JRNL-522136. Lawrence Livermore National Laboratory, 2012.

[8]   Bengt G Carlson, Kaye D Lathrop, et al. *Transport theory: the method of discrete ordinates.* Los Alamos Scientific Laboratory of the University of California, 1965.

[9]   K. M. Case, G. Placzek, and F. Hoffmann. *Introduction to the Theory of Neutron Diffusion.* Tech. rep. Los Alamos National Laboratory, 1953.

[10]   Boris Davison and John Bradbury Sykes. *Neutron transport theory.* Clarendon Press, 1957.

[11]   J. J. Duderstadt and W. R. Martin. *Transport theory.* 1979. URL: `http://adsabs.harvard.edu/abs/1979trth.book.....D`.

[12]   James J. Duderstadt and Louis J. Hamilton. *Nuclear Reactor Analysis*. en. Google-Books-ID: R057QgAACAAJ. Wiley, Jan. 1976. ISBN: 978-0-471-22363-4.

[13]   Gene H. Golub and Charles F. Van Loan. *Matrix Computations*. en. JHU Press, Dec. 2012. ISBN: 978-1-4214-0859-0.

[14]   A. Greenbaum. *Iterative Methods for Solving Linear Systems*. Philadelphia: Society of Industrial and Applied Mathematics, 1997.

[15]   U. Hanebutte and P. N. Brown. *ARDRA, Scalable Parallel Code System to Perform Neutron and Radiation Transport Calculations*. Tech. rep. UCRL-TB-132078. Lawrence Livermore National Laboratory, 1999.

[16]   T. R. Hill. "Efficient Methods for Time Absorption (a) Eigenvalue Calculations". In: *Proc. of Top. Meeting*. 1983.

[17]   Roger A. Horn, Roger A. Horn, and Charles R. Johnson. *Topics in Matrix Analysis*. en. Google-Books-ID: LeuNXB2bl5EC. Cambridge University Press, June 1994. ISBN: 978-0-521-46713-1.

[18]   Roger A. Horn and Charles R. Johnson. *Matrix Analysis*. en. Cambridge University Press, Oct. 2012. ISBN: 978-1-139-78888-5.

[19]   Ilse C. F. Ipsen. "Computing an Eigenvector with Inverse Iteration". In: *SIAM Review* 39.2 (1997), pp. 254–291. ISSN: 0036-1445. URL: `https://www.jstor.org/stable/2133109` (visited on 02/11/2019).

[20]   Konrad Jörgens. "An asymptotic expansion in the theory of neutron transport". en. In: *Communications on Pure and Applied Mathematics* 11.2 (May 1958), pp. 219–242. ISSN: 1097-0312. DOI: `10.1002/cpa.3160110206`. URL: `http://onlinelibrary.wiley.com/doi/10.1002/cpa.3160110206/abstract`.

[21]   Drew E. Kornreich and Barry D. Ganapol. "The Green's Function Method for Nuclear Engineering Applications". In: *Nuclear Science and Engineering* 126.3 (July 1997), pp. 293–313. ISSN: 0029-5639. DOI: `10.13182/NSE97-A24482`. URL: `https://doi.org/10.13182/NSE97-A24482` (visited on 03/05/2019).

[22]   Drew E. Kornreich and D. Kent Parsons. "Time–eigenvalue calculations in multi-region Cartesian geometry using Green's functions". In: *Annals of Nuclear Energy* 32.9 (June 2005), pp. 964–985. ISSN: 0306-4549. DOI: `10.1016/j.anucene.2005.02.004`. URL: `http://www.sciencedirect.com/science/article/pii/S0306454905000538` (visited on 09/10/2016).

[23]   Edward W. Larsen and Paul F. Zweifel. "On the spectrum of the linear transport operator". In: *Journal of Mathematical Physics* 15.11 (1974), pp. 1987–1997. URL: `http://scitation.aip.org/content/aip/journal/jmp/15/11/10.1063/1.1666570` (visited on 02/12/2016).

[24] Joseph Lehner and G. Milton Wing. "On the spectrum of an unsymmetric operator arising in the transport theory of neutrons". en. In: *Communications on Pure and Applied Mathematics* 8.2 (May 1955), pp. 217–234. ISSN: 1097-0312. DOI: 10.1002/cpa.3160080202. URL: http://onlinelibrary.wiley.com/doi/10.1002/cpa.3160080202/abstract (visited on 04/01/2017).

[25] Elmer Eugene Lewis and W. F. Miller. *Computational Methods of Neutron Transport*. en. Google-Books-ID: hRxRAAAAMAAJ. Wiley, 1984. ISBN: 978-0-471-09245-2.

[26] I. Lux and László Koblinger. *Monte Carlo particle transport methods: neutron and photon calculations*. en. Google-Books-ID: 4u7vAAAAMAAJ. CRC Press, 1991. ISBN: 978-0-8493-6074-9.

[27] R. S. Modak and Anurag Gupta. "A scheme for the evaluation of dominant time-eigenvalues of a nuclear reactor". In: *Annals of Nuclear Energy* 34.3 (Mar. 2007), pp. 213–221. ISSN: 0306-4549. DOI: 10.1016/j.anucene.2006.12.009. URL: http://www.sciencedirect.com/science/article/pii/S0306454907000060 (visited on 02/18/2016).

[28] R. S. Modak and Anurag Gupta. "A simple scheme for the direct evaluation of time-eigenvalues of neutron transport equation". In: *Annals of Nuclear Energy* 30.2 (Jan. 2003), pp. 211–222. ISSN: 0306-4549. DOI: 10.1016/S0306-4549(02)00050-6. URL: http://www.sciencedirect.com/science/article/pii/S0306454902000506 (visited on 11/30/2016).

[29] R. S. Modak, D. C. Sahni, and S. D. Paranjape. "Evaluation of higher K-rmeigenvalues of the neutron transport equation by Sn-method". In: *Annals of Nuclear Energy* 22.6 (June 1995), pp. 359–366. ISSN: 0306-4549. DOI: 10.1016/0306-4549(94)00091-R. URL: http://www.sciencedirect.com/science/article/pii/030645499400091R (visited on 02/11/2019).

[30] Mark Nelkin. "Asymptotic solutions of the transport equation for thermal neutrons". In: *Physica* 29.4 (Apr. 1963), pp. 261–273. ISSN: 0031-8914. DOI: 10.1016/S0031-8914(63)80286-4. URL: http://www.sciencedirect.com/science/article/pii/S0031891463802864.

[31] A. M. Ostrowski. *Solution of Equations and Systems of Equations: Pure and Applied Mathematics: A Series of Monographs and Textbooks*. en. Google-Books-ID: eHBdDAAAQBAJ. Elsevier, June 2016. ISBN: 978-1-4832-2364-3.

[32] Y. Ronen, D. Shvarts, and J. J. Wagschal. "A Comparison of Some Eigenvalues in Reactor Theory". In: *Nuclear Science and Engineering* 60.1 (May 1976), pp. 97–101. URL: http://epubs.ans.org/?a=26862 (visited on 09/09/2016).

[33] A. Sood, R. A. Forster, and D. K. Parsons. "Analytical Benchmark Test Set for Criticality Code Verification". In: *Progress in Nuclear Energy* 42.1 (2003), pp. 55–106.

[34] Richard S. Varga. *Matrix Iterative Analysis*. en. Google-Books-ID: ix_1MNMHfIC. Springer Science & Business Media, Dec. 2009. ISBN: 978-3-642-05154-8.

[35] Guillermo Velarde, Carolina Ahnert, and José M. Aragonés. "Analysis of the Eigenvalue Equations in k, λ, γ, and α Applied to Some Fast- and Thermal-Neutron Systems". In: *Nuclear Science and Engineering* 66.3 (June 1978), pp. 284–294. URL: `http://epubs.ans.org/?a=27213` (visited on 09/10/2016).

[36] J. S. Warsa et al. "Krylov Subspace Iterations for Deterministic k-Eigenvalue Calculations". In: *Nuclear Science and Engineering* 147.1 (2004), pp. 26–42.

[37] James S. Warsa et al. "Krylov subspace iterations for deterministic k-eigenvalue calculations". In: *Nuclear Science and Engineering* 147.1 (2004), pp. 26–42. URL: `http://www.ans.org/pubs/journals/nse/a_2416` (visited on 02/12/2016).

[38] Eugene P. Wigner. "Mathematical problems of nuclear reactor theory". en. In: *Proceedings of Symposia in Applied Mathematics*. Ed. by Garrett Birkhoff and Eugene Wigner. Vol. 11. Providence, Rhode Island: American Mathematical Society, 1961, pp. 89–104. ISBN: 978-0-8218-1311-9 978-0-8218-9226-8. URL: `http://www.ams.org/psapm/011` (visited on 07/07/2016).

[39] G. M. Wing. *An Introduction to Transport Theory*. en. John Wiley & Sons, 1962.

[40] Toshihiro YAMAMOTO and Yoshinori MIYOSHI. "Reliable Method for Fission Source Convergence of Monte Carlo Criticality Calculation with Wielandt's Method". In: *Journal of Nuclear Science and Technology* 41.2 (Feb. 2004), pp. 99–107. ISSN: 0022-3131. DOI: `10.1080/18811248.2004.9715465`. URL: `https://www.tandfonline.com/doi/abs/10.1080/18811248.2004.9715465` (visited on 02/11/2019).